PERFORMANCE EVALUATION AND REACTION KINETICS OF A PULSED HF LASER

J. D. McClure, et al

Boeing Company

Prepared for:

Air Force Weapons Laboratory

August 1973

AFWL-TR-73-7

AFWL-TR-
73-7

PERFORMANCE EVALUATION AND REACTION KINETICS OF A PULSED HF LASER

J. D. McClure
D. B. Nichols
K. H. Wrolstad

Boeing Aerospace Company

TECHNICAL REPORT NO. AFWL-TR-73-7

August 1973

AIR FORCE WEAPONS LABORATORY
Air Force Systems Command
Kirtland Air Force Base
New Mexico

AIR FORCE WEAPONS LABORATORY
Air Force Systems Command
Kirtland Air Force Base
New Mexico 87117

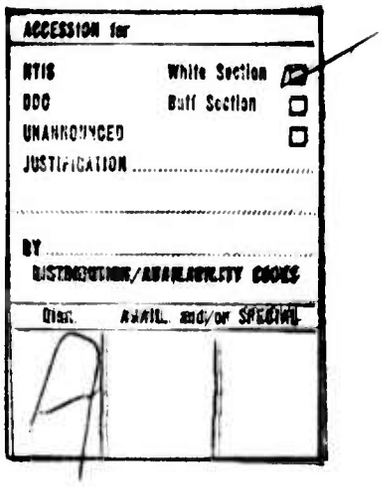

UNCLASSIFIED

Security Classification

AD-767230

DOCUMENT CONTROL DATA - R & D

(Security classification of title, body of abstract and indexing annotation must be entered when the overall report is classified)

1. ORIGINATING ACTIVITY *(Corporate author)*

Boeing Aerospace Company
Research & Engineering Division, PO Box 3999
Seattle, Washington 98124

2a. REPORT SECURITY CLASSIFICATION

Unclassified

2b. GROUP

3. REPORT TITLE

PERFORMANCE EVALUATION AND REACTION KINETICS OF A PULSED HF LASER

4. DESCRIPTIVE NOTES *(Type of report and inclusive dates)*

29 October 1971 through 28 October 1972

5. AUTHOR(S) *(First name, middle initial, last name)*

J. D. McClure, D. B. Nichols, K. H. Wrolstad

6. REPORT DATE	7a. TOTAL NO. OF PAGES	7b. NO. OF REFS
August 1973	~~124~~ 118	28

8a. CONTRACT OR GRANT NO. F29601-72-C-0008	9a. ORIGINATOR'S REPORT NUMBER(S)
b. PROJECT NO. 1256	AFWL-TR-73-7
c.	9b. OTHER REPORT NO(S) *(Any other numbers that may be assigned this report)*
d.	

10. DISTRIBUTION STATEMENT

Approved for public release; distribution unlimited.

11. SUPPLEMENTARY NOTES	12. SPONSORING MILITARY ACTIVITY
	AFWL (LRT) Kirtland AFB, NM 87117

13. ABSTRACT (Distribution Limitation Statement A)

Variation of performance of a laser-initiated HF laser with variation in reagent concentrations, reagent-diluent concentration ratio, and initial dissociation level is described. The HF laser intensity transients exhibit characteristic temporal structure representative of free-running chain reactions and collisional transfer processes in reacting H_2 - F_2 mixtures. Explicit exposure of underlying mechanisms is achieved by fast dissociation of F_2 via second harmonic radiation derived from a Q-switched ruby laser pulse, and by simultaneous time-resolved spectral measurements of laser emission on a number of vibration-rotation transitions. First initiation and large intensity fluctuations on lower P-branch transitions of the 2-1 and 1-0 vibrational bands are related on temporal grounds to consumption of photolytically generated F by the 'cold' F + H_2 reaction step. Transition from 'total' vibrational population inversions in an initial time range to a 'partial' population inversion at later times is implied by observation of the well known J-shift process predicted by existing model calculations based on the 'threshold gain' constraint and on the assumption of Boltzmann distribution of rotational states. Both time-order of line initiation and associated peak intensity exhibit strong correlation with expected gain of the transition. However, extended duration of moderate intensity emission on high J transitions results in large relative energy content compared to that of the high intensity, low J transitions. Continued laser emission over many chain-reaction steps, even for relatively low dissociation levels, supports the position that pulsed chemical lasers are attractive candidates for high power applications.

DD FORM 1 NOV 65 1473

ia

UNCLASSIFIED

Security Classification

14. KEY WORDS	LINK A		LINK B		LINK C	
	ROLE	WT	ROLE	WT	ROLE	WT
Pulsed HF chemical laser Laser photolysis reaction initiation Time resolved multi-line spectroscopy						

FOREWORD

This report was prepared by the Boeing Aerospace Company, Seattle, Washington, under Contract F29601-72-C-0008. The research was performed under Program Element 62301D, Project 1256, and was funded by the Advanced Research Projects Agency under ARPA Order 1256.

Inclusive dates of research were 29 October 1971 through 28 October 1972. The report was submitted 12 June 1973 by the Air Force Weapons Laboratory Project Officer, Captain William E. Thompson III (LRT).

This report has been reviewed and is approved.

William E. Thompson, III

WILLIAM E. THOMPSON, III
Captain, USAF
Project Officer

JOHN C. RICH
Lt Colonel, USAF
Chief, Advanced Technology Branch

DONALD L. LAMBERSON
Colonel, USAF
Chief, Laser Division

ABSTRACT

Variation of performance of a laser-initiated HF laser with variation in reagent concentrations, reagent-diluent concentration ratio, and initial dissociation level is described. The HF laser intensity transients exhibit characteristic temporal structure representative of free-running chain reactions and collisional transfer processes in reacting H_2 - F_2 mixtures. Explicit exposure of underlying mechanisms is achieved by fast dissociation of F_2 via second harmonic radiation derived from a Q-switched ruby laser pulse, and by simultaneous time-resolved spectral measurements of laser emission on a number of vibration-rotation transitions. First initiation and large intensity fluctuations on lower P-branch transitions of the 2-1 and 1-0 vibrational bands are related on temporal grounds to consumption of photolytically generated F by the 'cold' F + H_2 reaction step. Transition from 'total' vibrational population inversions in an initial time range to a 'partial' population inversion at later times is implied by observation of the well known J-shift process predicted by existing model calculations based on the 'threshold gain' constraint and on the assumption of Boltzmann distribution of rotational states. Both time-order of line initiation and associated peak intensity exhibit strong correlation with expected gain of the transition. However, extended duration of moderate intensity emission on higher J transitions results in large relative energy content compared to that of the high intensity, low J transitions. Continued laser emission over many chain-reaction steps, even for relatively low dissociation levels, supports the position that pulsed chemical lasers are attractive candidates for high power applications.

CONTENTS

CONTENTS (Continued)

ILLUSTRATIONS

ILLUSTRATIONS (Continued)

ILLUSTRATIONS (Continued)

ILLUSTRATIONS (Continued)

SECTION I

INTRODUCTION

The present study was undertaken with principal aims of: 1) determining the performance variation of a fast pulsed HF laser with variation of principal physical parameters governing the H_2 - F_2 reaction-deactivation processes, e.g., dissociation level, reagent concentration, and reagent/diluent concentration ratio; and 2) display of associated time-resolved vibration-rotation spectra of laser emission in order to further understanding of principal chemical mechanisms governing pulsed chemical laser performance. The work is based on use of laser-photolysis of F_2 described in section II-A1 which is accomplished on a time scale (~30-50 nanoseconds) that is short compared to characteristic times of relevant kinetic processes for the chemical conditions considered; H_2 - F_2 partial pressures are in the range 4-16 torr, total gas pressure in the range 40-160 torr. Use of collimated radiation of specified wavelength, in this case 3471 Å second harmonic radiation derived from a Q-switched ruby laser, has the additional advantage that the initial dissociation level is well specified. Thus, the initial chemical state when reaction begins is clearly defined, and the time evolution of chemical state is strictly governed by the propagating chain reactions, along with associated collision transfer and laser emission processes. Due primarily to practical considerations in acquisition of data, and for comparison of time-resolved line spectra for identical initial conditions, a unique capability for simultaneous measurement of transient intensity on a set of vibration-rotation transitions was developed during the program (section II-B).

Since demonstration of the first chemical laser by Kasper and Pimentel (Ref. 1) small chemical lasers based on photolytic initiation of reaction have provided a powerful investigative tool for study of

reaction mechanisms*. Notable examples of pulsed chemical laser studies undertaken prior to the work reported here include the HCl laser based on the Cl-HBr exchange reaction (Ref. 2) and use of several DCl/HF lasers for determination of relative partial reaction rates into individual vibrational levels by Pimentel and co-workers (Refs. 3, 4, and 5). At the time the present study was undertaken, however, existing studies of pulsed HF lasers pumped by the propagating chain reactions in H_2 - F_2 mixtures were quite preliminary in nature (Refs. 6, 7, and 8).

A common characteristic of conventional photolysis lasers is the finite duration of initiating light compared to characteristic reaction-deactivation times for reagent partial pressures of several torr and above. Furthermore, absolute intensity of the initiating light is difficult to determine in the conventional flash photolysis laser since the excessively low utilization of light per pass through slender tubes containing the reagent media necessitates use of external reflecting enclosures. Thus, the observed laser transients are governed by superimposed transient variation of photolysis products (specifically $F_2 + h\nu \rightarrow 2F$ for HF lasers based on H_2 - F_2 reagent mixtures), along with transient variation of vibration-rotation populations due to the propagating $F + H_2$ and $H + F_2$ production reactions, to collision induced energy transfer between vibrational states (V-V transfer), to collision induced removal of vibrational energy (V-T or, more properly, V-R transfer), to vibrational level change due to laser emission, and finally, due to variation of effective rotational temperature as the reactions proceed.

Although fast laser initiation of reaction eliminates temporal variation of photolysis products during the reaction transient, thus

---

* Although little attention has been given to development of high performance photolysis lasers for high power applications, a Boeing research/development program on high efficiency initiation of reaction along with high specific energy demonstrated at other laboratories for both HF and DF-CO_2 photolysis lasers provides a sound basis for such developments.

providing a clearly defined initial state, total intensity and individual line transients described in sections III-V and appendices I-II are quite complex in nature. For example, characteristic temporal behavior on radically different time scales varying from 10^{-8} - 10^{-5} sec is observed. This temporal structure is reproducible over an extensive set of data, and is a direct consequence of a more detailed exposure of governing mechanisms than has been possible with conventional 'slow' photolysis techniques. Initiation times of individual transitions and associated peak intensity correlate with threshold gain considerations based on known partial reaction rates of the F + H_2 reaction, assumption of Boltzmann rotational population distribution, and J-shifting processes associated with transition from 'total' to 'partial' population inversion as described by Airey (Ref. 2), Chester and Hess (Ref. 9), and Kerber et al. (Ref. 10). Total energy content of emission on individual lines shows little correlation with peak intensity or factors noted above, however, and is primarily determined by extended time duration of lines of higher rotational quantum number ($J \simeq 5$-6) that lase after transition to 'partial' state inversion has occurred. Extended duration of laser emission over many complete chain reaction steps, even for small dissociation level achieved with the laser-initiated chemical laser, has considerable significance with reference to high power laser applications (see section VII). For lower gas pressures (F_2:H_2:N_2 = 4:4:40 torr) evidence of a collisional energy transfer process circumstantially associated with ground state HF, and considerably more rapid than known deactivation processes involving the V = 1,2 upper vibrational levels, is obtained. However, the implied deactivation rate is not exceptionally fast compared to relaxation rates for V = 4,5 levels measured by Airey and Smith (Ref. 11).

Observed intensities of individual lasing transitions exhibit fluctuations whose magnitude and time duration correlate strongly with gain of the transition. Higher gain transitions typically exhibit one or two high intensity pulses of 40-80 nanosecond duration, intermediate gain transitions exhibit a larger number of fluctuations of moderate amplitude (relative to a 'quasi-steady' emission level) which in some

cases occur in a near periodic time sequence with relatively large separation between pulses (~1-2 μsec), and low gain transitions exhibit fluctuations whose amplitudes are small compared to a slowly varying 'mean' level. The rapid rise and fall of the higher intensity fluctuations are undoubtedly associated with resonator relaxation processes, i.e., resonator amplification of intensity and subsequent saturation or 'bleaching' of the gain media, that cannot be modeled utilizing the conventional threshold gain constraint. Although the principal energy content in emission from the laser-initiated chemical laser corresponds to lower gain transitions for which relaxation processes are of lesser significance, such processes may be an important factor in determining limitations on useful gain/pass in devices appropriate to higher power applications.

In addition to principal objectives described above, the subject program encompasses several supportive tasks designed to improve definition of experimental conditions associated with results reported here, and to extend present diagnostic capability for pulsed chemical laser applications. As described in section II-C, an HF probe laser was built and used to determine ground-state HF levels in the laser initiated chemical laser, and to define intra-cavity transmission losses, thus permitting an improved specification of threshold gain of the cavity. The measurements of HF concentration provide the basis for association of the fast deactivation process noted above with ground state HF (see section IV). As described in section II-D, capability for making time-resolved line strength measurements in reacting media would contribute significantly to improved experimental studies of reaction-deactivation kinetics in pulsed chemical lasers. Rationale for use of an HF laser-flame radiation source for such measurements as well as associated design considerations and characterization of a subsonic flow diffusion-flame radiation source are presented in sections II-D and VI.

SECTION II

EXPERIMENTAL CONSIDERATIONS

A. Laser-Initiated Chemical Laser

1. Initiation of Reaction

A schematic diagram of the laser-initiated chemical laser is shown by Fig. 1, and an overview photograph of the laser and associated spectroscopic instrumentation by Fig. 2. The H_2 - F_2 chain reactions are initiated through photo-dissociation of F_2 by second harmonic radiation derived from a Q-switched ruby laser. Second harmonic (2ν) pulses of .36 joule generated from 1.75 joules of primary radiation (conversion efficiency in excess of 20%) with ~60 nanosecond full width half maximum (FWHM) have been obtained from a KDP second harmonic generator, although 2ν levels of .15 - .2 joule are more typical in day-to-day operation. Alternative second harmonic generator materials ($LiIO_3$ and KD*P) tested before and during the contractual program did not produce significant 2ν conversion for the required incident power levels. Improved conversion efficiency and operating stability were achieved by improving beam quality of the ruby laser (beam divergence < $.8 \times 10^{-3}$ rad achieved by utilizing a 1.27 m cavity length and intracavity aperture), and by thermal isolation of the ruby laser mirrors. The 2ν radiation is introduced into the HF laser cavity via a sapphire Brewster flat as shown by Fig. 1. The 2ν energy/pulse used for HF laser initiation is monitored by an energy detector sensing the beam transmitted through the Brewster flat. This energy monitor was calibrated prior to HF laser operation by simultaneous measurement of the 2ν energy to the monitor detector and that passing through the reactor cell. The primary ruby light is excluded from the HF cavity by a cell containing $CuSO_4$ solution since otherwise damage of the HF laser mirrors occurs. Approximately 60% of the 2ν radiation is transmitted by the $CuSO_4$ of which ~60% is reflected by the Brewster flat (even though coated for 95% reflection of S-polarized 3471 Å radiation at 60° incidence) along the HF cavity axis. Approximately 80% of this beam fraction is transmitted by the sapphire

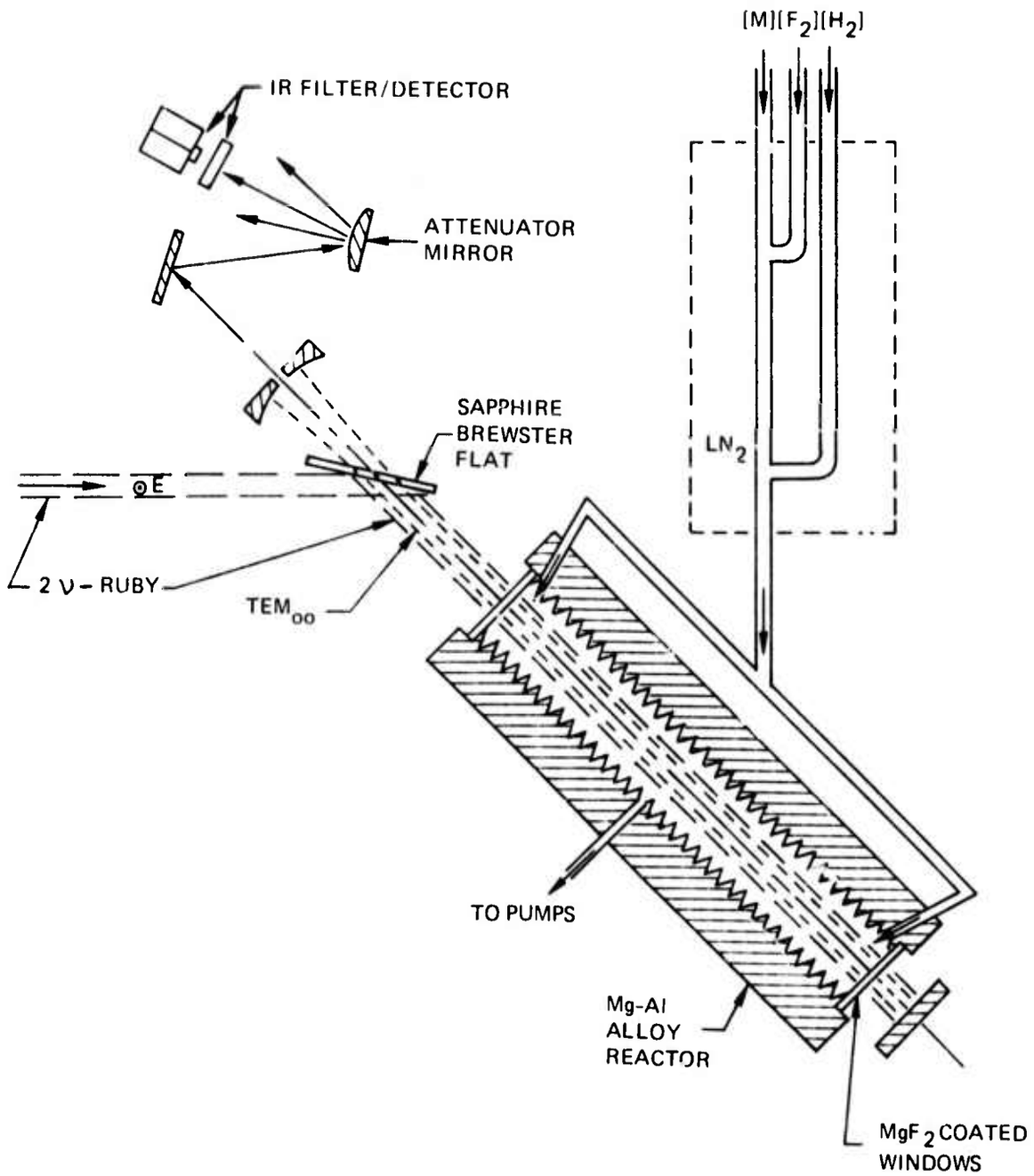

FIGURE 1. SCHEMATIC OF LASER INITIATED CHEMICAL LASER

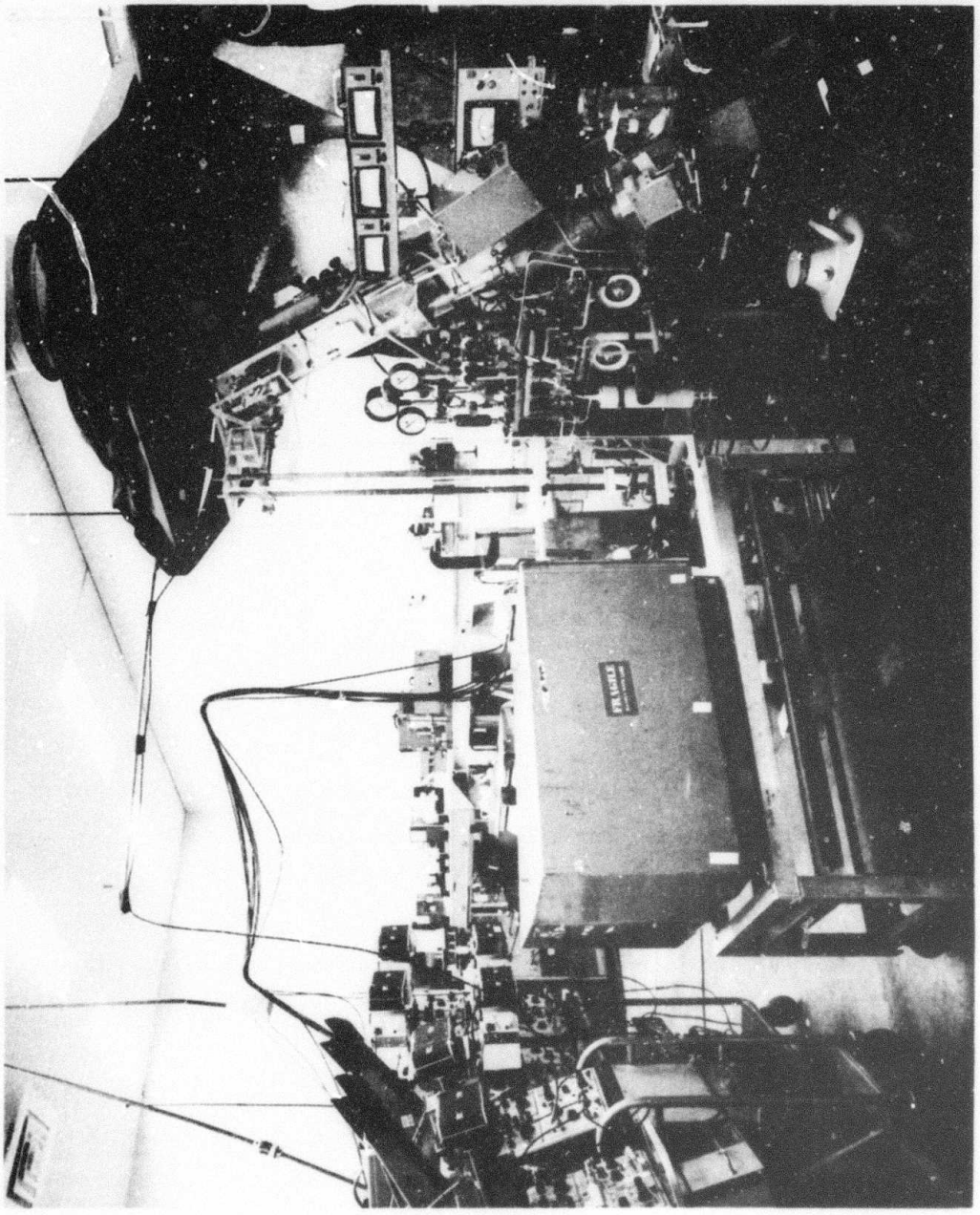

FIGURE 2. LASER INITIATED CHEMICAL LASER AND SPECTROSCOPIC INSTRUMENTATION

reactor end windows which are coated for infrared (IR) transmission but not for the ultraviolet (UV). Thus 50-75 millijoules of 2ν radiation is available for photolysis with a FWHM pulse duration of ~30 nanoseconds. The photo-dissociation cross section for F_2 at 3471 Å as given by Steunenburg and Vogal (Ref. 12) or Levy and Copeland (Ref. 13) is $.7 \times 10^{-20}$ cm^2. For double passage through the 30 cm long reactor, achieved by overcoating the lower HF laser mirror for high 2ν reflectivity, approximately 6% of the incident 2ν radiation ($3\text{-}4 \times 10^{-3}$ joules) is absorbed at an F_2 partial pressure of 4 torr and approximately 11% ($5\text{-}8 \times 10^{-3}$ joules) at 8 torr. As noted in section III, the corresponding dissociation level is $[F]/[F_2] = .8 - 1.2\%$ ($\Delta[F_2]/[F_2] = .4 - .6\%$).

2. Premixing and Prereaction

The chemical reactor is fabricated from a Mg-Al alloy with 60° threads machined into the 1 cm diameter x 30 cm internal bore to reduce spurious internal reflections. The choice of a non-transition metal cell is based on experience of Levy and Copeland (Refs. 13, 14, and 15) in successfully containing sufficiently dilute H_2 - F_2 mixtures without incurring spontaneous 'dark reaction'. Prior to this contract UV absorption instrumentation (xenon arc lamp, 2880 Å narrow band filter, 1P28 phototube detector) was set up to determine the rate of 'dark' reaction in static F_2 - H_2 - N_2 mixtures in this Mg-Al cell. Cell filling by adding F_2 - N_2 mixtures to pure H_2 with concentration ratios, F_2:H_2:N_2, in the range 1:1:10 to 1:1:20 and total pressure in the range 100-700 torr resulted in quite stable mixtures with 'half lives' in excess of one hour, i.e., the F_2 concentration slowly decreased from the initial value (determined by partial pressure measurements and confirmed by initial UV absorption measurements based on prior calibration in pure F_2) to one half that value in periods of one hour and greater. The cell was initially passivated with pure F_2 for extended periods (48 hours and more). The passivation process was frequently repeated for periods of one hour or more after the cell had been exposed to an untrapped mechanical vacuum pump over night. In general, however, the rate of 'dark reaction' was found to be stable and independent of successive passivation. Reverse filling procedure by adding N_2 - H_2 mixtures to

pure F_2 resulted in explosion. This result might well be expected since studies of explosion limits (Ref. 16) show that F_2 - rich mixtures without diluent are unstable, a condition that can occur here due to preferential diffusion of H_2 into F_2.

Since the rates of dark reaction found above (~1%/minute) could lead to undesirable levels of ground state HF in the time-period required for diffusive mixing of reagents in a 'static fill' mode, the 'slow flow' purging configuration illustrated by Fig 1 in which more rapid premixing occurs in small bore supply lines was implemented. Glass tubing was initially used in the supply lines. Continued visual checks for etching of the glass by HF gave no indication of pre-reaction during laser studies at lower total pressure levels (40-80 torr). Due to evidence of burning in the premixer at increased pressure, however, a more conservative premixer was fabricated from Al tubing. The main N_2 flow-tube is 1/4 inch OD, F_2 and H_2 are introduced into the main tube through three small orifices in the wall of 1/8 inch supply lines that penetrate the wall of the larger tube. The H_2 injection point is at the bottom of a U-tube configuration which can be immersed in liquid nitrogen, is located 80 cm downstream from the F_2 injector, and is 40 cm upstream from the flow entry to the reactor. The gas residence times in the reactor are typically 2-3 seconds. For the total pressure levels used in the laser measurements, the corresponding flow velocities in the supply lines (50 cm/sec and less) give adequate transit time for complete diffusive mixing of F_2 - N_2 before H_2 injection, for complete mixing of H_2 - F_2 - N_2, and for warming the mixture to ambient temperature before the mixture reaches the reactor. The premixer modification was made after the laser transient measurements of section III and prior to the spectroscopic measurements of sections IV and V.

As described in sections II-C2, IV and V, typical steady-state HF concentrations in the reactor after premixer modification as determined by absorption measurements are in the range .017 - .022 torr for the premixer at ambient temperature, and .002 - .005 torr for the premixer refrigerated to liquid nitrogen (LN_2) temperature. These steady state concentrations are independent of specific ways of starting the

flow so long as reasonable care is exercised, i.e., the flows can be established at low pressure and the gas pressure increased to the desired value by partially closing a valve in the exhaust line, or the pure N_2 flow can be first restricted to the desired partial pressure with subsequent introduction of H_2/F_2. Higher level prereaction transients follow initiation of gas flow, but decay to steady state levels in reproducible periods of time.

3. Resonator Configuration

The HF laser cavity consists of interchangeable spherical output couplers of 10 m radius of curvature and a flat dielectric coated total reflector with 113 cm mirror separation. The total reflector is overcoated for high reflectivity at 3471 Å in order to more efficiently utilize the 2ν radiation. First laser measurements (section III) were performed with a hole-coupled spherical mirror (1/2 mm diameter hole giving $\lesssim$ 1% coupling fraction for a 3.5 mm diameter TEM_{oo} mode), and the spectroscopic measurements (sections IV and V) were performed with a bare germanium spherical mirror antireflection (AR) coated on the second surface for the HF wavelength range (T = 70% $\pm$ 1% through the wavelength range of interest). A 15% transmitter was also used briefly but radiation damage occurred (presumably from the high power 2ν beam). The mode volume external to the reactor cell was enclosed by tubes purged continuously with dry nitrogen. The reactor end windows are of sapphire with AR coating of magnesium fluoride. The AR coatings are impervious to exposure to HF and F_2 as determined by visual inspection. Optical properties of the end windows and other intracavity components are described in subsection C-3.

4. Miscellaneous Instrumentation

In the initial part of the program concentration ratios were determined by calibrated leak valves. Due to frequent needs to change valve conductance and excessive burden of recalibration, Matheson Linear mass-flow meters were installed and have given excellent service. Total gas pressure was measured by use of Leybold-Hereaeus Di-Vac gauges. A fast photodiode detector was used to monitor the ruby laser transient, thereby establishing a time base for the reaction and HF-laser transients. Corresponding energy/pulse was monitored with an energy thermopile.

B. Transient Emission Spectroscopy

1. Rationale and Configuration for Multi-Channel Spectroscopic Capability

The advantages of using a high power Q-switched laser dissociation source for initiating chemical reaction are described in section I. However, the rate of acquisition of data is limited by the low repetition rate inherent to this technique, especially since the set of vibration-rotation transitions of interest for HF lasers based on H_2 - F_2 chain reactions is large. Consequently, capability for simultaneous measurement of transient line spectra on a set of 10 transitions was developed. Ability to define characteristic temporal structure of emission on various lines involving radically different time scales (sections IV/V) has depended strongly on this multi-channel capability.

An overview of the Jarrell-Ash .75 m grating spectrograph and optical components for leading the beam from the HF laser to the spectrograph is shown by Fig. 2, and a photograph of the spectrograph/detector arrangement is shown by Fig. 3. A 'pellicle' beam splitter (~8μ thick) directs a fraction of the HF laser beam to a Ge:Au total intensity detector located at the upper end of the optical strongback shown by Fig. 2. The remaining beam fraction is focussed onto the spectrograph entrance slit (lower right corner of Fig. 3). The spectrograph interior and lucite dry-box containing the beam steering components are purged with dry N_2 (relative humidity of 15-17% in the dry-box causes a maximum attenuation of 20% or less on the HF line spectrum).

As shown by Fig. 3 the individual IR detectors are inset into sliding mounts that can be precisely positioned (tolerance of ± .15 mm) in the direction parallel to the spectrograph 'camera' slit. The Ge:Au detectors are of the 'end-viewing'type and the mounts are equipped with polished metal 'pickup' mirrors 1 mm in width. Thus, provision of multiple tracks for the sliding detector mounts eliminates the mechanical constraint otherwise imposed by the .75 inch dewer diameter on simultaneous detection of adjacent spectral lines. Constraints on spectral resolution due to placement of detectors behind the focal plane of the spectrograph 'camera' mirror are discussed below.

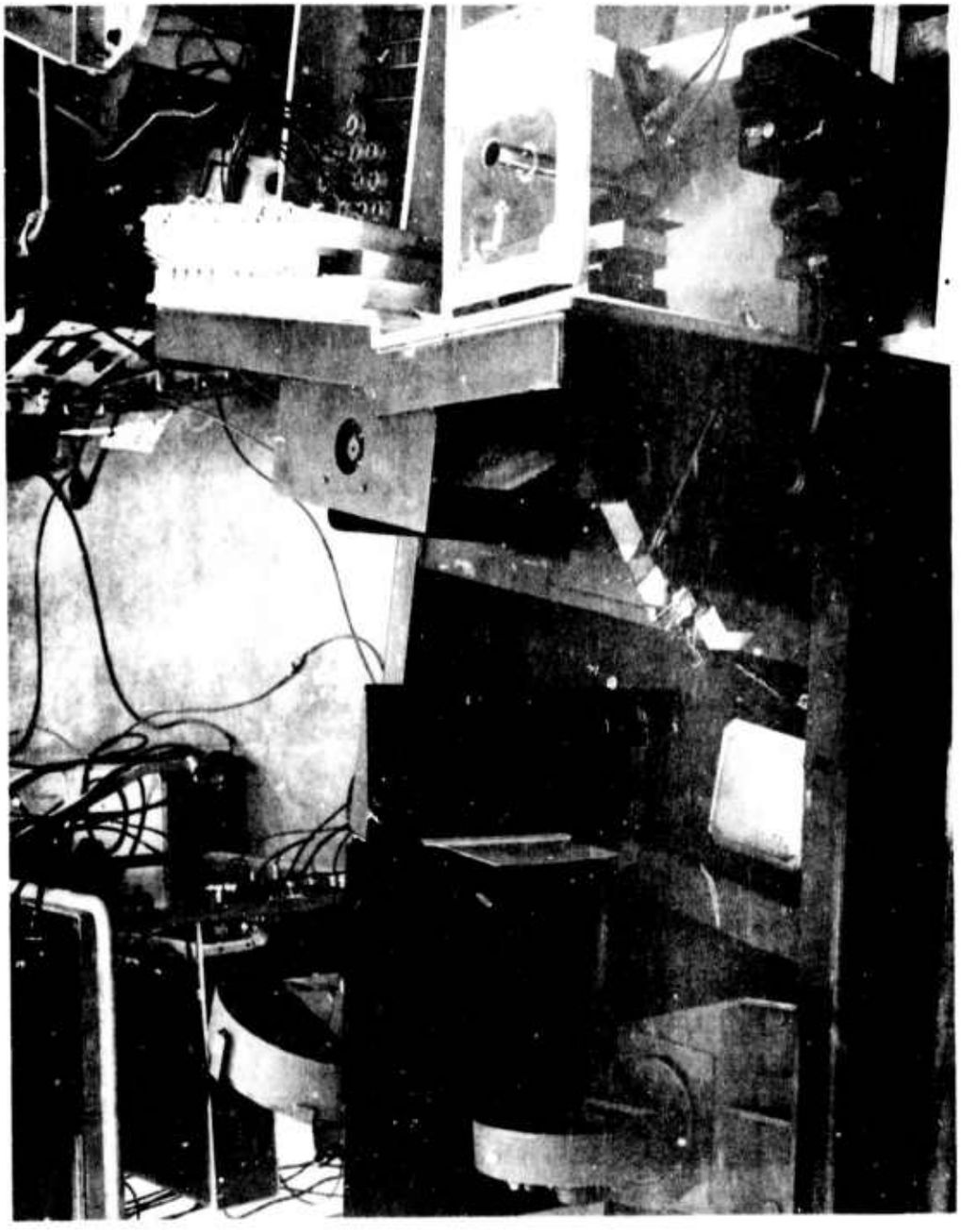

FIGURE 3. SPECTROGRAPH AND MULTI-CHANNEL DETECTOR CONFIGURATION

2. Spectrograph Calibration and Resolution

Reliable pre-positioning of the detectors for multichannel transient spectroscopy of non-repetitive events requires careful definition of optical properties of the spectrograph. In principle, definition of spectrograph optics is straightforward. The position (Y) of any diffracted beam measured parallel to the spectrograph exit slit in a given detector plane is a function only of the included angle $\phi = \theta_D - \theta_I$ between the incident and diffracted beams where θ_D/θ_I are the diffraction/incidence angles measured with respect to the grating outward normal. Calibration of the spectrograph requires determination of the function $Y(\phi)$ for each detector which, ideally, is accomplished by measuring Y as a function of grating angular position for simple reflection of a He-Ne laser alignment beam. For a given grating angle and spacing of rulings d, the included angle ϕ for a particular wavelength λ is determined from the grating equation,

$$\sin \theta_I + \sin \theta_D = m \frac{d}{\lambda}$$

thus yielding the required detector position from the predetermined $Y(\phi)$.

The practical difficulty to be overcome in the calibration procedure outlined above is determination of the grating orientation (i.e., true θ_I for given indicated grating angle $\tilde{\theta}$) with adequate accuracy. An angular error $\Delta\theta = .005°$ produces a shift in diffracted position of $\sim$.1 mm at the camera plane which is in turn equivalent to a wave number error of .25 - .5 cm^{-1} in the 2.5 - 3μ wavelength range for a 300 line/mm grating. This angular accuracy was achieved by spring-loading the grating holder to eliminate backlash, and by determining the effective gear ratio between the grating angle indicator and the grating shaft with high precision. This gear ratio appears as a constant C in the relationship between true and indicated grating angles, $\theta_I = C\,(\tilde{\theta} - \tilde{\theta}_o)$, where $\tilde{\theta}_o$ is the indicator reading for normal grating incidence. Empirical determination of the constant C permits evaluation of the calibration function $Y(\phi)$.

Self consistency and error bounds utilizing the calibration procedure described above were established by determining the error between measured and calculated positions of 0th, 4th, 5th, and 6th order beams of a He-Ne alignment laser as the grating angle was varied (i.e., the diffracted beams were swept across the full 1.5 cm 'camera' slit). The inherent limitation on the calibration technique is due to periodic error in the grating drive and to error in measuring the position of the focussed He-Ne beam at the camera plane (± .1 mm). Visual positioning of the IR detectors introduces a slightly larger error bound (~.4 - .7 cm^{-1} wave number error) which is still smaller than resolution limits discussed below.

The principal factors limiting resolution of the multiple channel measurements result from the fact that the detectors are positioned behind the instrument focal plane. Three semi-independent sources of error arise: 1) divergence of the diffracted beams behind the focal plane according to the relation $t \equiv \Delta\nu \frac{dY}{d\nu} \simeq \ell/f$ where t is beam width, $\Delta\nu$ is the equivalent wave number increment (resolution limit), $\frac{dY}{d\nu}$ is the dispersion relation, f is the f-value, and ℓ is distance behind the focal plane, 2) shift in transverse position ΔY of the diffracted beams due to a change of position of the entering beam at the entrance slit according to $\Delta Y = \frac{dY}{d\theta_I} \frac{\Delta Y_{in}}{75} = \frac{d\theta_D}{d\theta_I} \frac{\Delta Y_{in}}{75} (75 + \ell)$ where ΔY_{in} is the shift in position of the entering beam, all distances measured in cm, and 3) the usual grating resolution limit, which for first order diffraction is $\Delta\nu/\nu = \frac{1}{N} \simeq f/(3000 \times 75)$ where N is the number of rulings illuminated for the 300 line/mm grating. Error 2) above can be reduced to a noncritical value by using small entrance slit-width (i.e., by ensuring the He-Ne calibration beam and HF beam enter at the same location with adequate precision) and will not be considered further. Factors 1) and 3) together set the resolution limits and the optimum f-value. Choice of f = 125 (achieved by aperturing the incident beam between collimator mirror and grating) yields a resolution of 2-5 cm^{-1} in the wavelength range of interest. Beam steering mirrors are, of course, designed to give a similar f-value since otherwise excessive intensity loss or degradation of resolution by 3) will occur.

Prior to time-resolved measurements discussed in sections IV/V, the HF probe laser described in subsection C-1 was used to recheck the calibration procedure. Subsequent measurements of diffracted beam widths of the HF laser confirm operation with resolution approximately equal to the design value.

C. Initial [HF] Concentration and Cavity Diagnostics

After encountering evidence of prereaction in the initial 'slow flow' mixing configuration and consequent redesign of the premixer (section II-A2), it was deemed necessary to establish ground state HF concentration for typical operating conditions. Importance of a quantitative definition of low level initial [HF] as related to performance of the laser-initiated HF laser for low pressure operation is demonstrated by results reported in section IV. Definition of transmission properties of the intracavity Brewster flat and reactor end-windows, with particular reference to correct orientation of the sapphire substrates for transmission of plane-polarized HF radiation without loss due to depolarization, was also made. Methods used for accomplishing these tasks and associated results are described in the following subsections.

1. Line Selected HF Probe Laser

A small HF probe laser pumped by the $F + H_2$ reaction initiated by repetitive discharge dissociation of SF_6 in $SF_6 - H_2 - He$ mixtures was built and operated in a line-selected mode on 15 P-branch transitions in the 2-1 and 1-0 vibrational bands (operation on 3 R-branch transitions in the 2-1 band was also possible). The basic probe laser configuration, which is similar to that reported by Ultee (Ref. 17) is shown by Fig. 4. The cavity consists of a 600 line/mm Littrow mounted grating and an aluminized 'pellicle' ($R \simeq 85\%$) with approximately 90 cm mirror separation. Principal output coupling is the specular reflection from the grating. The line-selected probe intensity varies by $\sim$25% as the cavity resonator frequencies (free spectral range = .0056 cm^{-1}) are swept slowly across the gain profile via a piezoelectric translator. As

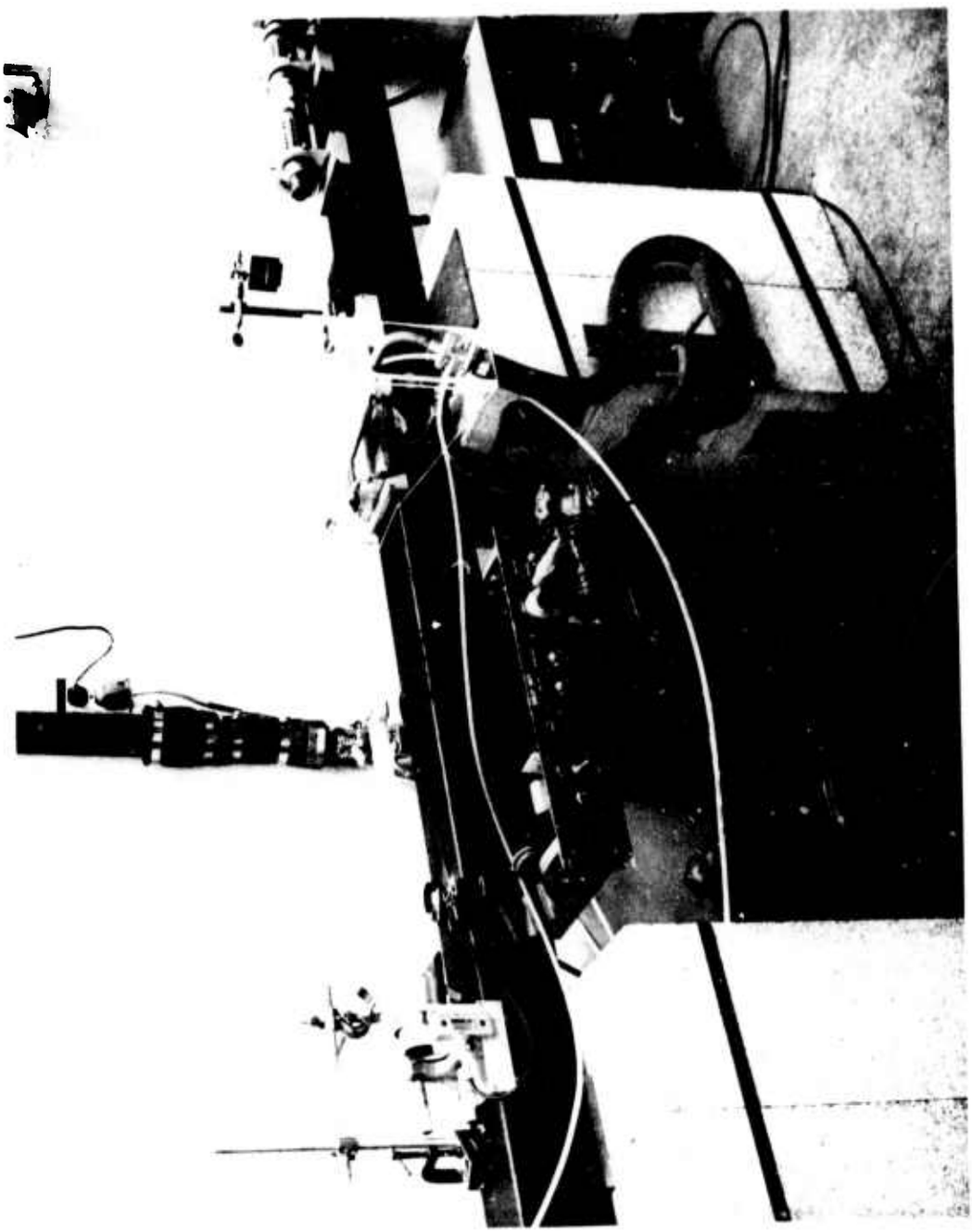

FIGURE 4. HF PROBE LASER

noted below, operation in a single longitudinal mode is not essential for our application (i.e., the width of the HF absorption profile for conditions of interest is large compared to the ± .0025 - .005 cm^{-1} uncertainty in probe laser wave number).

2. Measurements of Ground State HF in the Laser Reactor Cell

Absorption measurements of ground state HF in the 'slow flow' purge reactor configuration of Fig. 1 were made with the probe laser operating on the P(2) transition of the 1-0 vibrational band. A small fraction of the probe beam was directed by a beam splitter into a reference detector before passing the principal beam fraction through the reactor cell for attenuation measurements.

Absorption due to HF in the reactor was measured for typical laser mixtures $H_2:F_2:N_2$ = 4:4:40 torr and 8:8:80 torr, with and without LN_2 cooling of the premixer, and at 16:16:160 torr for the ambient temperature premixer. The Voigt profile was assumed for the HF line shape, with the Lorentz width taken from the work of Shaw and Lovell (Ref. 18) for CO_2, i.e., for the P(2) line, $\Delta\nu_L\,(cm^{-1}) = .1 \times P_{N2}\,(atm)$. This usage is conservative (i.e., a given measured attenuation level yields higher HF concentration) relative to the expression used by Emanuel et al. (Ref. 19). Self broadening of HF by HF is negligible for conditions of interest, as are pressure induced line shifts. For conditions of interest the ratio of Lorentz to Doppler linewidths (more properly, the quantity $Y = (\Delta\nu_L/\Delta\nu_D)\,(\ln 2)^{1/2}$) is unity and greater. Therefore association of the measured probe laser attenuation (recall the small wavelength uncertainty noted in subsection C-1) with the Voigt line center absorption coefficient, i.e., $I/I_o = \exp(-k_{\nu o} L)$, leads to an error of 5% or less in $k_{\nu o}$. The reference Doppler coefficient, $k_o = (S/\Delta\nu_D)\,(\ln 2/\pi)^{1/2}$, and thus the corresponding line strength S, are determined from $k_{\nu o}$ via the Voigt line center relation, $k_{\nu o}/k_o = \exp(Y^2)\,\mathrm{erfc}\,(Y)$. The HF concentration is determined from S via the calculations by Meredith and Kent (Ref. 20).

Steady-state HF concentrations so determined for the 4:4:40 torr mixture are .022 torr and .005 torr for the premixer at ambient and LN_2 temperatures, respectively, and corresponding HF concentrations for the 8:8:80 torr mixture are .017 torr and .002 torr. HF concentration for 16:16:160 torr for the ambient temperature premixer is in the range .010 - .015 torr. Reproducibility of attenuation measurements to within ± 5% yield corresponding uncertainties in $k_{\nu o}$, and therefore HF concentration, of ~30% at the higher concentration levels and ~50% at the lower concentrations. As indicated in subsection A-2, transient HF levels of larger magnitude occur when the reagent flows are first turned on, but decay to these reproducible steady-state levels in well-defined time intervals. The HF levels above correspond to a residence time of ~3 sec in the reactor. Increase of residence time to ~6 sec leads to a factor of two increase in HF concentration. It is of interest to note that the steady-state levels imply a dark reaction rate that is consistent with those measured in quiescent $H_2 - F_2 - N_2$ mixtures in the Mg-Al reactor cell prior to beginning work on this contract (subsection A-2).

3. Intracavity Losses and Definition of Threshold Gain

An assessment of intracavity losses in the laser initiated HF laser was undertaken with the two-fold objectives of an improved definition of threshold gain associated with the cavity and/or to identify and reduce transmission losses that could adversely affect laser performance. These measurements and associated component changes, undertaken after the laser transient measurements of section III, reduced intracavity losses by a factor of 3-4 and permit specification of threshold gain with an accuracy of 5-30% over the wavelength range of interest. Subsequent measurement of laser transients showed no basic change in the temporal structure described in section III, although the total intensity was increased considerably.

A bare intracavity sapphire Brewster flat (60° material) used for performance measurements of section III exhibited significant optical imperfections when viewed in a cross-polarizer. Initial azimuthal orientation of the Brewster flat was made by viewing a polarized He-Ne

alignment beam through a cross-polarizer after transmission through the Brewster flat. The flat was oriented so as not to disturb the intensity null established before insertion of the flat. Existence of rapid changes in the He-Ne intensity so observed with variation in azimuthal angle of the flat introduced uncertainty as to whether correct orientation had been achieved for passage of P-polarized radiation of all wavelengths without de-polarization, which would lead to transmission loss in subsequent passes. The desired condition is, of course, that of propagating the polarized beam as either an ordinary or extra-ordinary wave in the sapphire.

The polarized 1P(2) line from the HF probe laser was used to check transmission losses of the Brewster flat in the configuration used for laser measurements of section III. The measured transmission loss was ~1% with a confidence level of ~3%. Subsequent changes in azimuthal orientation showed well-behaved variation of transmission with orientation, the losses increasing to 15-20%/pass at 45° from the correct azimuthal orientation.

Similar measurements were made for a second sapphire flat (used for measurements of sections IV and V) of improved optical quality and coated for high reflectivity of S-polarized 3471 Å radiation at 60° incidence angle. Transmission losses were found to be negligibly small in the vicinity of the correct orientation, although complex lobular loss patterns were observed for large changes in azimuthal angle. Therefore, proper orientation of sapphire Brewster flats is quite important for reducing transmission loss, and the use of polarized laser light in the visible as described above provides a convenient technique for correct orientation.

The reactor end-windows consist of (60°) sapphire substrates AR coated with MgF_2 for nominal reflectance of 2%/surface or less in the 2.5-3μ wavelength region. Unsatisfactory vendor documentation of transmission properties of an initial set of windows, used for laser transient measurements of section III, motivated an improved definition of transmission utilizing a Cary Model 14 broadband spectrophotometer and the

2.58μ 1P(2) probe laser line. These windows exhibit a broadband loss varying from 7 1/2 - 16% over the 2.5-3 micron wavelength interval, thus indicating possible two-surface interference losses in the range 0-15% at 2.5 microns and 0-32% at 3 microns. The narrow-band (probe line) loss for this window is 12 ± 2% at 2.58 microns. The polarized HF probe beam and a Brewster flat in tandem with the reactor window were used to confirm that correct azimuthal orientation ($\phi = 0$) of the window for transmission of plane polarized radiation had been used for previous measurements.

A second set of end-windows used for spectroscopic measurements of sections IV and V exhibit 2 1/2 - 4 1/2% broadband losses over the 2.5-3 micron interval. The narrow probe line shows no measurable loss at normal incidence at 2.58 microns (confidence level of measurement ±2%). A scan of probe beam attenuation over a complete free-spectral-range of optical path (achieved by tilting the window) was indicative of the periodic variation expected for two-surface interference, but the ±2% confidence level precludes a definitive conclusion on this point. The polarized probe beam and tandem Brewster flat were used, as above, to establish that de-polarization losses of the end-windows are negligibly small near the correct orientation $\phi = 0$ (for purposes of comparison, such losses increase to ~30% at $\phi = \pm 45°$). These end-windows were installed in the reactor at $\phi = 0$, and with opposing 8×10^{-3} rad angles of incidence to preclude mutual interference effects.

Under the conservative assumption that the 2 1/2 - 4 1/2% broadband loss of the reactor end-windows used for measurements of sections IV and V corresponds to an averaged two-surface interference loss in the range 0 - 5% at 2.5 microns and 0 - 9% at 3 microns, the uncertainty in threshold gain, $G = -\frac{1}{2L} \times \ln \prod R_i T_j \simeq .022/cm$, is ~5% at 2.6 microns and ~30% at 3 microns for a cavity configuration $R_1 = 1$, $R_2 = .3$ (70% output coupler), $\prod T_j = T^4$ where T is the individual window transmission/pass. The higher loss end-windows used for measurements of section III along with small output coupling (1/2 mm hole coupler) correspond to considerably larger uncertainty in threshold gain.

D. CW Laser - Flame Radiation Source

1. State Concentrations from Transient Line-Strength Measurements

Time-resolved spectroscopic measurements of pulsed laser emission described in sections IIB and IV/V provide a useful diagnostic tool for defining underlying kinetics processes. However, associated time-evolution of specific vibration-rotation state populations cannot be directly determined from such measurements. Absorption-gain measurements in the reacting media utilizing an appropriate probe laser operating at a fixed frequency ν_1 provides a direct measure of concentration difference only if the line shape of corresponding transitions in the reacting media and the probe frequency ν_1 are accurately known. Consequently, this latter technique is also inappropriate for direct concentration measurements in pulsed chemical laser applications since the transient pressure and temperature, and hence the line shape, are usually not known.

Capability of direct measurement of line strength S would give concentration differences via the relation,

$$S = \frac{\lambda_o^2}{8\pi c} A_{21} \left(N_1 - g_{1/g_2} N_2\right) \qquad (1)$$

where the line strength is defined as the wave number integral of the absorption/gain coefficient for the transition of interest, i.e., $S = \int k_\nu \, d\nu$, and where N_2/N_1 are the desired upper/lower state concentrations, λ_o the line-center wavelength, A_{21} the Einstein spontaneous emission coefficient for the transition, and g_i the appropriate statistical weights.

Direct measurement of S can be accomplished in certain cases by utilizing a radiation source with near constant intensity I_o/unit wavenumber over the line width $\Delta\nu_A$ of the absorption/gain media, and by restricting to a moderate optical thickness of absorption/gain media, i.e., by requiring $k_\nu L << 1$ where L is the physical path. Under these conditions, $I_\nu/I_o = \exp(-k_\nu L) \simeq 1 - k_\nu L$, which upon integration over the emission band yields the desired relation for S:

$$S \simeq \frac{\Delta\nu_E}{L}\left(1 - \frac{P_{(L)}}{P(0)}\right) \tag{2}$$

where $P(0) = \int_{\Delta\nu_E} I_o d\nu$ is the power at a receiver in the absence of absorption/gain media, $P_{(L)} = \int_{\Delta\nu_E} I_\nu d_\nu$ is the corresponding received power with absorption/gain media present, and $\Delta\nu_E$ is the bandwidth of the probe radiation. As anticipated, equation (2) does not explicitly contain properties of the unknown absorption/gain profile.

An estimate of the error due to finite optical path (FOP) is readily developed by retaining the second order term in the expansion of I_ν/I_o in the derivation of equation (2) and is given by:

$$\Delta S/S\Big|_{FOP} \simeq \frac{1}{2}\,\frac{S}{\Delta\nu_A} \equiv \frac{L\langle k_\nu\rangle}{2} \tag{3}$$

Thus the estimated FOP error is given by the known L, measured S, and estimated $\Delta\nu_A$ (which provide an estimate of the average absorption coefficient $\langle k_\nu \rangle$). For properly chosen optical path, accurate knowledge of $\Delta\nu_A$ is not required for application of equation (2) with good confidence level.

The error due to variation of intensity in the emission profile is developed by noting

$$P_{(L)} = P_{(0)} - \int_{\Delta\nu_A}\left[1 - \exp\,(-k_\nu L)\right] I_o\, d\nu$$

$$\simeq P_{(0)} - L\int_{\Delta\nu_A} k_\nu\, I_o\, d\nu \tag{3'}$$

which with equation (2) yields:

$$S \simeq \frac{\Delta\nu_E}{P(0)} \int_{\Delta\nu_A} k_\nu\, I_o\, d\nu$$

or

$$\Delta S \simeq \frac{\Delta\nu_E}{P(0)} \int_{\Delta\nu_A} k_\nu \, \Delta I_o d\nu$$

Introducing the averaged variation of incident intensity over the absorption gain profile,

$$\langle \Delta I_o \rangle_A \equiv \frac{\int_{\Delta\nu_A} k_\nu \Delta I_o d\nu}{\int_{\Delta\nu_A} k_\nu \, d\nu \equiv S}$$

and a similar averaged intensity over the emission profile, $\langle I_o \rangle_E \equiv \int_{\Delta\nu_E} I_o d\nu/\Delta\nu_E = P(0)/\Delta\nu_E$ gives the variation in measured S due to variation of emission intensity as:

$$\Delta S/S \Big|_{\Delta I_o} \simeq \langle \Delta I_o \rangle_A / \langle I_o \rangle_E \qquad (4)$$

This error relation is readily expressed in terms of bandwidth ratio for typical cases of interest by comparison of Doppler emission and absorption/gain profiles, i.e., $I_o \sim \exp - [2\ (\ln 2)^{1/2}\ (\nu - \nu_o)/\Delta\nu_E]^2$, $k_\nu \sim \exp - [2\ (\ln 2)^{1/2}\ (\nu - \nu_o)/\Delta\nu_A]^2$, $\Delta\nu_E >> \Delta\nu_A$, to obtain

$$\Delta S/S \Big|_{\Delta I_o} \simeq .8 \left(\frac{\Delta\nu_A}{\Delta\nu_E}\right)^2 ; \ \frac{\Delta\nu_A}{\Delta\nu_E} << 1 \qquad (4')$$

To summarize, equations (2), (3), and (4)/(4') imply a set of interrelated constraints for accurate experimental determination of line strength. Equations (4)/(4') require an emission profile considerably broader than the absorption/gain profile. Equation (3) requires that the average attenuation over the absorption/gain profile be small. Using equation (3') to express the normalized difference in received power in terms of the bandwidth ratio and average absorption/gain coefficient, and imposing the constraints $\Delta S/S \Big|_{FOP}$, $\Delta S/S \Big|_{\Delta I_o} \sim .1 - .2$ yields:

$$\left[P_{(0)} - P_{(L)}\right] \Big/ P_{(0)} \simeq \frac{\Delta\nu_A}{\Delta\nu_E} \times L \times \langle k_\nu \rangle \simeq .4 \times .2$$

Thus P(L)/P(0) ≃ .9 which with equation (2) implies that ±2% reliability in determination of P(0) and P(L) would be required for determination of S with ±20% reliability. These constraints can be relaxed by use of a high resolution spectrograph in combination with a relatively broad emission bandwidth, but with additional experimental difficulty.

2. Desired Properties of a Flame Emission Source

Provided that adequate intensity can be achieved, line shapes for emission from $H_2 - F_2$ flames have ideal characteristics for direct line strength measurements. Spectroscopic studies of such flames have been reported by Mann et al. (Ref. 21) and Benedict et al. (Ref. 22). In the latter case flame emission on a number of transitions in both 1-0 and 2-1 bands was observed in the temperature range 2700 - 5300°K at pressures of 1-5 atm. Corresponding Doppler widths are of the order .03 - .05 cm^{-1} and typical Lorentz widths (see section II-C2) are expected in the range,

$$\Delta\nu_L = \left(\frac{300}{T°K}\right)^{1/2} \times .1 \times P_{(atm)} \qquad (5)$$

$$\simeq .025 - .12 \text{ cm}^{-1}$$

These line widths are in the appropriate range to satisfy requirements for line strength measurements established in the preceding paragraphs. In the studies referenced above, the emission intensities were not adequately high for use in transient measurements, i.e., time-integration of modulated emission was required for adequate signal-to-noise ratio. As noted in sections II-D4 and VI, however, CW chemical laser technology provides the base for considerable improvement in flame sources relative to the simple concentric-tube burners used in the investigations above.

3. Line Width Constraints of a Low-Q Resonator

The possibility of utilizing a low-Q resonator configuration for increasing the emission intensity from inverted HF pumped by chain reactions in H_2 - F_2 mixtures, while retaining a reasonably broad emission profile, has been investigated. A condition to be imposed on such a resonator configuration is that the variation of cavity 'Q' over a free spectral range of frequency shall not be large, i.e., the usual constraint of high-Q cavities characterized by a discrete set of frequencies at which lasing occurs would have to be relaxed. The desired resonator behavior can be treated in a semi-quantitative manner by considering the radiation intensity transmitted through a plane mirror of reflectivity $\tilde{R}$ due to a source of coherent radiation of wave number ν contained between this mirror and a parallel total reflector. The ratio of transmitted to source intensity is found by summing the transmitted amplitudes associated with internal reflected waves and is given by:

$$\eta = \frac{t^2}{(1-\rho)^2}\left[1 - \frac{4\rho}{(1-\rho)^2}\sin^2\sigma\right]^{-1}$$

where $\rho = R^{1/2}$, t is the amplitude transmission coefficient of the transmitting mirror, and $\sigma = 2\pi D\nu$ is the usual phase factor for normal incidence radiation and mirror separation D. The bracketed phase function above corresponds identically to the expression for transmission through a symmetric two-surface interferometer of reflectivity $\tilde{R} = \rho$. For $R \ll 1$, the maximum variation in transmitted intensity with wave number is:

$$\frac{\Delta\eta}{\eta_{max}} \simeq 4\,R^{1/2} \qquad (6)$$

Due to the $R^{1/2}$ dependence, the mirror reflectivity must be extremely low to achieve modest variation of effective Q with ν, e.g., $\Delta\eta/\eta_{max} = .1 - .2$ implies R - .06% - .25%. Thus, adequate gain/pass to operate with nearly 100% output coupling must be achieved before broad-line resonator operation would be feasible.

4. Device Considerations

A small HF laser-flame apparatus was built and characterized under this program with the view of assessing feasibility for line strength measurements in pulsed chemical laser applications. The device is described here and results of characterization studies are reported in section VI. The basic requirements for maximum flame emission intensity and for low-Q laser operation are similar in some respects, e.g., rapid mixing and reaction to maximize excited HF* concentrations with adequate flow speed to provide high emission intensity over an extended volume are required.

In order to minimize development effort and uncertainity, a subsonic mixer-reactor device based on the pioneering work of Cool and coworkers (Ref. 23) was chosen. Although preliminary consideration was given to discharge dissociation of F_2 for initiation of reaction, dissociation by the NO + F_2 reaction, again pioneered by Cool, was chosen since capability of establishing a wide range of dissociation fraction $[F]/[F_2]$ can be provided. For example, numerical solution of the associated rate equations,

$$\frac{d[F_2]}{dt} = -k_1 [NO] [F_2] \tag{7}$$

$$\frac{d[F]}{dt} = k_1 [NO] [F_2] - k_2 [M][NO][F]$$

for typical [He] and [NO] third body concentrations, and based on the recent rate measurements of Kim et al. (Ref. 24), show that dissociation levels $[F]/[F_2]$ = .01 - .2 can be achieved for $[NO]/[F_2]$ = .01 - .5.

An overview photograph of the device is shown by Fig. 5 and a detail of the H_2 injector and reactor by Fig. 6 (the injector details are exposed by removing the channel cover and by separating internal plates used to maintain constant channel height through the injector region). The option of injecting diluent at the upstream end of a 1.25 x 14.8 cm premixer channel (lower left corner Fig. 5) is provided, F_2 is injected through a linear array of 60 equally spaced orifices located

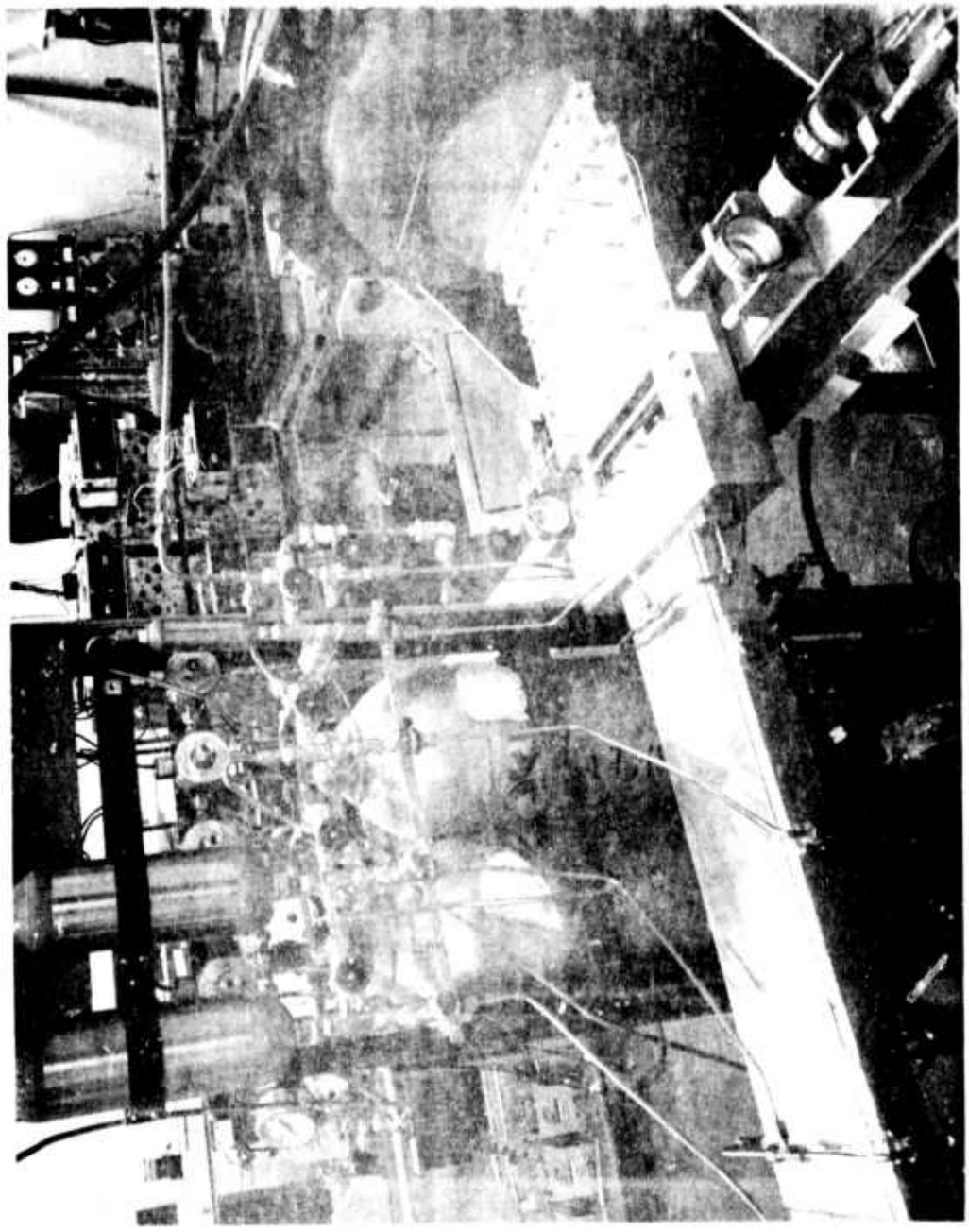

FIGURE 5. CW LASER–FLAME APPARATUS

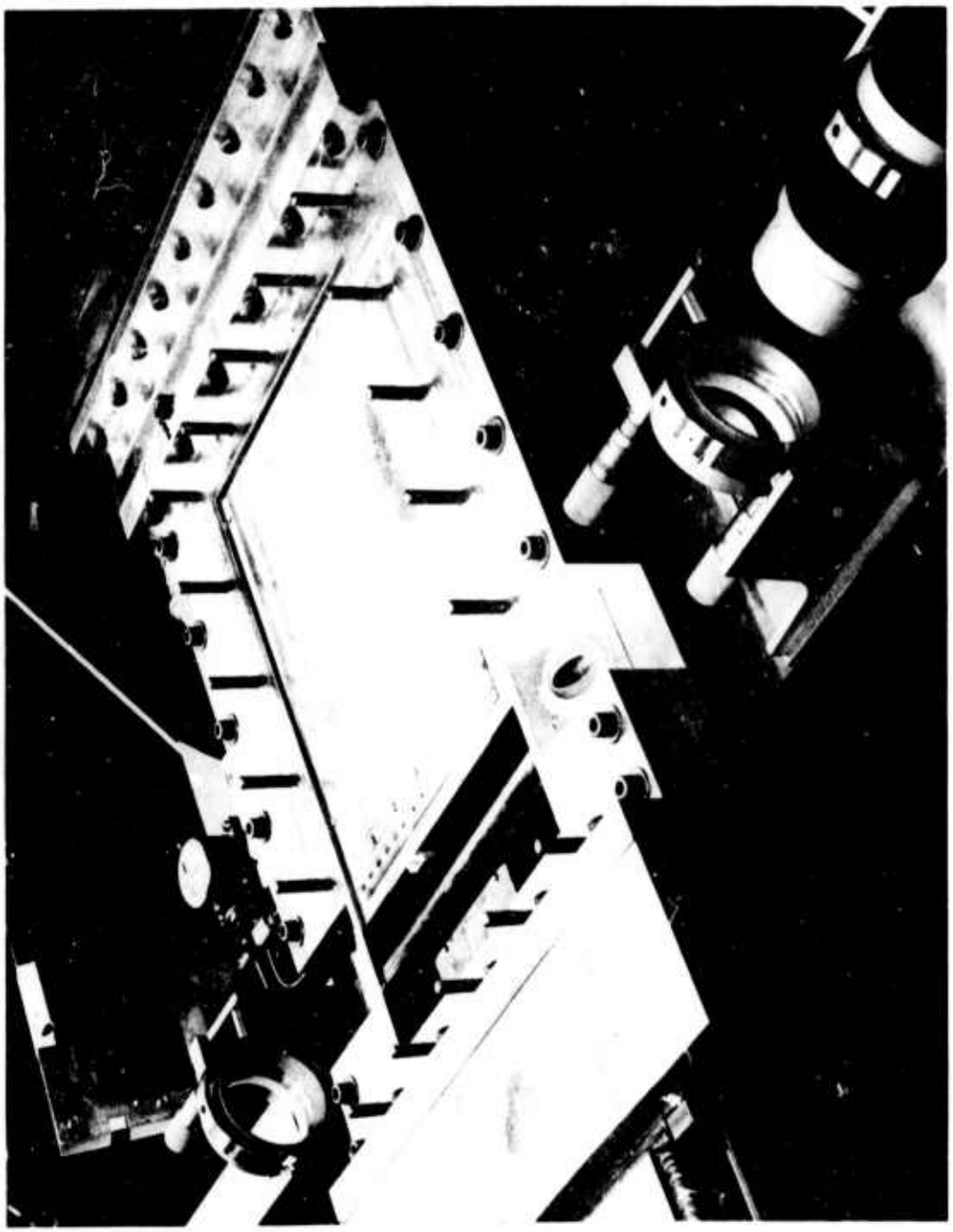

FIGURE 6. CW LASER–FLAME APPARATUS WITH H_2 INJECTOR DETAIL

~80 cm upstream from the H_2 injector. NO is introduced through a similar array at a point ~50 cm upstream from the H_2 injector. With nominal operation at M = .5 in typical He - F_2 mixtures at 5 - 10 torr pressure levels, the latter distance provides adequate transit time for diffusive mixing of NO through the F_2 - bearing stream, and for the NO + F_2 dissociation reaction to proceed. The streamwise position of the H_2 injector is adjustable over a distance 0-5 cm upstream from the transverse optical axis. Two H_2 injectors were built, the first (Injector I) consists of 59 .107 cm OD stainless steel tubes each equipped with 11 transverse injector orifices ~.02 cm in diameter and arranged in a staggered 6-5 configuration (vertical spacing of H_2 injection points of .079 cm over an 8 mm height). The second (Injector II) is similar to the one described above except that the injector tubes are unobscured when viewed along the optical axis, each injector tube has 9 injector orifices ~.01 cm diameter arranged in a 5-4 configuration, and extending over a 6.5 mm height (the latter is adequate for providing a series of H_2 streams that cover typical TEM_{oo} mode diameters for small scale stable laser resonators). The channel sidewalls are parallel to the external surfaces that position NaCl Brewster flats, and the upstream flow passes outside the H_2 injectors, thus shielding the small window wells from deactivated HF. Reagent and diluent gases are supplied through fast acting solenoid valves in series with needle metering valves, and the system is 'pumped' by a 360 liter ballast chamber through a sonic slot. This arrangement provides capability for maintaining steady-state flow condition for ~.25 sec (equivalent to 1-2 x 10^3 liters/sec pumping speeds) at any desired pressure level. The latter feature is quite important for this application since population inversion for CW lasers operation can be maintained only at low pressure (5-10 torr), whereas capability for operation at somewhat higher pressure was desired for optimization studies of flame emission characteristics.

SECTION III

VARIATION OF [HF] LASER INTENSITY TRANSIENTS WITH DISSOCIATION LEVEL AND REAGENT/DILUENT CONCENTRATIONS

A quantitative description of HF-laser transients including laser initiation time-delay, pulse duration, relative energy/pulse, and peak intensity as functions of 2ν - light level ($[F]/[F_2]$ in the range 1/3 - 3/4%) are reported below for nominal chemical configurations: $[F_2]:[H_2]:[N_2]$ = 4:4:40 torr, 4:4:80 torr, 8:8:40 torr, and 8:8:80 torr. (The concentration ratios are correct as stated, the total pressure is slightly less than the nominal value.) A principal feature of all observed transients is the existence of high intensity 'precursor' pulses of extremely short time duration (25-150 nanoseconds) followed by low level transients of extended duration (1 - 30 microseconds). Total intensity measurements obtained with the hole-coupled resonator configuration described previously are reported in this section, and detailed spectroscopic measurements obtained with a partially transmitting mirror are reported in the following two sections.

These data exhibit qualitatively correct trends of pulse initiation times with variation of 2ν - light level and $[F_2]/[H_2]$ concentrations. Evidence presented below shows that the first precursor pulse is associated with disappearance of initial [F] via the 'cold' reaction, $F + H_2 \rightarrow HF^* + H$, and that the second pulse, when it appears, is governed by processes for which the 'hot' $H + F_2$ reaction is the rate limiting step. Existence of high intensity precursor pulses is attributed in part to the fast 'cold' reaction rate in the initial step, and in part to unsteady resonator processes. These intensities are contrasted to the low-level, long-term transient which must depend on complete chain propagation.

A series of aperturing measurements indicate that the observed transients are mainly representative of oscillation in the TEM_{oo} mode. A few measurements with 15% and 70% transmitting mirrors show the same time structure as those with the hole-coupled output mirror, but with increased intensity.

Oscillograms illustrating typical precursor and long-term structure are shown by Fig. 7. Although the temporal structure is quite complex, it is to be emphasized that the main features are reproducible and characteristic of all measurements reported here. Corresponding nomenclature used to characterize the laser transient is shown by Fig. 8. Fig. 9 shows the observed variation of properties of the laser transient with 2ν light intensity for $[F_2]:[H_2]:[N_2]$ = 3.7:3.7:37 torr. Similar data are shown by Fig. 10 for 3.7:3.7:74 torr, by Fig. 11 for 7:7:35 torr, and by Fig. 12 for 7.5:7.5:75 torr. The quantity $E_{2\nu}$ represents energy of second harmonic (2ν) ruby light transmitted through the reactor in millijoules as determined by the method described in subsection II-A1.* The intensity data of Figs. 9-12 is given in terms of voltage across a 25 ohm load in series with a Raytheon Ge:Au detector and having an estimated responsivity of .25 volts/watt.

It is important to note that certain features of the intensity transients are well behaved and others are less so, or ambiguous. Specifically, the initiation times, τ_1 and τ_2, the intensity-time products (relative energy), ε_1 and ε_2, and to slightly less degree the pulse FWHM, $\Delta\tau_1$ and $\Delta\tau_2$, are well behaved. Total pulse duration, $\Delta\tau_{TOTAL}$, and total intensity-time product, ε_T, are difficult to determine without

---

* For the measured attenuation factor 1.29 of the reactor end-windows at 3471 Å (the windows are AR coated for infrared only), we have $[F]/[F_2] = 2N_{ph} \times \sigma/A_{2\nu} = 1.29 \times E_{2\nu} \times K \times (1 + \eta)$, where $K = 2\ \sigma/\varepsilon_{ph}\ A_{2\nu} = 6.96 \times 10^{-5}$/millijoule. N_{ph} is the total number of 2ν photons passing through the cell, σ the photo dissociation cross section (subsection II-A1), $A_{2\nu}$ the 2ν beam cross section, ε_{ph} the average 2ν photon energy, and η is the probability of second passage of a 2ν photon through the reactor due to reflection by the laser end-mirror ($R \simeq 100\%$). Since we do not know the reflectance/absorptance ratio of the end-windows, we have $.6 \leq \eta \leq 1.0$. Taking $\eta = .8$, $[F_1]/[F_2] = (1.60 \pm .167) \times 10^{-4} \times E_{2\nu}$ (millijoules).

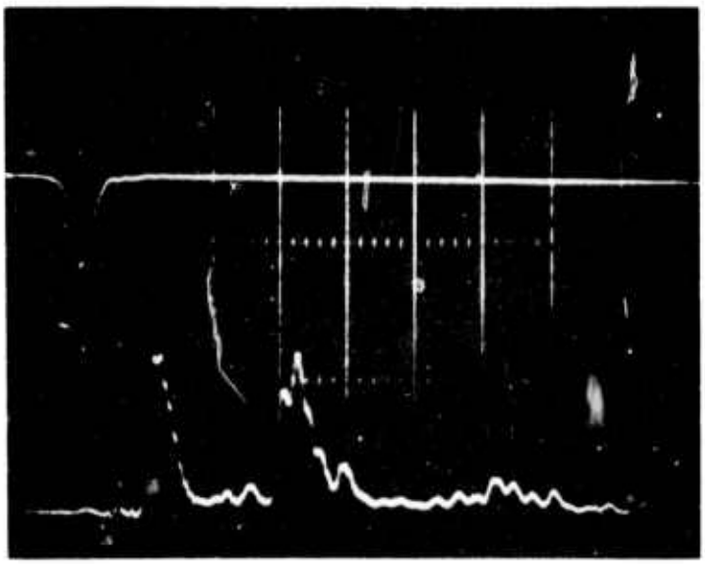

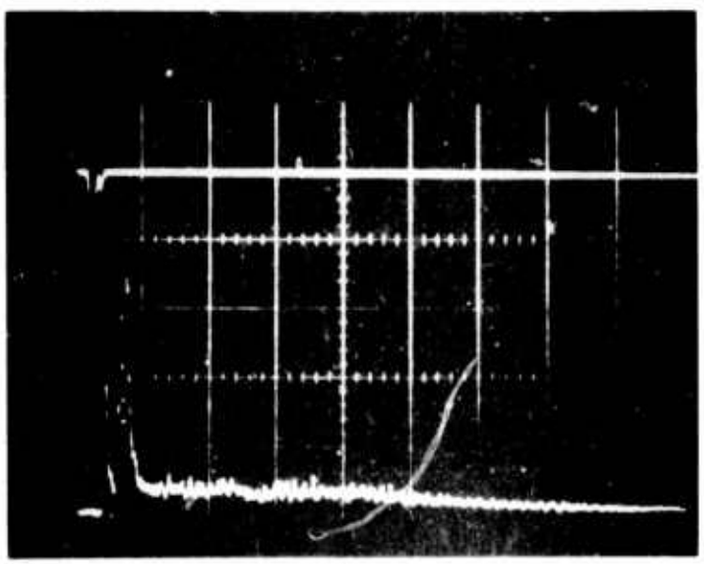

FIGURE 7. HF LASER TRANSIENT FOR $F_2 : H_2 : N_2$ = 3.7 : 3.7 : 74 TORR

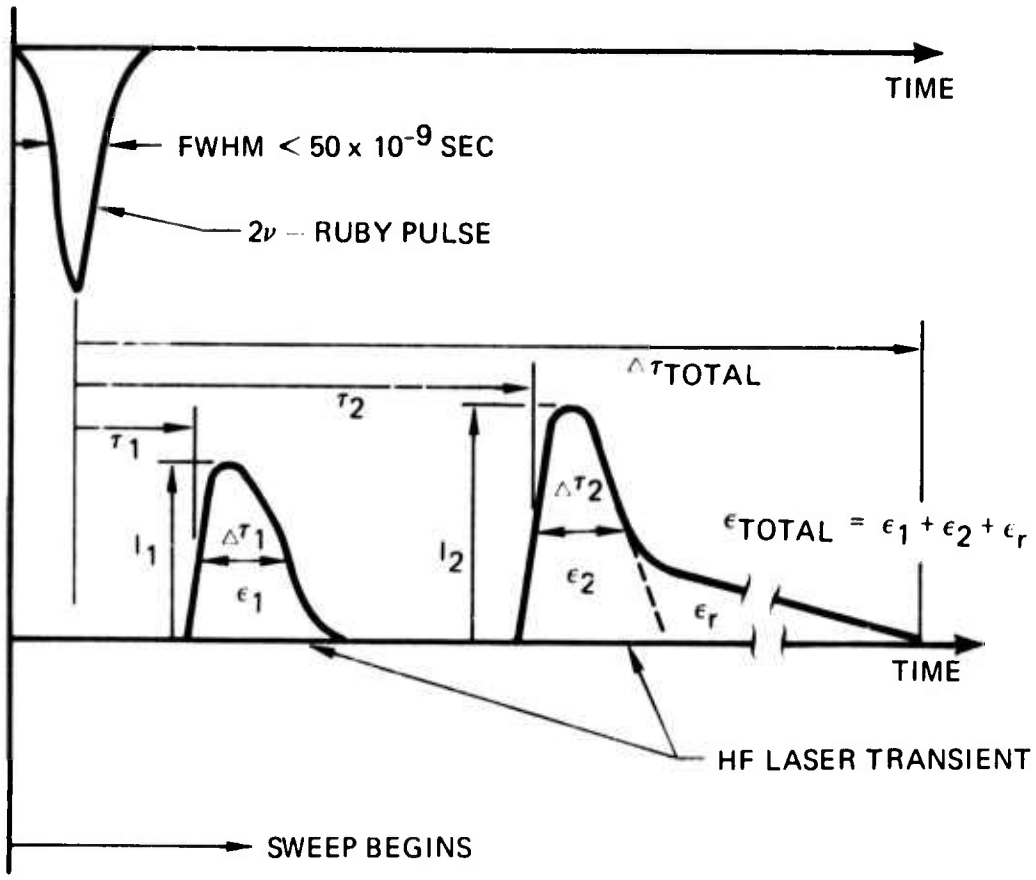

FIGURE 8. NOMENCLATURE FOR HF LASER TRANSIENT

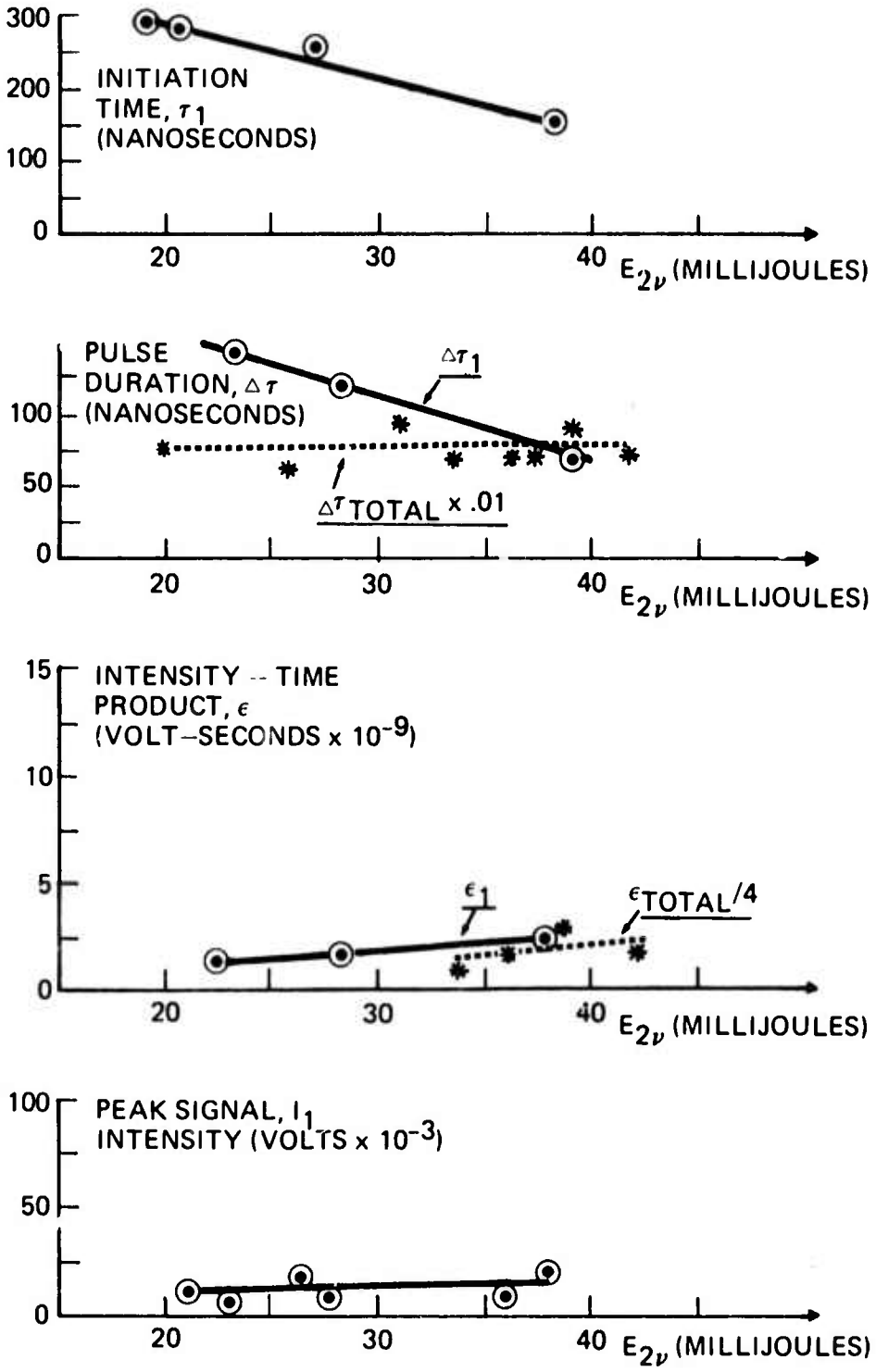

FIGURE 9. HF LASER TRANSIENT PROPERTIES FOR $F_2 : H_2 : N_2 = 3.7 : 3.7 : 37$ TORR

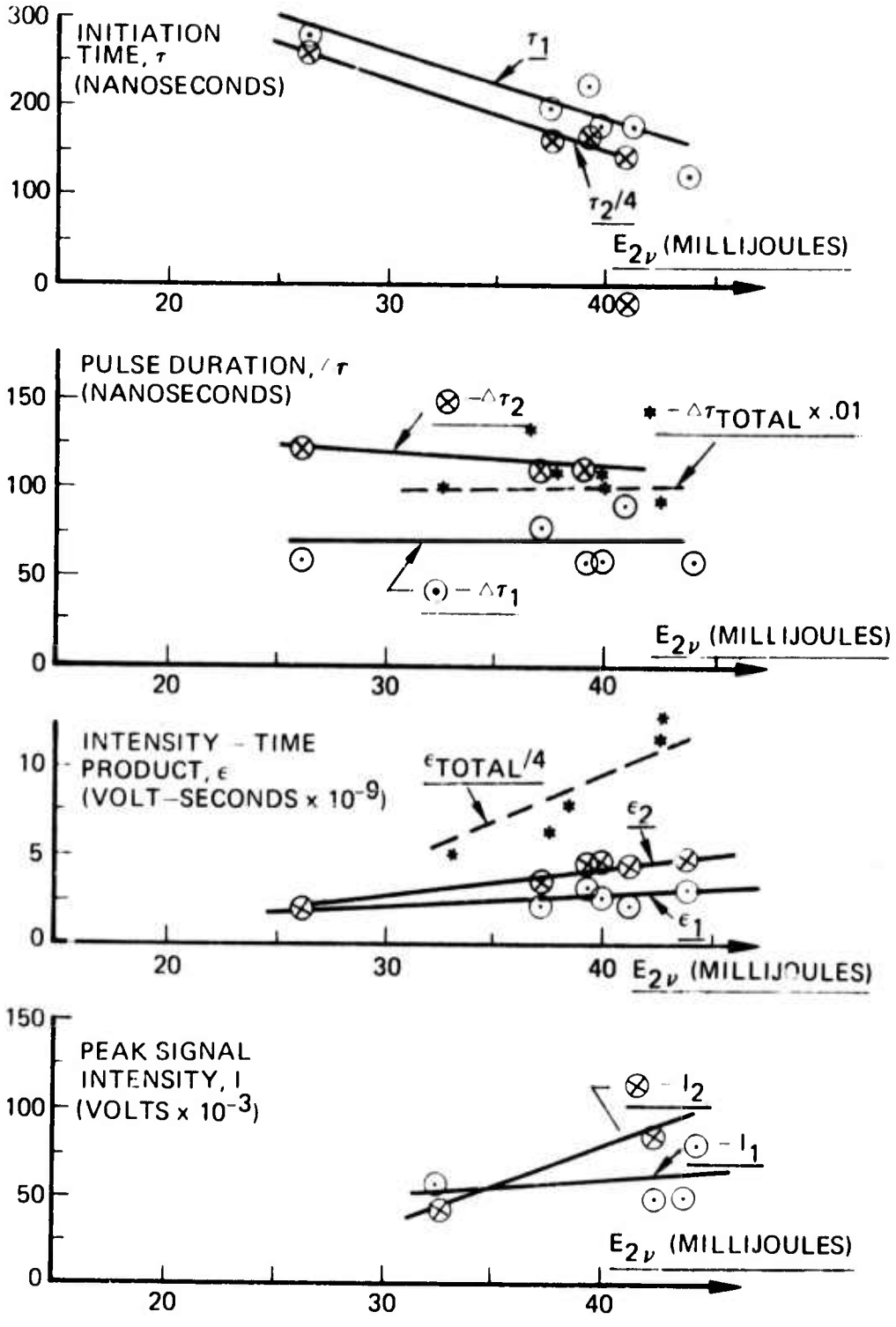

FIGURE 10. HF LASER TRANSIENT PROPERTIES FOR $F_2 : H_2 : N_2 = 3.7 : 3.7 : 74$ TORR

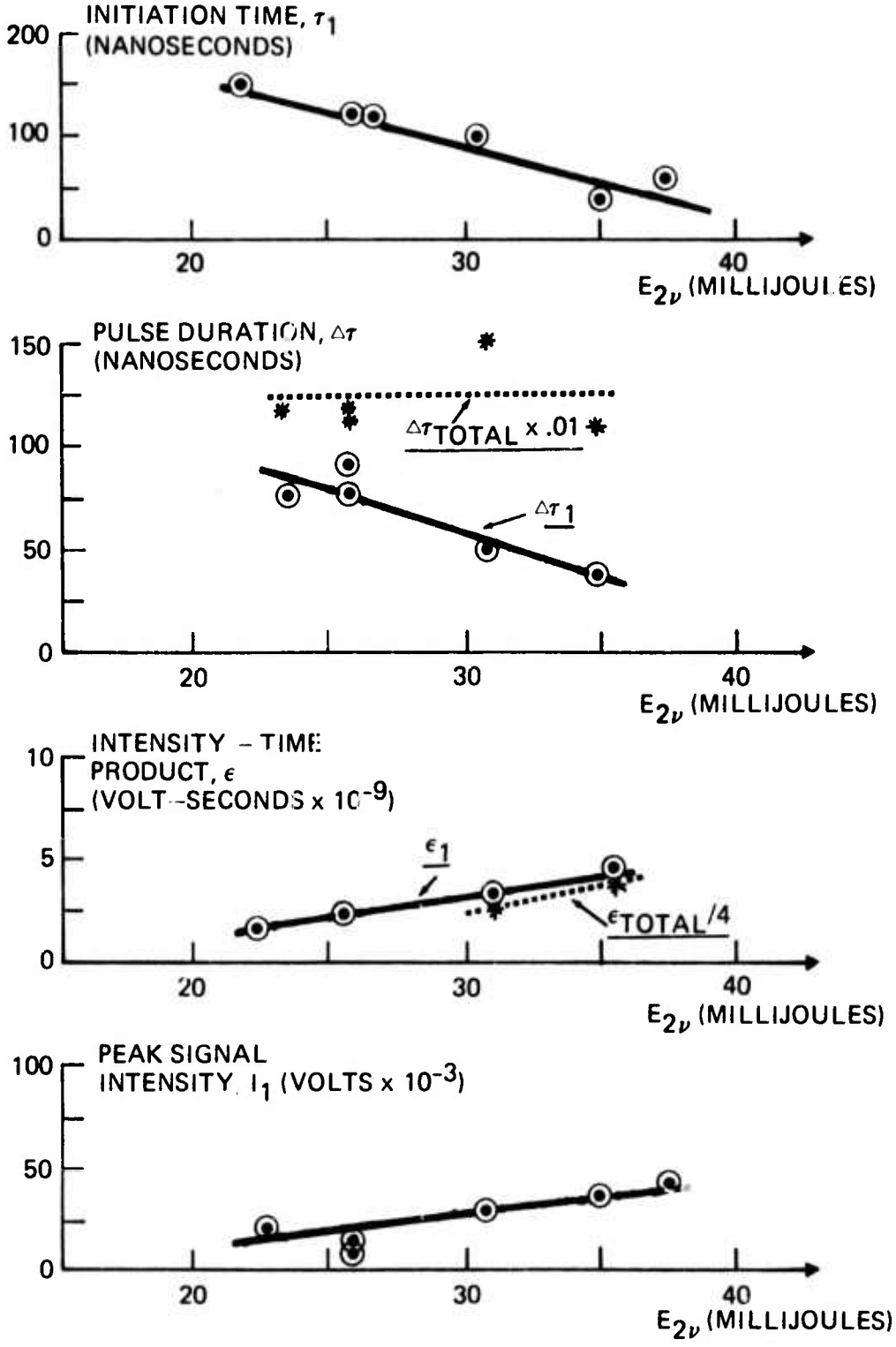

FIGURE 11. HF LASER TRANSIENT PROPERTIES FOR $F_2 : H_2 : N_2 = 7 : 7 : 35$ TORR

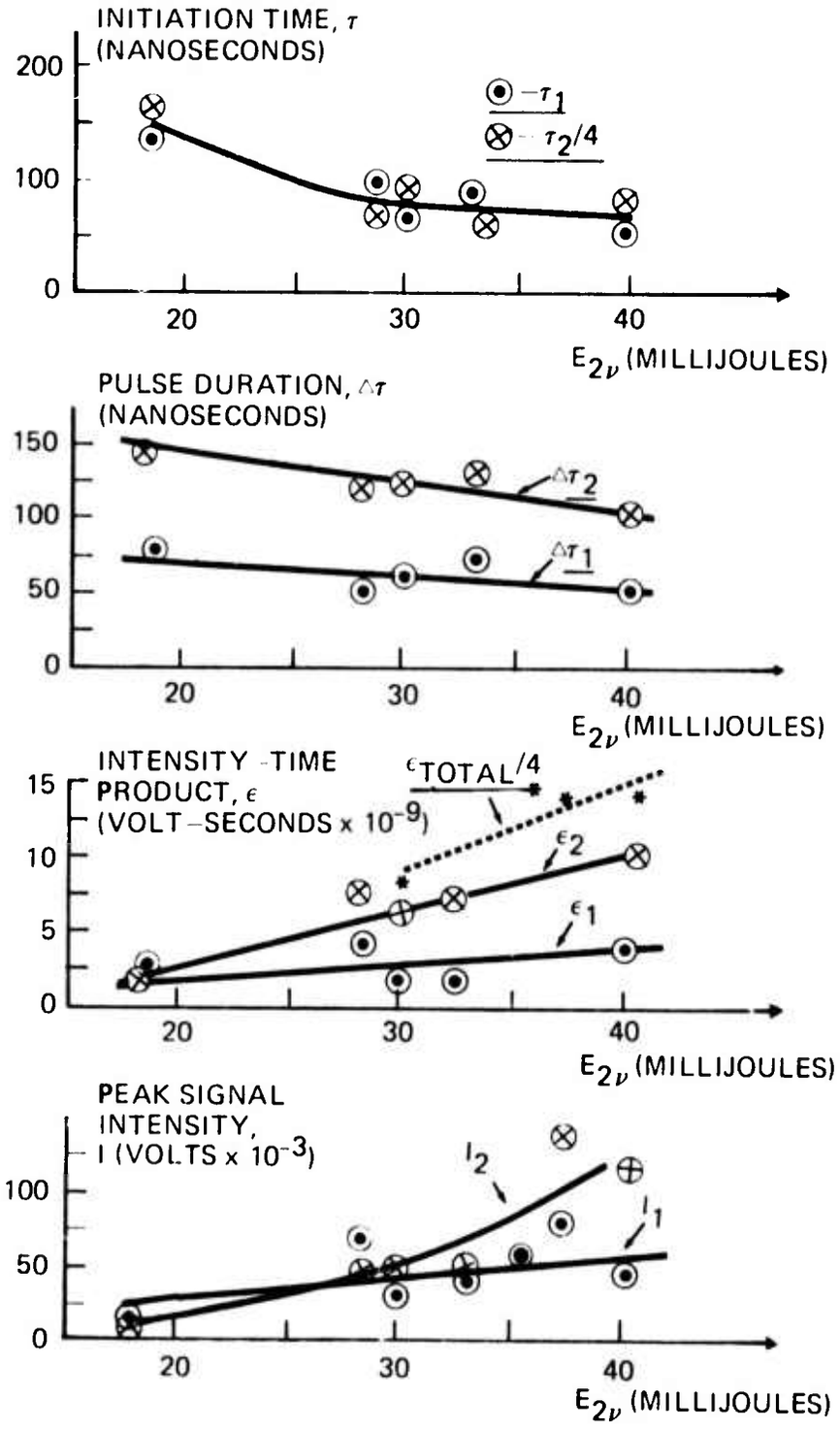

FIGURE 12. HF LASER TRANSIENT PROPERTIES FOR $F_2 : H_2 : N_2 = 7.5 : 7.5 : 75$ TORR

ambiguity. Due apparently to phase variation of high frequency oscillations (which we associate with transverse mode beating) relative to time of peak intensity, precursor peak intensities, I_1 and I_2, show somewhat larger scatter than the corresponding ε_1 and ε_2.

The data for 35/37 torr N_2 (Figs. 9 and 11) exhibit a single precursor peak, whereas those for 74/75 torr N_2 (Figs. 10 and 12) exhibit two peaks. Similar data for 160 torr N_2 (not shown) exhibit double pulse structure for all reagent concentrations considered*. Increase of H_2/F_2 partial pressures by a factor of two (compare Figs. 9 and 11 or 10 and 12) reduces the pulse initiation times by a factor of two or more, as does a factor of two increases in $E_{2\nu}$. This is expected since the number of propagating chains is doubled in both cases and the rate of propagation also increases at increased reactant pressure. Increase of N_2 pressure by a factor of two has no significant effect on initiation time (compare Figs. 9 and 10 or 11 and 12). This is also expected since excess moderator should be unimportant in the initial stages of reaction (i.e., significant temperature rise has not yet occurred and HF deactivation by N_2 is not significant on this time scale). Pulse FWHM tends to shorten with increasing reagent pressure, although the effect is less straightforward, particularly in the double pulse cases. Both pulse and total energy content increase with H_2/F_2 pressure (compare Figs. 9 and 11 or 10 and 12), but the most dramatic increase is associated with increased N_2 pressure (results of premixer cooling reported in the following section suggest this effect may be due to suppressed formation

* Data obtained for concentration ratios 1:1:40, 1:1:20, and 1:1:10 at a total pressure of 160 torr are qualitatively consistent with results reported here. All data presented in this section correspond to an ambient temperature premixer fabricated from glass tubing. Due to evidence of prereaction for the 160 torr pressure (no such indications occurred for the 40-80 torr cases reported here), a more conservatively designed premixer was installed and ground state [HF] concentrations were monitored for measurements reported in subsequent sections.

of initial HF due to prereaction). Note that in all cases, the precursor energy content is $\simeq$ 25% of the total even though the corresponding time duration is 1/2 - 1% of the total. Peak intensity variations tend to track changes in energy content, although as noted above, with increased scatter.

Although a complete description of the reaction-deactivation system associated with HF lasers pumped by H_2 - F_2 chain reactions requires simultaneous solution of a large number of rate equations, a partial interpretation of the data reported here can be developed on a much simpler base. Consumption of initial [F] generated by 2ν - photolysis, which underlies initial generation of excited HF*, proceeds via the reaction:

$$\frac{d[F]}{dt} = -k_4 [F] [H_2]_o \tag{8}$$

where k_4 is the 'cold' reaction rate constant and $[H_2]_o$ is the initial hydrogen concentration. H produced by the above reaction is consumed according to:

$$\frac{d[H]}{dt} = -k_5 [H] [F_2] \tag{9}$$

where k_5 is the 'hot' reaction rate constant and, for time-ranges associated with precursor processes, $[F_2]$ can be taken as the initial fluorine concentration. For initial times then, populations of individual vibrational levels are generated by sub-reactions of the two types described by (8) and (9) with e-fold times at T = 300°K given by:

$$\begin{aligned} \tau_{C(\mu\text{-sec})} &= 1.7/P_{H_2(\text{torr})} \\ \tau_{H(\mu\text{-sec})} &= 8/P_{F_2(\text{torr})} \end{aligned} \tag{10}$$

The above relations are developed on the basis of rate data obtained by Homann and Albright and compiled by N Cohen (Ref. 25).

Fig. 13 displays times of initial pulse termination (defined as initiation time plus FWHM) of the first precursor pulse for the conditions noted above. The 'cold' reaction e-fold time from equation (10) is displayed as dashed lines in Fig. 13. Two facts immediately apparent from Fig. 13 are: 1) a factor of two change in $[N_2]$ has little effect on pulse termination time although some reproducible differences for rich and lean mixtures are apparent, and 2) first pulse termination occurs before complete consumption of initial [F] and before the 'hot' reaction has reached maximum production rate. It is important to note also that Figs. 10 and 12 show τ_1 and τ_2, the initiation times of the first and second precursor pulses to be in the ratio

$$\tau_2/\tau_1 \simeq 4$$

over a 4-6 fold variation of τ_1 and τ_2 resulting from variation of $E_{2\nu}$ and/or reagent partial pressure. The time of first pulse termination relative to τ_C and τ_H ($>> \tau_C$) indicates the first precursor pulse results from 'cold' reaction processes (data at pressures up to 16:16:160 torr also agree with this observation). The fact that the initial [F] has been consumed before initiation of the second pulse, and close coincidence between the ratio τ_2/τ_1 and τ_H/τ_C (k_4/k_5) over a wide range of initiation times, implies the second precursor pulse results from processes that are rate-limited by the 'hot' reaction. One may note in passing that Jacobson and Kimbell (Ref. 26) have identified similar precursor pulses sequences with a 2P(5) - 3P(4) cascade process. A simple cascade process of this type is not supported by the present observations since quiescent periods exist between first and second precursors at low pressure.

The decreasing first pulse termination time relative to the 'cold' reaction e-fold time with increasing $E_{2\nu}$ (stronger reaction), and the fact that the low level long-term transient is contiguous with second pulse termination provide evidence that pulse termination is not a direct consequence of a rapid decrease in HF production. In any event, no chemical process is adequately rapid to correspond to the termination

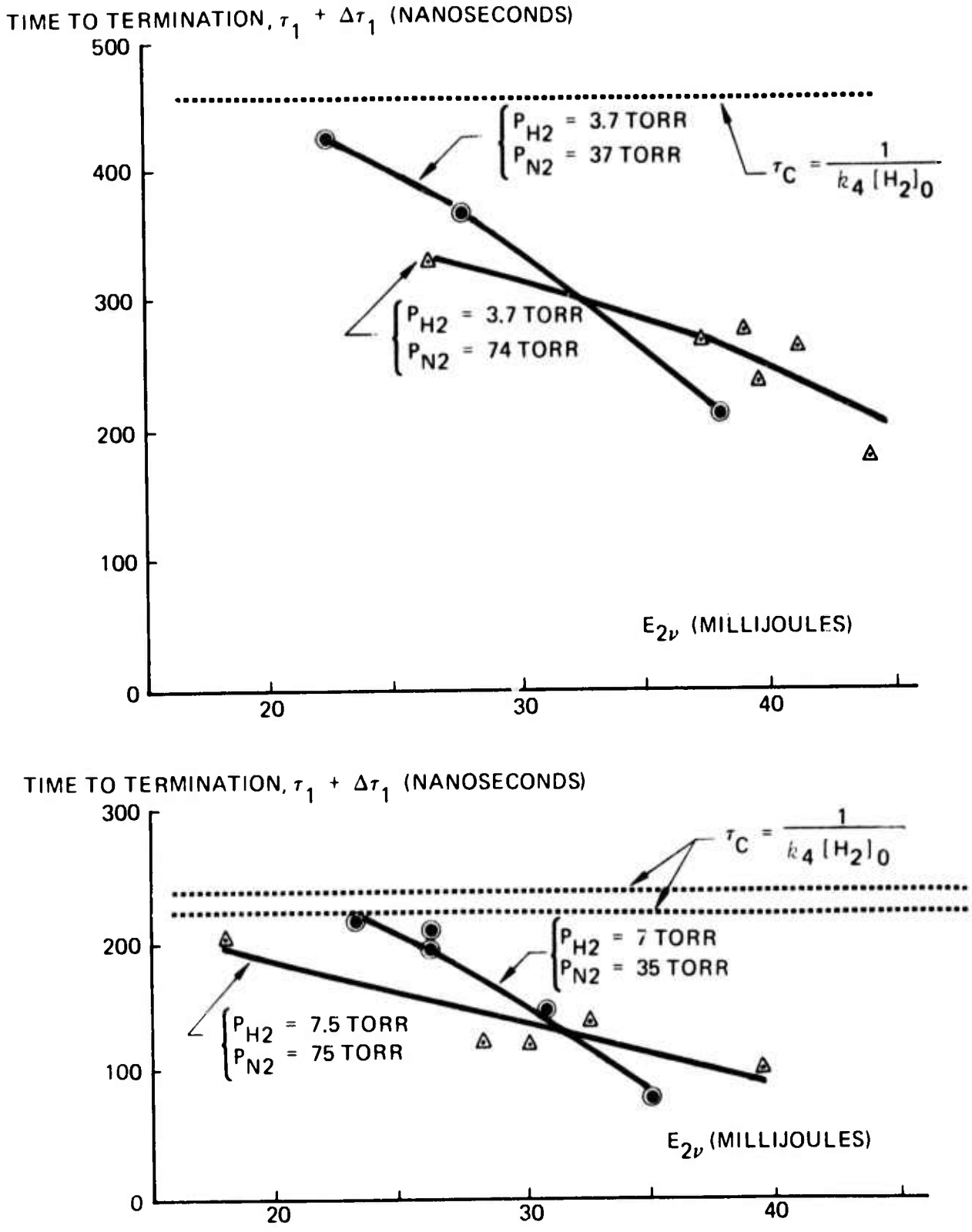

FIGURE 13. TERMINATION OF INITIAL PULSE

transients. The possibility that pulse termination might be associated with switching from a transverse mode with high centerline intensity to one with a centerline null in conjunction with hole-coupler sampling was investigated by a series of aperturing measurements for the condition $[F_2]:[H_2]:[N_2] = 7.5:7.5:75$ torr. Ratios of aperture diameters used to the $1/e^2$ fundamental mode diameter are .97, .90, and .76. These correspond to a geometric 'shadowing' (intensity-area product) of the TEM_{oo} mode varying from 20-35%. Similar 'shadowing' of the TEM_{10} mode is approximately constant at 72%, and that of the TEM_{01} varies from 48-70%. Although the smallest aperture caused attenuation of HF laser intensity by approximately a factor of 2, as noted above, no changes in relative precursor/long term intensity were observed. Therefore, oscillation in higher order modes, if present, has no significant effect on observed precursor/long term temporal structure. High frequency, small amplitude oscillations that persist through the long term transient were affected somewhat by aperturing. As the aperture size is decreased, these tend to become more distinctly periodic, and the amplitudes attenuate slightly more rapidly than that of the long term mean level. Two distinct frequency components, 8-10 MHz and 25-30 MHz, have been observed, sometimes concurrently. These frequencies are compatible with those expected for beating of low order transverse modes and lead us to believe that higher order modes may oscillate, even though they do not contribute materially to present observations.

Centerline measurements with a 15% transmitting mirror show the same temporal structure as described above. Several measurements with the spherical mirror removed (semi-open cavity) showed similar first pulse structure, suppression of the second pulse, and lasing over several microseconds at reduced intensity and with a somewhat erratic multiple pulse structure.

The fast termination of precursor pulses are in all probability due to unsteady resonator processes, i.e., reduction of inversion density below the threshold value by the higher intensity cavity radiation associated with the pulse (see Ref. 27). The precursor pulse structure

observed here is qualitatively similar to the extremely high-power pulses observed elsewhere in fast discharge initiated chemical lasers. It is also of interest to note that the long term low-level transient depends on operation of the complete reaction chain as it approaches quasi-steady propagation.

SECTION IV

TIME-RESOLVED [HF] LASER EMISSION SPECTRA FOR $[F_2]:[H_2]:[N_2]$ = 4:4:40 TORR

Results of extensive time-resolved spectroscopic measurements of emission from the laser initiated HF laser are reported in this section for the initial chemical state, $[F_2]:[H_2]:[N_2]$ = 4:4:40 torr, and in the following section for an 8:8:80 torr mixture. The spectral survey at the lower pressure includes the 10 lowest P-branch transitions in the 1-0 and 2-1 vibrational bands, and the higher pressure survey includes lower J transitions in the 3-2 and 4-3 bands also. The resonator configuration used in all measurements in this and the following section is a 10 m radius spherical mirror with T = 70% ± 1% across the HF wavelength range and a flat total reflector with 113 cm mirror separation. Throughout the following discussion terminology for line designation, VP(J) indicating lasing from the (V, J-1) vibration-rotation state to the (V-1, J) state is used. For the 4:4:40 torr case, cooling the gas premixer to liquid nitrogen (LN_2) temperature is found both to have strong beneficial effects on laser performance, and to reduce the steady state concentration of $[HF]_o$ due to pre-reaction from approximately .022 torr to .005 torr (the absorption measurements used to determine $[HF]_o$ concentration are described in section II-C2). Implications of an assumed casual relationship between variations of $[HF]_o$ and laser performance (with reference to deactivation by HF - HF collisions) are discussed below.

Fig. 14 illustrates typical transient behavior of total laser intensity (upper two oscillograms) and single line transients, all measured simultaneously in a single laser pulse. In all cases zero time base is taken at the maximum of the ruby laser signal displayed in the upper left trace. The initial signal peak in all single line traces (but not total intensity traces) is associated with instrument 'pickup' from the ruby laser signal and provide a convenient zero time reference. Signal levels for the total intensity trace may not be compared directly with those for individual lines due to differences in optical transmission

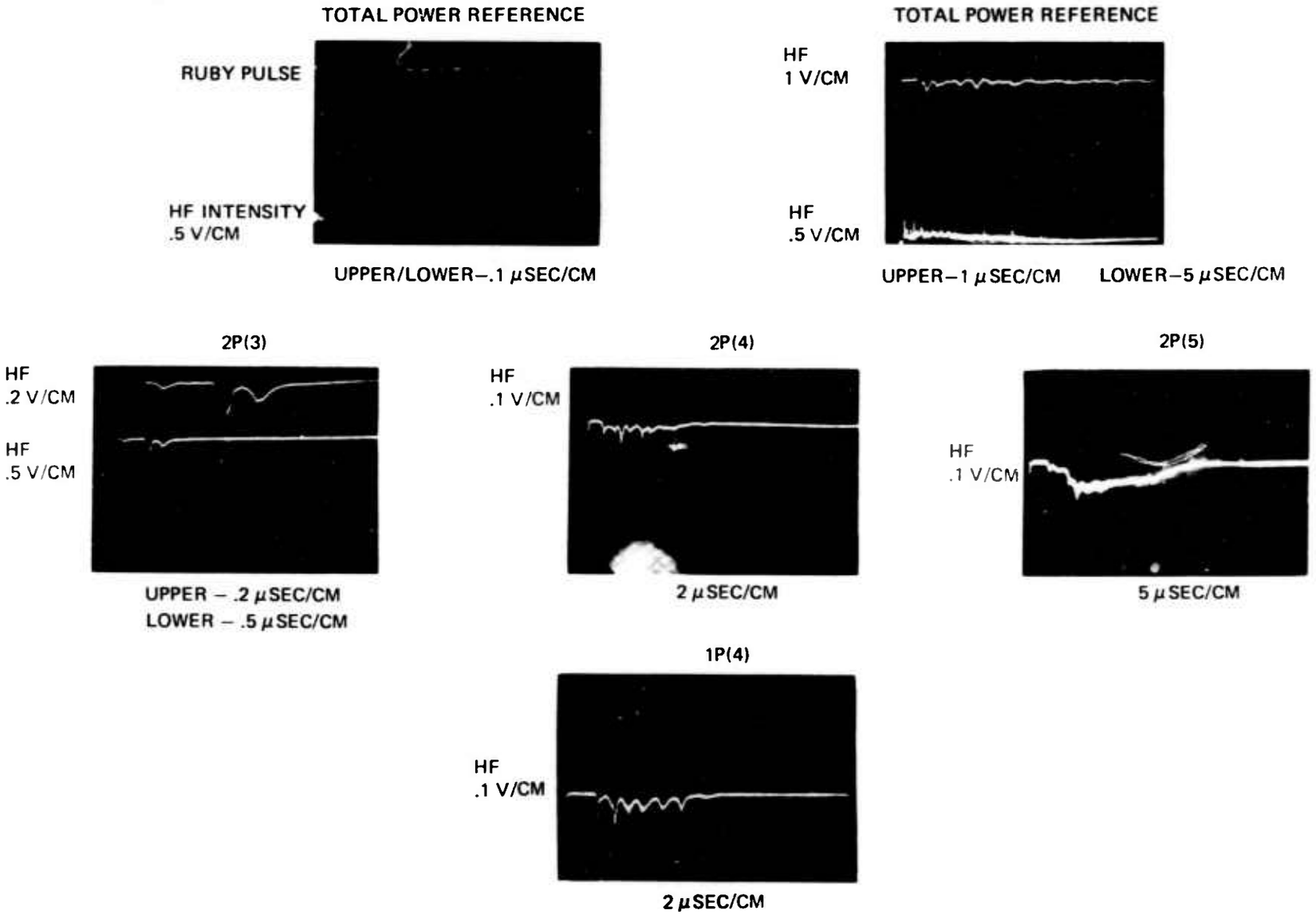

FIGURE 14. TIME RESOLVED HF LASER INTENSITY AND LINE SPECTRA FOR $F_2 : H_2 : N_2$ = 4 : 4: 40 TORR, $E_{2\nu}$= 37 MILLIJOULES

factors. However, comparison of relative intensity between individual lines can be made directly from the oscillograms. For reference with later discussion, the transients of Fig. 14 correspond to the cold gas premixer.

The total intensity transients of Fig. 14 exhibit relatively intense 'precursor' and 'low-level, long term' structure reported for prior measurements (section III). Laser initiation on the 2P(3) line is coincident with the 'precursor' peak and exhibits a peak intensity considerably larger than other observed lines. Note, however, that the time-duration of the 2P(3) transition is typically 1-2 orders of magnitude less than duration of the other transitions, and consequently the relative contribution of 2P(3) to total energy/pulse is small. First initiation on 2P(3) is expected from threshold gain considerations based on known partial reaction rates into given vibrational levels and on assumed Boltzmann rotation distributions, but near simultaneous initiation on 2P(3) and 2P(4), along with continued emission on 2P(4) is not consistent with the foregoing considerations. Although superficial examination of onset times for 2P(3) and 1P(4) transitions might suggest cascade behavior, the brief duration and low relative energy of 2P(3) emission cast doubt on significance of such interpretation.

It is to be emphasized that the relatively complex temporal structure exhibited by single line traces of Fig. 14 is characteristic of the large number of oscillograms associated with results discussed below. Specifically, the 2P(3) transition invariably exhibits fast high intensity fluctuations, 2P(4) and 1P(4) exhibit moderately large, near cyclic fluctuations of relatively long period (.5-1 μsec compared to .1 - .2 μsec for 2P(3)), and 2P(5) exhibits fluctuations that are usually small in amplitude compared to the slowly varying mean level. It is believed that the increasing violent intensity fluctuations for higher gain lines represents a dynamical coupling between the resonator and gain media that is not modeled by most existing computer simulations of pulsed chemical lasers, i.e., a defect of the threshold gain constraint. Such resonator relaxation processes in chemical lasers have recently been discussed by Molina and Pimentel (Ref. 27).

Estimates of excited vibrational populations during the early part of the observed laser transients suggest that the measured .022 torr $[HF]_o$ concentration due to prereaction in the ambient temperature premixer could have significant influence on laser emission in the 1-0 band. Experimental verification of increased emission on the 1P(4) line with the LN_2 cooled premixer ($[HF]_o \simeq .005$ torr) was made. Associated increase in time duration of total laser intensity in a time regime following termination of the 1P(4) line indicated that these effects were more extensive than had been expected. Consequently, surveys of the laser emission spectrum were made for both the LN_2 cooled and ambient temperature premixer. Detailed variation of HF laser properties with $E_{2\nu}$ for both room temperature and LN_2 cooled premixer is presented in appendix I.

Figs. 15 and 16 display a compacted characterization of the principal features of the HF laser transients as extracted from appendix I. Fig. 15 corresponds to results for the ambient temperature premixer, and Fig. 16 to the LN_2 temperature premixer. These figures show total intensity and individual line properties for three different dissociation levels: $E_{2\nu}$ = 50 millijoules corresponds to $[F]/[F_2]$ = .8%, $E_{2\nu}$ = 35 millijoules to $[F]/[F_2]$ = .56% and $E_{2\nu}$ = 20 millijoules to $[F]/[F_2]$ = .32%. Time duration of emission relative to the peak of the initiating light pulse is shown by insets to the left, relative peak intensity (open bars) and relative energy/pulse (shaded bars) are given in the insets to the right. As in the oscillograms described above (Fig. 14), total intensity power/energy characteristics may not be directly compared to individual line characteristics, but individual line intensities may be directly compared with each other.

Comparison of Figs. 15 and 16 clearly illustrate the dramatic effects of premixer cooling on all observed lines (in some cases effects on relative energy/pulse are best understood from detailed properties presented in appendix I since the large variation in magnitude causes difficulties in adequate display for all transitions in the compacted representation). Specifically, duration of emission and energy/pulse

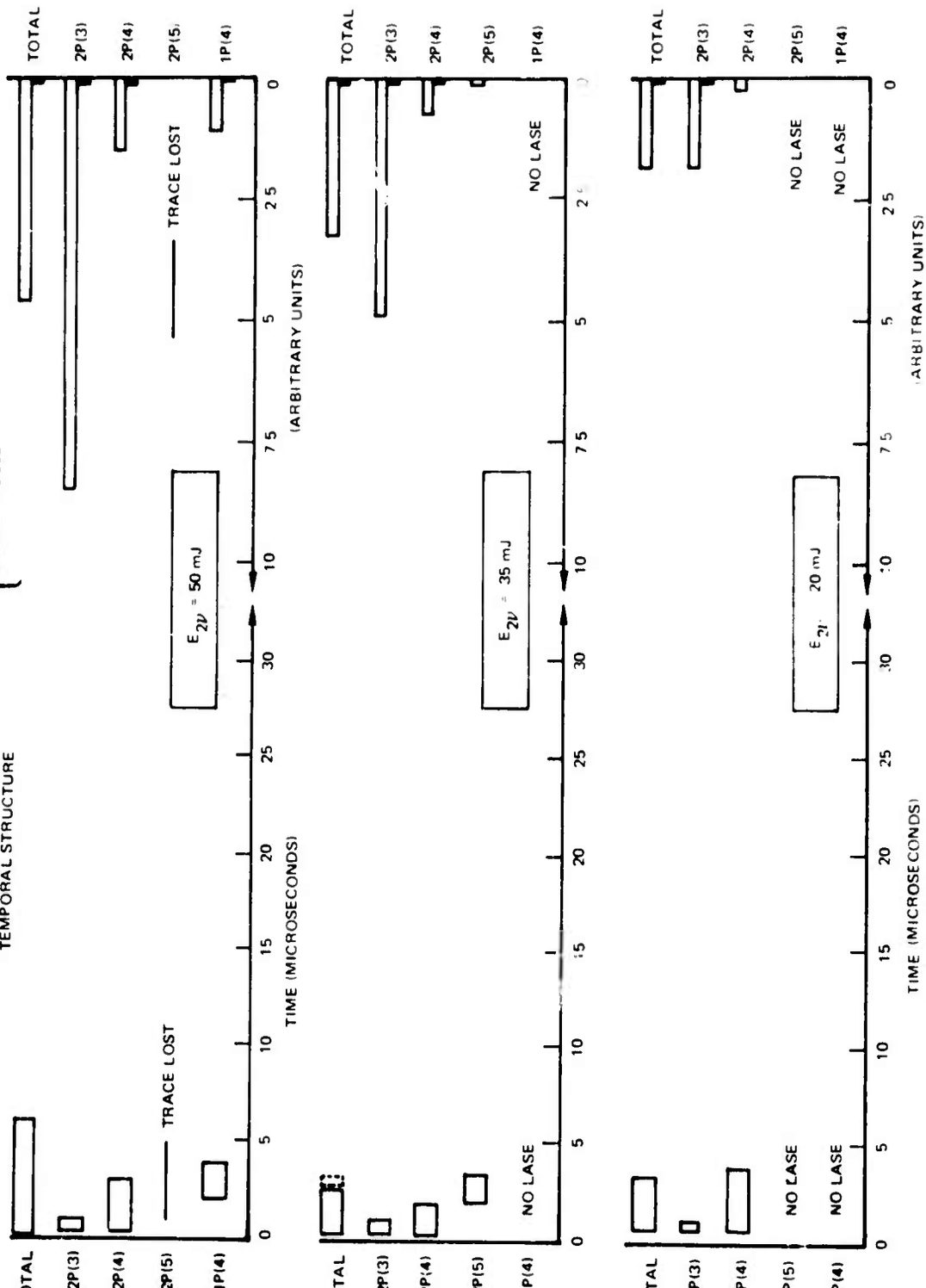

FIGURE 15. SUMMARY OF HF LASER TRANSIENT PROPERTIES FOR $F_2 : H_2 : N_2 = 4 : 4 : 40$ TORR, INITIAL $[HF]_o \cong 0.022$ TORR

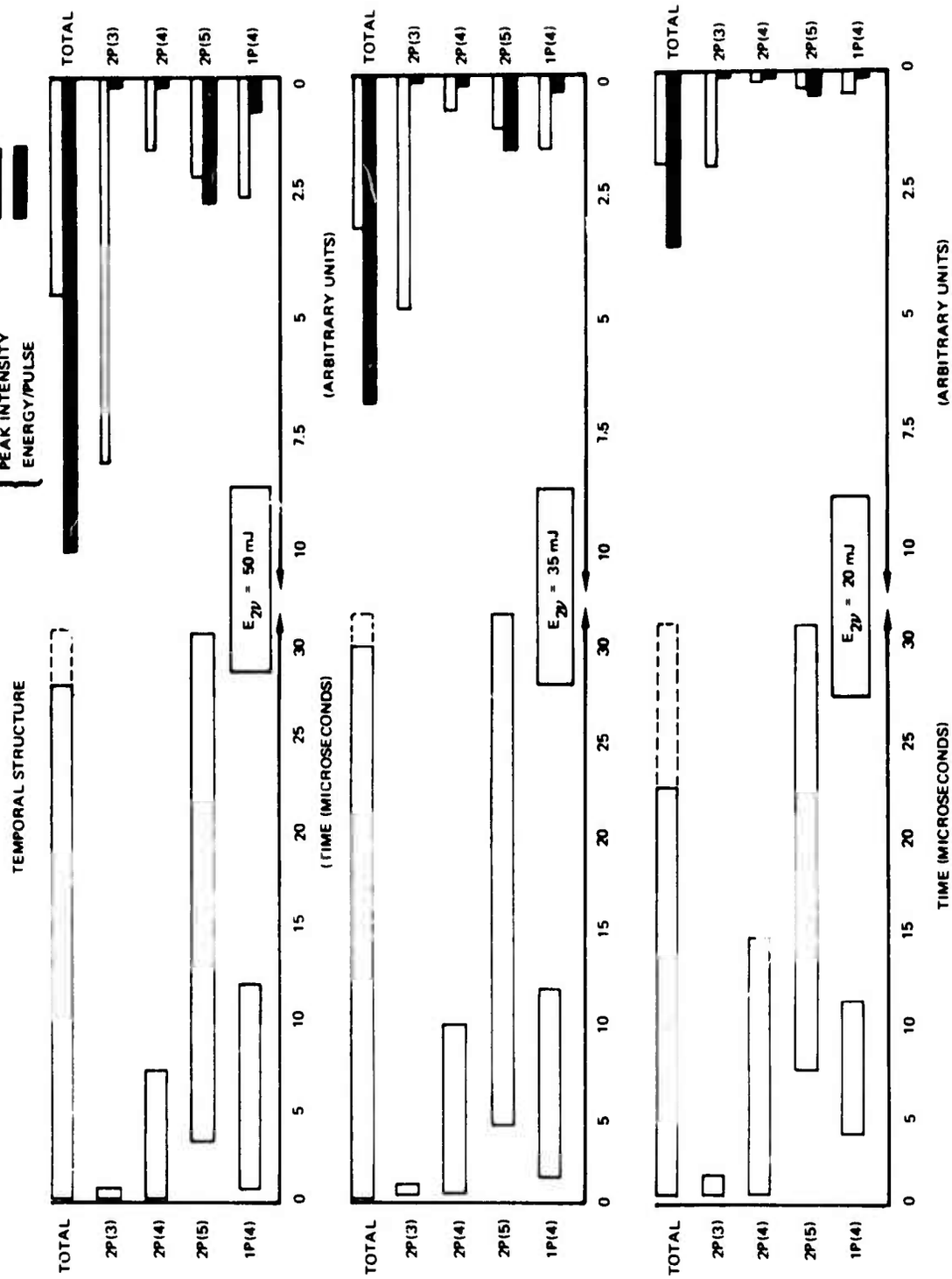

FIGURE 16. SUMMARY OF HF LASER TRANSIENT PROPERTIES FOR $F_2 : H_2 : N_2 = 4 : 4 : 40$ TORR, INITIAL $[HF]_o \cong 0.005$ TORR

for all observed lines are significantly increased by premixer cooling. Perhaps the most striking effect is on the 2P(5) line which lases only intermittently for the warm premixer, but contains by far the largest energy/pulse for the cooled premixer. Further, the ratio of energy/pulse values on a particular line with LN_2 cooling to corresponding values with the warm premixer uniformly increases in proportion to time-duration of emission from 1-2 for the 2P(3) line with ~2 μsec duration of emission to > 10 for the 2P(5) line with 25-30 μsec duration of emission. It is also important to note that the time of initiation and peak intensity for lines that exhibit 'precursor' behavior in the .2 - .75 μsec range are relatively unaffected by LN_2 cooling. These features, along with 4-5 fold reduction of initial ground state [HF] due to LN_2 cooling strongly suggest that the observed change in laser performance is due to increased collisional deactivation in the warm premixer case. Association of these effects with the observed values of ground state $[HF]_o$ would imply a characteristic $p\tau$ product of ~.15 - .3 μsec torr.

This $p\tau$ product is somewhat less than that measured by Airey and Smith (Ref. 11) for deactivation of HF (V = 2, 3) by HF(0) ($p\tau$ = 1.67 μsec torr and 1.56 μsec torr, respectively), but are of the same order as the rates for higher vibrational levels (< .6 μsec torr for V = 4, < .4 μsec torr for V = 5). The effects on laser performance observed here do not appear to be consistent with simple deactivation from HF (V = 2) by ground state HF. Nevertheless, the unknown process is not excessively fast relative to other deactivation processes for HF-HF collisions. Finally, it should be noted that auxiliary absorption measurements for several gas flow configurations do establish that the decreased $[HF]_o$ for the LN_2 cooled premixer is a consequence of suppressing reaction in the premixer (i.e., is not due to trapping HF contamination in the reagent gas supply). Measurements to rule out an alternative possibility that the effect of premixer cooling on laser performance might be associated with trapping other unknown contaminant species from the reagent supply are straightforward, but could not be undertaken under this program.

The emission spectra displayed in Fig. 16 form a characteristic pattern that will apply also to the more extensive set of lines for higher reagent pressure (section V). As noted in the discussion of oscillograms above, threshold gain calculations based on known partial rates of the $F + H_2$ reaction determined by Polanyi, et al. (Ref. 28) and on assumed Boltzmann distribution of rotational states predict initiation on the 2P(3) transition. Transition from total vibrational inversion to partial inversion due either to collisional deactivation or to laser-induced depletion of upper state population causes shift of maximum gain to higher J-levels as observed in the 2-1 band in Fig. 16.

Although Fig. 16 shows that peak emission intensity on individual lines correlates strongly with expected gain, energy content of individual lines shows no such correlation. The latter fact is due, of course, to extended time duration of the higher J transitions. It is also of interest to note, for the 4:4:40 torr initial state, that the characteristic reaction times for the 'cold' $F + H_2$ reaction and the 'hot' $H + F_2$ reaction are initially $\tau_C \simeq .4$ μsec and $\tau_H \simeq 2$ μsec. Therefore, the 'precursor' behavior is predominately associated with consumption of photolytically produced [F], whereas extended emission on high J transitions is necessarily a consequence of the propagating chain reactions. Extended laser emission over many chain reaction steps, shown both by Fig. 16 and in the following section, for small dissociation levels appropriate to these measurements is of considerable significance for high power laser applications (see section VII).

SECTION V

TIME-RESOLVED [HF] LASER EMISSION SPECTRA FOR $[F_2]:[H_2]:[N_2] = 8:8:80$

Results of time-resolved spectroscopic measurements of HF laser emission for the reagent mixture $[F_2]:[H_2]:[N_2] = 8:8:80$ torr are described below. Except where noted these data correspond to the LN_2 cooled premixer and a typical ground state HF concentration due to prereaction of .002 torr as determined by absorption measurements on the 1P(2) transition.

Fig. 17 shows a tabulation of observed transitions along with several transitions on which no observable intensity was found. Superscripts on several weak lines indicate proximity to wavelengths of nearby lines. In only two cases, the 1P(9) - 3P(2) pair and the 3P(5) - 4P(1) pair, are the line separations less than the 2-5cm^{-1} instrument resolution. In the latter case identical temporal structure clearly indicates that the weak 4P(1) signal is spurious. Although with adequate effort the set of observations could be readily extended to include transitions of higher V, J quantum numbers and R-branch transitions as well, it was deemed more important within the contractual constraints to develop a quantitative characterization of the subset of strong transitions appearing in Fig. 17.

Figs. 18 and 19 illustrate sets of transients taken in two typical laser pulses with $E_{2\nu}$ = 38 millijoules and 25 millijoules, respectively. As in the previous oscillograms for 4:4:40 torr these results exhibit complex temporal structure on both nanosecond and microsecond time scales (the leading pulse in single line transients is again due to 'pick-up' from the ruby laser pulse and provides convenient zero-time base). The total intensity transient exhibits first and second precursor pulses as in the 8:8:80 torr data discussed in section III. Note that the indicated figures show a high degree of reproducibility of characteristic time structure for different lines. This characteristic structure is typical of the large set of data discussed below.

VIBRATIONAL BAND	LOWER J VALUE (P-BRANCH)									
	1	2	3	4	5	6	7	8	9	10
1–0	○	○	+	◈	◈	◈	○	+ (3P1)	+ (3P2)	○
2–1	+ (1P5)	+	◈	◈	◈	◈	○	+	○	○
3–2	+ (1P8)	+ (1P9)	+	○	◈	+	○	○	---	---
4–3	▨ (3P5)	+	○	○	---	---	---	---	---	---

LEGEND

+ WEAK LINE

◈ STRONG LINE

○ INTENSITY NOT OBSERVABLE

--- NO OBSERVATION MADE

▨ ERROR SIGNAL DUE TO INADEQUATE RESOLUTION

(iPj) IDENTIFICATION OF ADJACENT LINE

FIGURE 17. LINES OBSERVED AT $F_2 : H_2 : N_2 = 8 : 8 : 80$ TORR

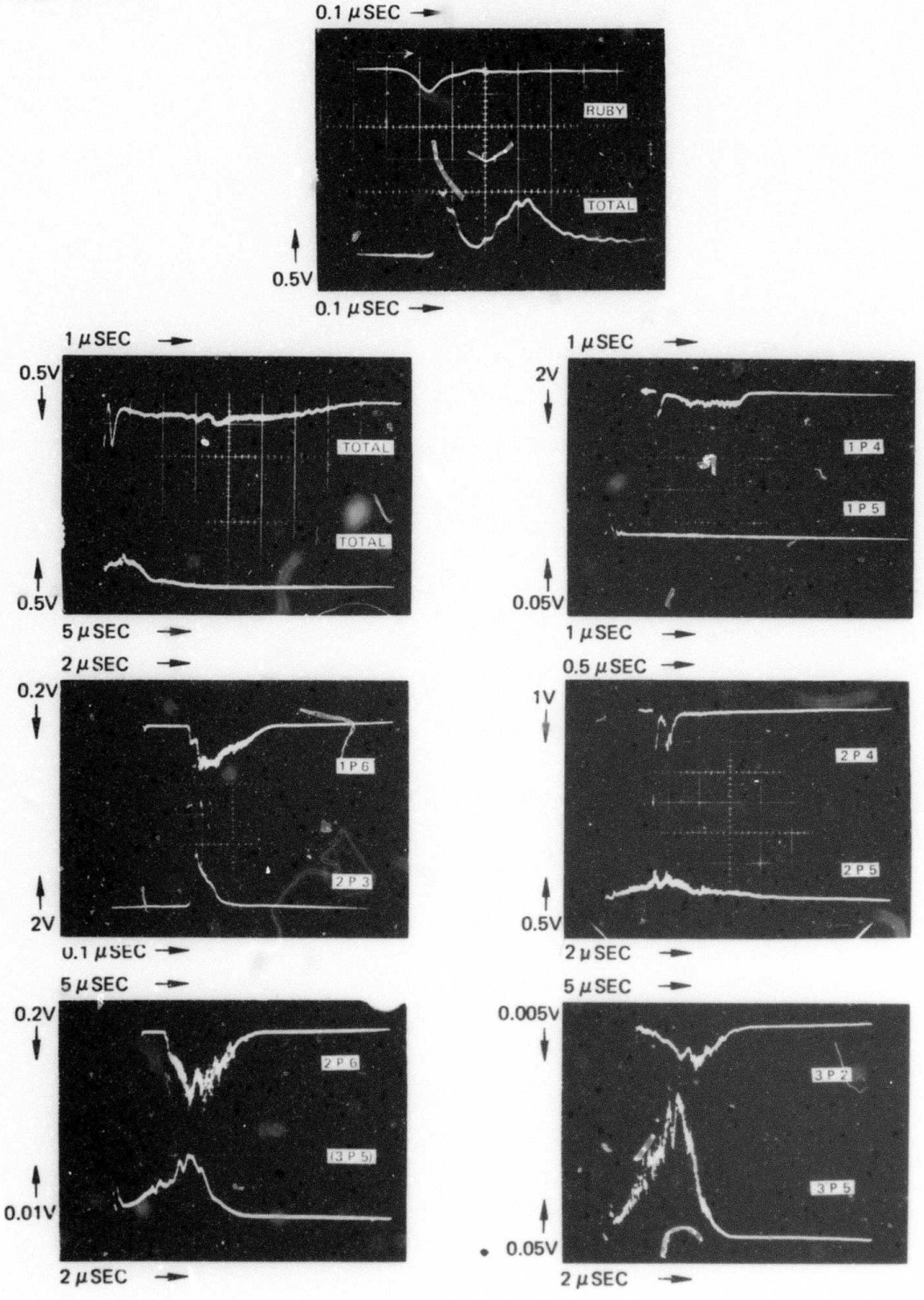

FIGURE 18. TIME–RESOLVED HF LASER INTENSITY AND LINE SPECTRA FOR $F_2 : H_2 : N_2 = 8 : 8 : 80$ TORR, $E_{2V} = 25$ MILLIJOULES

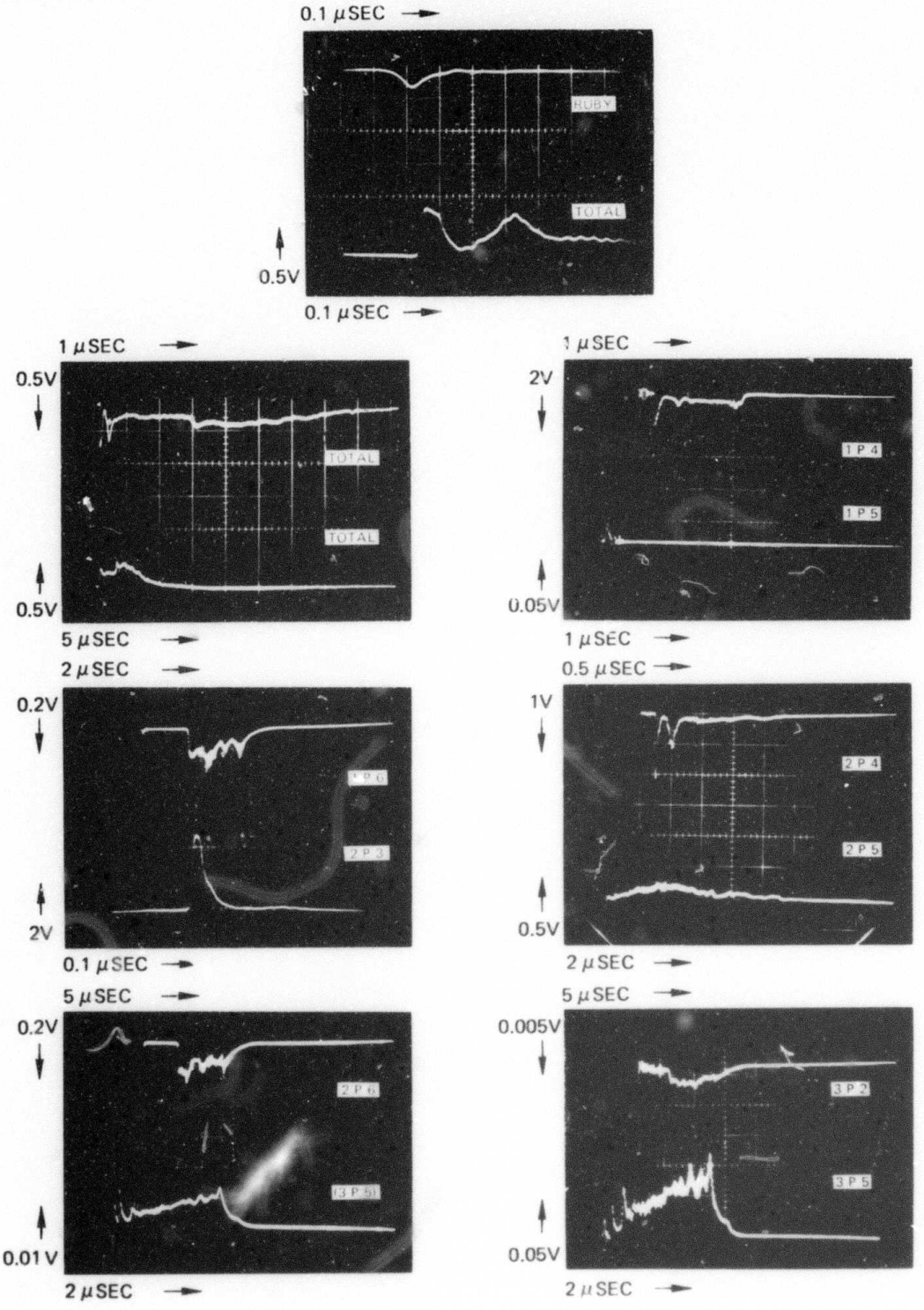

FIGURE 19. TIME–RESOLVED HF LASER INTENSITY AND LINE SPECTRA FOR $F_2 : H_2 : N_2 = 8 : 8 : 80$ TORR, $E_{2V} = 38$ MILLIJOULES

A useful classification of temporal structure suggested by oscillograms of Fig. 14 for the 4:4:40 torr reagent mixture is appropriate also to Figs. 18 and 19. The low J transitions in the 2-1 and 1-0 bands (2P(3), 2P(4), 1P(4)) which, based on the known partial F + H_2 reaction rates into individual vibrational levels along with assumed Boltzmann distribution of rotational states, are expected to have high gain initially, are seen to exhibit 'precursor' intensity fluctuations of large magnitude. In contrast, the intensity fluctuation on higher J lines (2P(5), 2P(6), 1P(6)) are less severe relative to the overall intensity level.

Detailed variation of principal features of the stronger lines with E_{2v} (dissociation level) are shown in appendix II. A few data points shown in appendix II for the ambient temperature premixer (for which measured ground state $[HF]_o$ levels due to prereaction are typically .017 torr) tend to show slight adverse effects on laser performance due to warming the premixer. However, these effects are much less distinct than was the case for the 4:4:40 torr mixture, hence measurements were mainly limited to the LN_2 cooled premixer configuration.

A compacted characterization of the principal features of the data presented in appendix II is shown by Fig. 20. The total intensity features shown by the figure can be compared directly with those of Fig. 16 for the 4:4:40 torr mixture. Again unknown differences in transmission efficiencies to the total intensity and individual line detectors preclude direct comparison of intensity, although relative intensities between individual lines can be so compared. Realignment of the spectrograph between the 4:4:40 torr data set of Fig. 16 and the subject 8:8:80 torr case most probably invalidates quantitative comparison of individual line intensities for the two cases. Finally, it may be noted that measurements of the geometric width of a spectrally resolved beam at a typical detector position are in agreement with a predicted FWHM approximately equal to the 1 mm width of the detector pickup mirrors. Therefore, typical detector positioning errors of $\pm$ .15 mm lead to expected relative intensity errors between different lines of 20-30%.

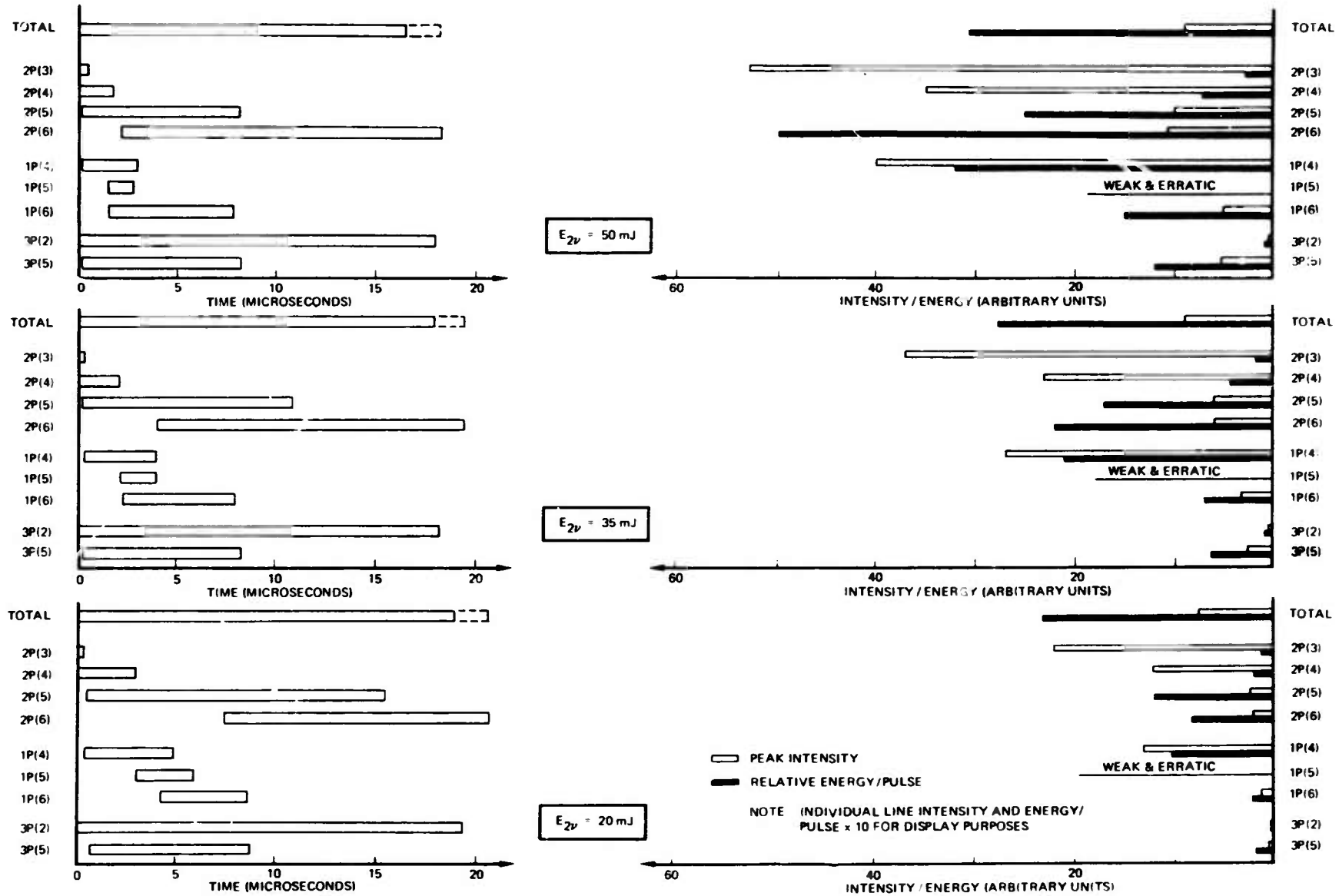

FIGURE 20. SUMMARY OF HF LASER TRANSIENT PROPERTIES FOR $F_2 : H_2 : N_2$ = 8 : 8 : 80 TORR, INITIAL $[HF]_o \simeq 0.002$ TORR

Fig. 20 clearly illustrates characteristic line behavior shown by the 4:4:40 torr data (Fig. 16) and noted in part in the discussion of oscillograms above. On the 2-1 and 1-0 bands, time delay between initial F_2 dissociation and laser initiation increases with increasing J-level. As expected the delay to laser initiation increases at decreased dissociation level (E_{2v}). The J-shift process is attributed to a transition from total vibrational population inversion initially (as expected from known partial reaction rates into individual vibrational levels) to a partial inversion at later times with the decreasing vibrational population inversion being offset at higher J levels by the rotational state distribution.

The peak intensity data for the 2-1 and 1-0 bands is entirely consistent with the above interpretation, showing very high 'precursor' intensity for the low J, high gain transitions and lower intensity for larger J. As in the 4:4:40 torr data, however, the energy content on lines in the 2-1 band shows no correlation with maximum gain and peak intensity. This result is, of course, a consequence of the long time duration of emission on the higher J lines. Lines in the 1-0 band fit this same general pattern except that the 1P(4) line exhibits intermediate behavior, i.e., relatively high precursor intensity and moderate time duration with relatively high energy content. Aside from the increased number of lasing transitions at higher pressure, comparison of Figs. 16 and 20 shows that increased reagent pressure tends to cause the behavior of individual lines to shift from 'low gain' toward 'high gain' character (compare intensities of 2P(4) and 1P(4) lines relative to the 2P(3) transition).

Results shown by Fig. 20 for the 3-2 vibrational band are of special interest since these transitions are pumped by the 'hot' H + F_2 reaction. For the given initial conditions, the corresponding e-fold time is $\tau_H \simeq 8$ μsec torr/$P_{F_2(\text{torr})}$ = 1 μsec. Thus Fig. 20 (see appendix II) shows that the 3-2 transitions initiate well before completion of the first complete chain step.

A second feature peculiar to the 3-2 transitions shown by Fig. 20 is that the lower J transitions are weak relative to 3P(5). This may result from a favored pumping of higher J levels by the 'hot' H + F_2 reaction although the set of observed transitions is not sufficiently extensive to corroborate this point. One may also note an apparent anomaly in the long duration and extremely low intensity of the 3P(2) line. It is quite possible that the observed emission is a combination of 3P(2) and the weak 1P(9) line since this wavelength separation is $\sim 1\ cm^{-1}$. Despite the inability to clearly resolve these lines, however, the early initiation time associated with the 3P(2) line in Fig. 20 is substantiated by late observed initiation ($\cdot$ 5 μsec from the photolysis pulse) on the 1P(9) detector, and by the J-progression of other lines in the 1-0 band.

The relation for the rate limiting 'hot' reaction time constant above, combined with the known initial dissociation level, permit an upper bound to be established on rate of completion of reaction. For example for initial $[F]/[F_2] = 8 \times 10^{-3}$ ($E_{2\nu}$ = 50 millijoule), the initial rate of completion of reaction is 1.6%/μsec. Thus Fig. 20 shows that, even for these very low dissociation levels, laser emission continues until a large fraction of the reagents have been consumed.

SECTION VI

CHARACTERIZATION OF CW LASER-FLAME SOURCE

Section II shows that a flame emission source of adequate intensity could provide direct line-strength measurements for a pulsed chemical laser medium. The device described in section II-D4 utilizes subsonic diffusion-mixing, and F_2 dissociation by the NO + F_2 reaction. Results from this device are presented here.

A. CW Laser Characterization

Characterization of the CW chemical laser used with a conventional stable resonator was chosen as a point of reference since required laboratory setups are similar to, and in some respects less critical than, those for flame characterization. Properties of the CW laser are of interest in their own right, and similarities in conditions required for lasing and enhanced flame emission lead to related optimization procedures.

Although simultaneous solution of the NO + F_2 and NO + F rate equations along with existing literature on subsonic CW chemical lasers provides expected operating conditions, laboratory optimization of relative flow rates (He, 50-50 He-F_2, NO, and H_2), injector location, and output coupling fraction were made. Laser power measurements were made with a Ge:Au detector having a 2 mm diameter active element; the cavity was ~1 meter in length with a 10 m radius spherical output mirror and a flat total reflector. The cavity volume external to the flow channel was enclosed by ~1 inch diameter tubes which were continuously purged with dry nitrogen.

Variation of laser power with upstream position of the H_2 injector orifices measured from the optic axis is shown by Fig. 21. Laser power increases monotonically with decreasing injector distance until the TEM_{oo} mode volume becomes obscured by a part of the H_2 injector manifold. Optical obstruction for Injector I (see section II-D4) extends 6 mm downstream from the injection point; that length was reduced to

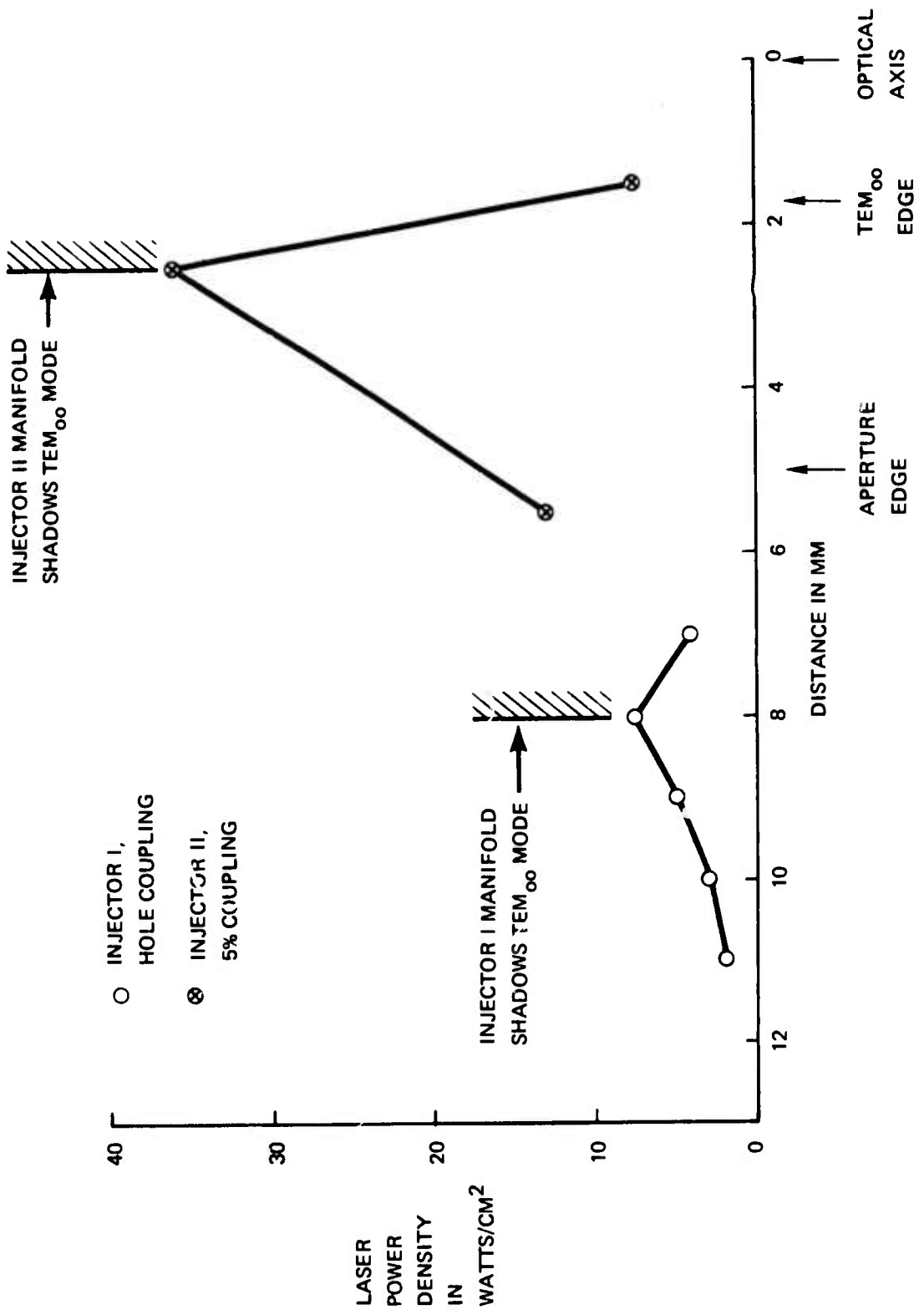

FIGURE 21. VARIATION OF LASER POWER DENSITY WITH POSITION OF H_2 INJECTION

0.5 mm for Injector II. The small optimum injector-cavity separation for this device apparently results from fine-scale H_2 injection, since power variation for similar devices reported in the literature is relatively insensitive to injector position for separation distances less than 1 cm. Rapid decrease of output power with increasing injector stand-off distance from the optimum valve and spectroscopic observations discussed below indicate rapid collisional deactivation in the immediate region downstream from the H_2 injector.

Variation of CW laser power density with output coupling fraction measured with a set of 10 m radius partially transmitting mirrors is shown by Fig. 22. These power densities correspond to optimized gas conditions defined by the lower portion of Fig. 22. The highest power density corresponds to ~3 watts average power and is relatively insensitive to output coupling fraction in the range 15-30%. The most significant variation in optimum gas mixture is the increased amount of F_2 for Injector II (decreased stand-off distance) at the smaller coupling fractions.

Relative spectral intensities for the CW laser for 15% mirror transmission and optimized injector locations are shown by Fig. 23 for Injector I and by Fig. 24 for Injector II. Intensities of the 18 observed transitions listed in the first column of Fig. 23 correspond to a 'standard' gas mixture defined by the figure; all tabulated intensities are normalized to the 1P(6) intensity. The remaining columns of Fig. 23 show the effects of the independent variation of H_2, F_2 and NO flow rates as defined in the lower part of the figure. During initiation and termination of gas flow, many transitions exhibit transient peak intensities comparable to the 'standard' 1P(6) value even though the corresponding average intensity values are small. In several cases the gas mixture was 'tuned' to produce uniform emission levels comparable to the transient peak values noted above. It is expected, therefore, that the laser could operate on a relatively large number of lines at one to several watt power levels with appropriate adjustment of gas conditions.

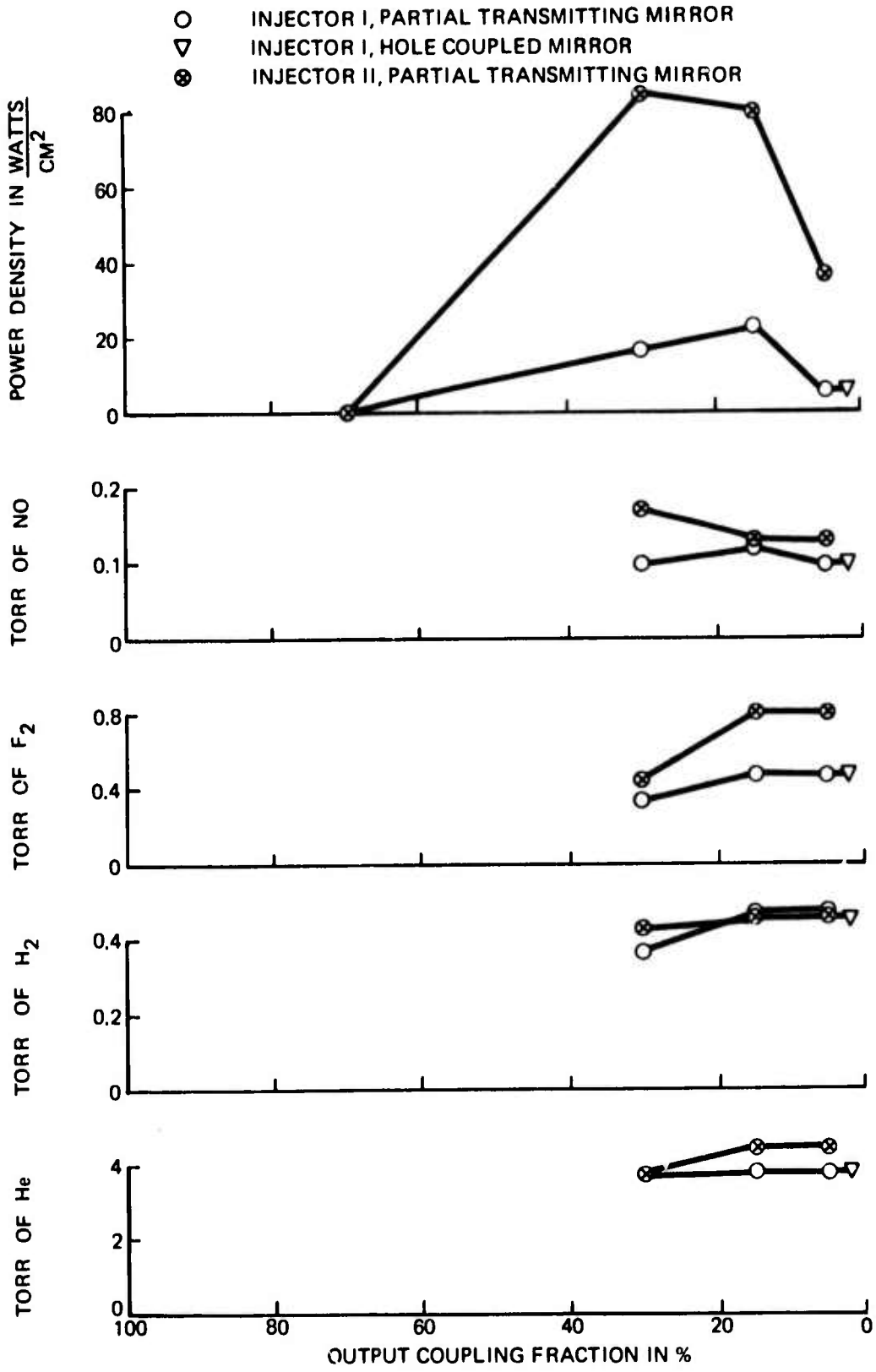

FIGURE 22. OPTIMIZED POWER DENSITY AND GAS MIXTURE VERSUS OUTPUT COUPLING

LINE DESIGNATION	RELATIVE INTENSITY									
1P(1)	0									
1P(2)	0									
1P(3)	10^{-5}									
1P(4)	.08	–	.75	.01	–	1.3	1.1	.23	.19	.27	0
1P(5)	.08	.01	$.2\times10^{-2}$	$.7\times10^{-3}$	–	–	0	$.2\times10^{-2}$	$.8\times10^{-2}$	.23	0
1P(6)	1.0	.26	–	.2	.42	.1	0	.13	.67	.18	0
1P(7)	–										
1P(8)	$.3\times10^{-2}$										
1P(9)	$.15\times10^{-2}$										
1P(10)	1×10^{-6}										
2P(1)	$.15\times10^{-2}$										
2P(2)	.08										
2P(3)	.03	.02	$.4\times10^{-2}$	.02	.02	$.6\times10^{-2}$	.01	.02	.03	.03	–
2P(4)	.01	.1	0	.01	0	10^{-5}	0	.02	.07	$.3\times10^{-2}$	.06
2P(5)	$.5\times10^{-2}$	$.1\times10^{-2}$	0	$.3\times10^{-3}$	$.1\times10^{-3}$	0	0	$.1\times10^{-2}$	$.3\times10^{-3}$	.17	.1
2P(6)	.06	$.2\times10^{-2}$	0	0	0	0	0	0	0	.33	0
2P(7)	10^{-5}										
2P(8)	0										
2P(9)	0										
2P(10)	0										
3P(1)	2×10^{-5}										
3P(2)	10^{-5}										
3P(3)	10^{-5}										
3P(4)	2×10^{-5}	–	0	0	0	0	0	10^{-4}	10^{-4}	3×10^{-4}	10^{-4}
3P(5)	0	0	0	0	0	0	0	0	0	0	0
3P(6)	0										
3P(7)	0										
3P(8)	0										
4P(1)	0										
4P(2)	0										
4P(3)	0										
4P(4)	0										
RELATIVE MASS FLOW $\dot{M}_{H_2}$	1.0	1.5	.5	1.0	1.0	1.0	1.0	1.0	1.0	1.0	1.0
$\dot{M}_{F_2}$	1.0	1.0	1.0	1.4	.6	.4	.2	1.0	1.0	1.0	1.0
$\dot{M}_{NO}$	1.0	1.0	1.0	1.0	1.0	1.0	1.0	2.4	1.7	.6	.3
$\dot{M}_{He}$	1.0	1.0	1.0	1.0	1.0	1.0	1.0	1.0	1.0	1.0	1.0

NOTE: SPECTRAL SURVEY NOT EXTENDED THROUGH CROSS HATCHED AREAS

LEGEND: 0 ZERO OBSERVED INTENSITY
– NO DATA ACQUIRED

NOTE: RELATIVE MASS FLOW RATES EQUAL TO UNITY CORRESPOND TO:
0.5 TORR H_2
0.6 TORR F_2
0.1 TORR NO
4.1 TORR He

FIGURE 23. AVERAGE CW LASER LINE INTENSITIES, H_2 INJECTOR I, 15% MIRROR TRANSMISSION

J	1P(J)	2P(J)	3P(J)	4P(J)
1	4×10^{-5}	7×10^{-5}	2.1×10^{-3}	0
2	0	4×10^{-4}	0	4×10^{-4}
3	0	2×10^{-3}	0	1.4×10^{-4}
4	4×10^{-5}	1.4×10^{-3}	7×10^{-5}	1.8×10^{-4}
5	1.4×10^{-2}	2.5×10^{-3}	4×10^{-5}	– –
6	1.0	.29	1.4×10^{-4}	– –
7	9.1	1.1	1.4×10^{-4}	– –
8	.11	5.4×10^{-4}	0	– –
9	4×10^{-4}	0	– –	– –
10	5×10^{-4}	0	– –	– –

FIGURE 24. AVERAGE CW LASER LINE INTENSITIES, H_2 INJECTOR II, 15% MIRROR TRANSMISSION

A feature evident in the data of Fig. 24, and even more pronounced in that of Fig. 23 for which H_2 is injected further upstream, is the relatively high intensity of V = 1-0 lines despite preferred pumping rates into the V = 2 vibrational level. This result suggests that significant collisional transfer occurs in the region adjacent to the H_2 injector. Fig. 23 shows that the variation of any constituent gas flow typically had quite different effects on different lines. It appears that such variation shifted the position of the inversion region for each transition relative to the cavity location; i.e. 'tuning' the gases also 'tuned' the spatial coincidence of inversion and cavity volumes.

B. Flame Source Characterization

Although identifiable laser emission was observed only for coupling fractions less than 70% (Fig. 22), observable emission occurred with the resonator removed. Fig. 25 illustrates variation of flame emission intensity with static pressure (measured ~4 cm downstream from the optical axis) for Injector I. These emission levels correspond to a wavelength range ~1-6μ, defined at the short-wavelength end by the Ge:Au detector cutoff, and at the long-wavelength end by a sapphire entrance window. The lowest emission value of 1/3 mW/cm^2 corresponds to a 'standard' CW laser mixture, F_2:H_2:He: NO = 0.5:0.5:4:0.1 torr. The remaining values correspond approximately to 1:1:1 mixtures of F_2/H_2/He. For a total pressure of 25 torr, variation of NO concentration by factors of 2 and 0.5 from the nominal value produced no observable effect on emission intensity.

The highest emission level shown by Fig. 25 is 180 times larger than that observed under conditions appropriate to CW laser operation. The reagent flow rates at 25 torr were the largest that could be safely handled in this apparatus with a sonic slot downstream designed for a 'cold flow' mach number of .5. Since increase of the distance between Injector I and optic axis from .5 to 3.0 cm decreased the emission intensity by only 25-30%, a 5 times smaller sonic throat area was installed to reduce the flow speed, thus further increasing the reacting gas pressure at constant mass flow. As shown by Fig. 25, the associated emission

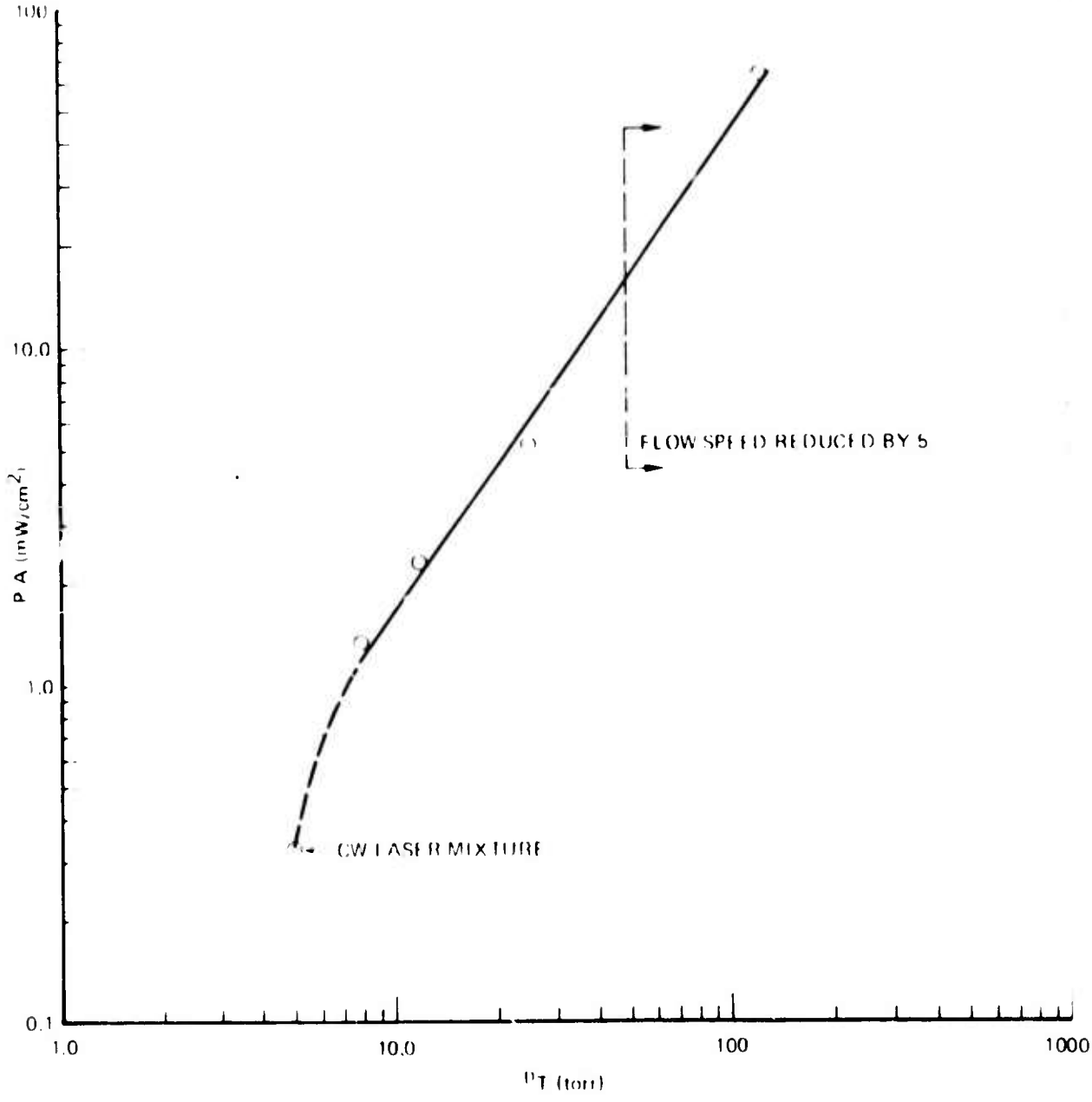

FIGURE 25. FLAME EMISSION INTENSITY

intensity increased by an order of magnitude. The character of visible emission changed markedly with changing gas conditions in the range covered by Fig. 25. For the low pressure dilute mixture corresponding to CW laser conditions, the soft orange flow associated with HF overtone emission was observed. Visible emission for the 'richer' mixture at intermediate pressures was a brilliant blue, changing to intense white at high pressure. The IR emission levels were inadequate to observe single line emission using a fast IR detector and the multichannel spectrograph configuration described in section II.

For the conditions indicated by the two higher points of Fig. 25, an optical cavity consisting of metal coated flat and 10 m spherical mirror equipped with .5 mm coupling hole was placed across the reaction channel as a test for gain. Neither visible nor IR lasing was observed under these conditions of optimized emission with Injector I. Similar single mirror tests gave no indication of enhancement of emission.

For the high-speed flows at 25 torr and below, the emission intensity from Injector I was approximately constant over the duration of near-steady flow conditions, whereas the emission intensity for the low-speed, high-pressure flow increased rapidly throughout the flow time. This behavior was attributed to 'thermal runaway' due to heating of Injector I. During installation of Injector II, it was apparent that Injector I had been thermally damaged during the slow-flow tests. For this reason, Injector II was operated only in the fast-flow mode, and hence only to approximately 25 torr. Despite increased CW laser emission for Injector II, emission levels with resonator removed were similar to those obtained using Injector I. Again, absence of IR or visible lasing indicated very low gains, and single line emission levels were not observable.

SECTION VII

SUMMARY AND RECOMMENDATIONS

Performance evaluation and spectroscopic studies of an HF chemical laser based on laser-initiated reaction in dilute H_2 - F_2 mixtures have been described. Use of 2ν radiation generated by a Q-switched ruby laser for photolysis of F_2 provides a simple and well-defined initial state. The corresponding HF laser transients are somewhat complex in nature, but exhibit temporal structure that is directly representative of the evolving chemical state. In an initial time regime, for example, the laser intensity exhibits 'precursor' pulses associated with lower P-branch transitions of the 2-1 and 1-0 vibrational bands. The initial 'precursor' pulse, associated with the 2P(3) transition, is representative of a 'total' vibration population inversion for a Boltzmann distribution of rotational states in the ambient temperature reagent mixture. This initial pulse is shown to be a consequence of the F + H_2 reaction alone, since the corresponding intensity reaches maximum amplitude and terminates well before consumption of photolytically generated F and before the H + F_2 reaction has reached a significant production rate. This characteristic of first pulse termination time, which decreases with increasing dissociation level, is indicative of unsteady resonator processes not modeled by simulation codes based on the 'threshold gain' constraint.

The J-shift process attributed to transition from 'total' to 'partial' inversion of vibration-rotation populations in threshold gain models is observed in the HF laser emission spectra. In some instances, however, higher J transitions initiate in near coincidence with low J transitions, and continue to lase during and following low J emission. Amplitudes of intensity fluctuations about a 'quasi-steady' mean value correlate strongly with expected gain of the transition, as does peak emission intensity. Relative energy content shows no such correlation with gain, however, and is much larger for the higher J transitions which lase at lower intensity, but for extended time periods compared to low J transitions.

These experiments clearly show that even for low dissociation levels ($[F]/[F_2] = 3 - 8 \times 10^{-3}$) laser emission is maintained by long chain propagation. For an 8:8:80 torr F_2-H_2-N_2 mixture, for example, the characteristic time per chain step decreases from an initial value of ~1 μsec to .25 μsec and less as the reaction proceeds. Associated laser emission periods of approximately 20 μsec correspond to many chain propagation steps and to significant completion of reaction.

Concurrent variation of HF laser performance and ground state HF concentration (section IV) is indicative of a deactivation process depleting the V = 2 upper state at faster rates than would be expected on the basis of known relaxation rates. Since effects of this process are considerably smaller for the 8:8:80 torr measurements (section V), they appear to be of concern only for low pressure laser operation. One would expect, of course, that this deactivation process would be less significant for higher dissociation levels.

As noted above, a common characteristic of conventional photolysis lasers is inefficient utilization of dissociating light, due both to excessively slow flashlamp emission and to small optical thickness of F_2 in slender quartz tube containers. An independent Boeing research/development program has shown that correctly designed photolysis lasers will require an (electrical) initiation energy in the range 1.5 - 6 k-cal/mole of HF under typical conditions for effective laser operation. Demonstrated capability for near reaction-free premixing utilizing refrigerated premixers (sections IIA, IV, and V) establishes a basis for relatively straightforward design of devices sized for efficient initiation of reaction. Ability to maintain specific energy levels demonstrated in conventional photolysis lasers for devices utilizing initiation technology described above would establish the pulsed chemical laser as a formidable competitor for high power laser applications.

APPENDIX I

VARIATION OF PROPERTIES OF [HF] LASER EMISSION SPECTRA WITH INITIATING LIGHT $F_2:H_2:N_2$ = 4:4:40 TORR

Figs. 26-45 to follow exhibit detailed properties of total power and single line HF laser emission transients discussed in section IV for the initial chemical state $F_2:H_2:N_2$ = 4:4:40 torr. In each case the property is plotted against 2ν energy, $E_{2\nu}$, and the figures are grouped to show a specific property in the order: total intensity/2P(3)/2P(4)/2P(5)/1P(4). Figs. 26-30 display laser initiation times relative to peak 2ν emission, Figs. 31-35 display time duration of observable laser emission, Figs. 36-40 peak emission intensity, and Figs. 41-45 relative energy/pulse. Principal characteristics of these transient properties are summarized by Figs. 15 and 16.

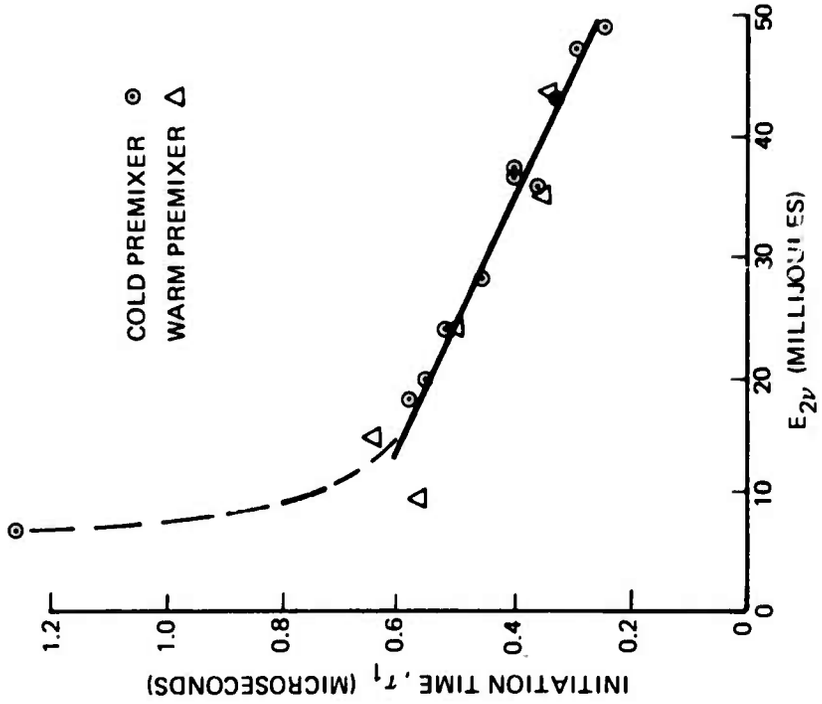

FIGURE 27. 2P(3) INITIATION TIME, $F_2 : H_2 : N_2 = 4 : 4 : 40$ TORR

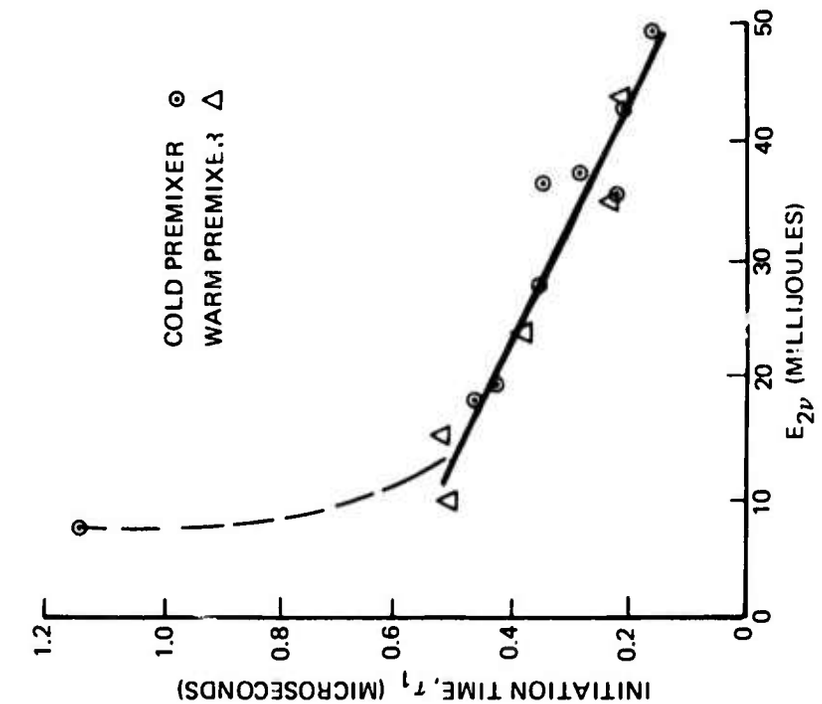

FIGURE 26. TOTAL–POWER INITIATION TIME, $F_2 : H_2 : N_2 = 4 : 4 : 40$ TORR

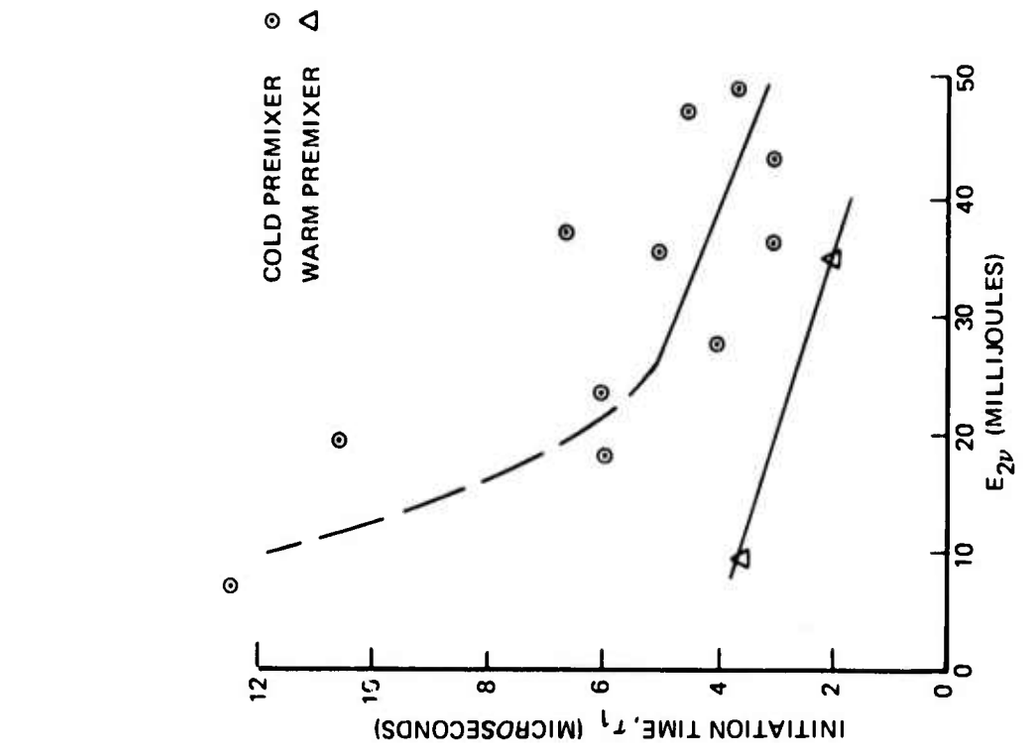

FIGURE 29. 2P(5) INITIATION TIME, $F_2 : H_2 : N_2 = 4 : 4 : 40$ TORR

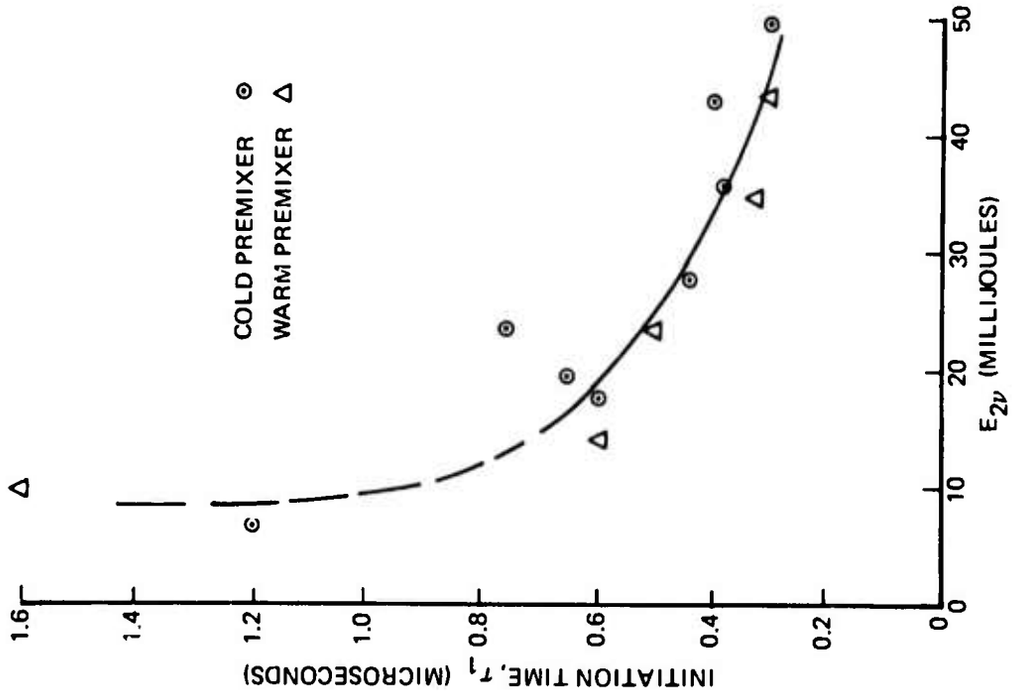

FIGURE 28. 2P(4) INITIATION TIME, $F_2 : H_2 : N_2 = 4 : 4 : 40$ TORR

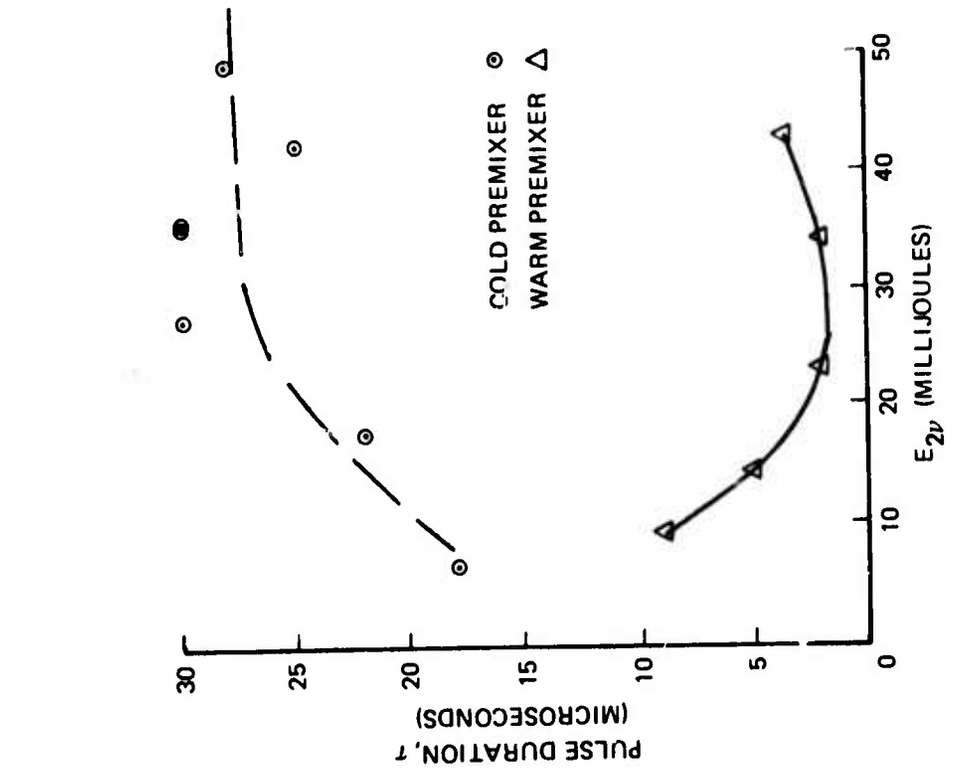

FIGURE 31. TOTAL–POWER PULSE DURATION, $F_2 : H_2 : N_2 = 4 : 4 : 40$ TORR

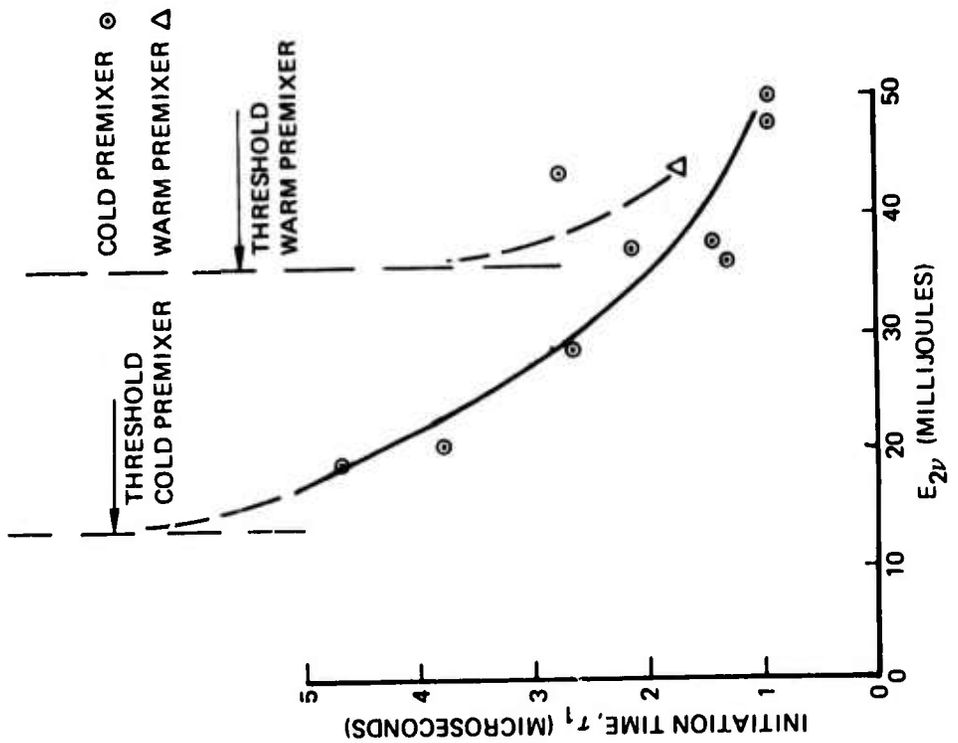

FIGURE 30. IP(4) INITIATION TIME, $F_2 : H_2 : N_2 = 4 : 4 : 40$ TORR

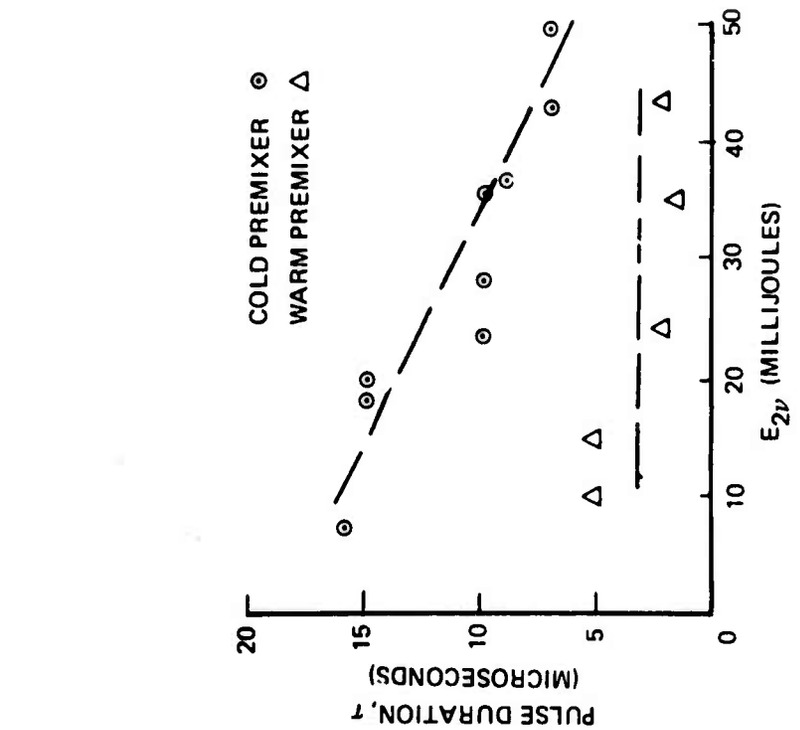

FIGURE 33. 2P(4) PULSE DURATION, $F_2 : H_2 : N_2 = 4 : 4 : 40$ TORR

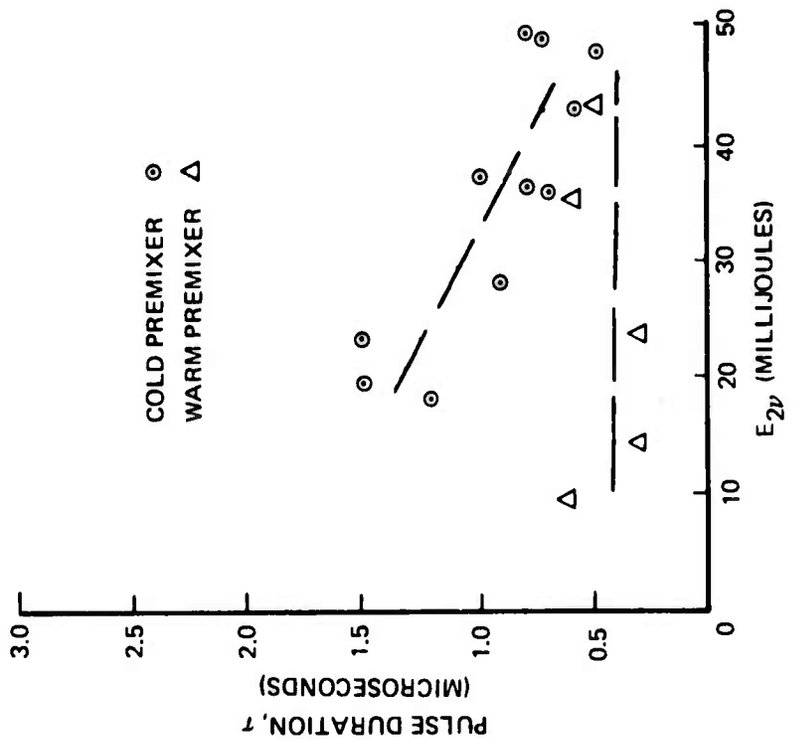

FIGURE 32. 2P(3) PULSE DURATION, $F_2 : H_2 : N_2 = 4 : 4 : 40$ TORR

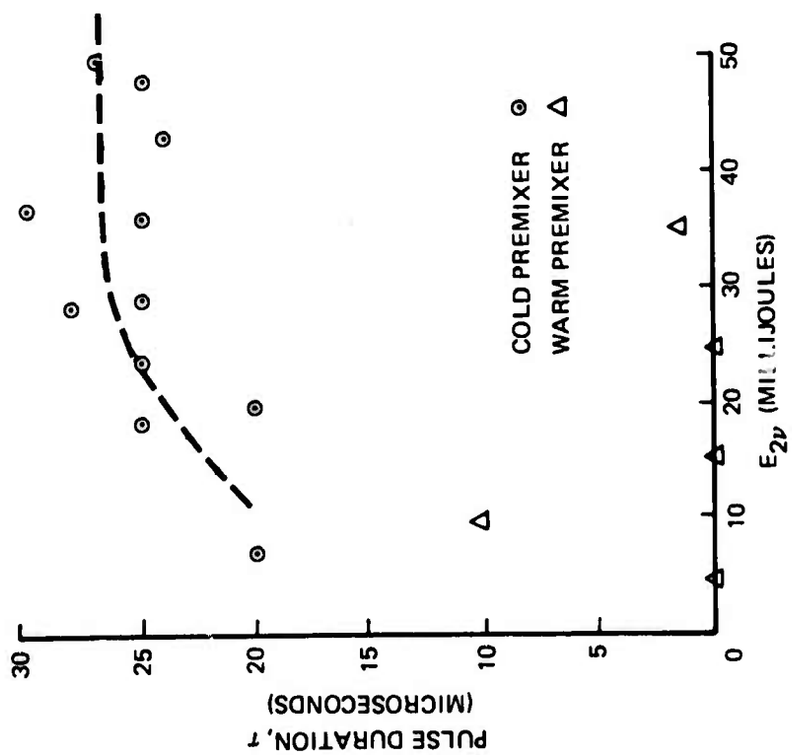

FIGURE 34. 2P(5) PULSE DURATION,
$F_2 : H_2 : N_2 = 4 : 4 : 40$ TORR

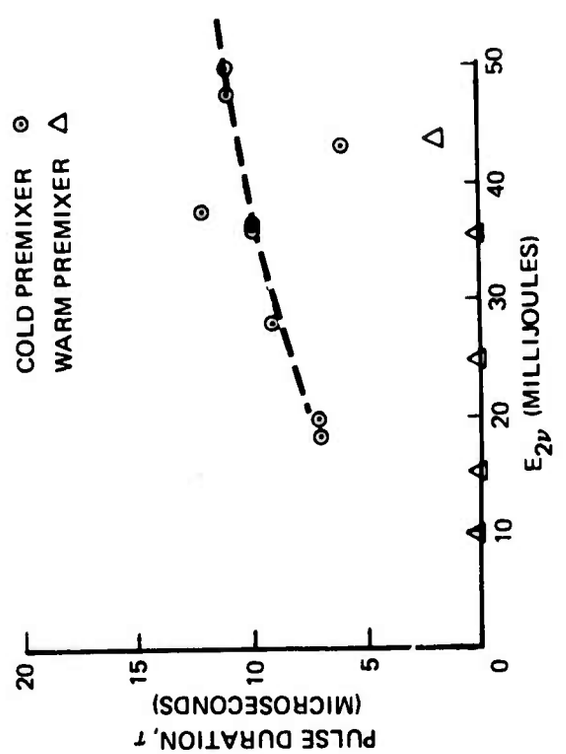

FIGURE 35. IP(4) PULSE DURATION,
$F_2 : H_2 : N_2 = 4 : 4 : 40$ TORR

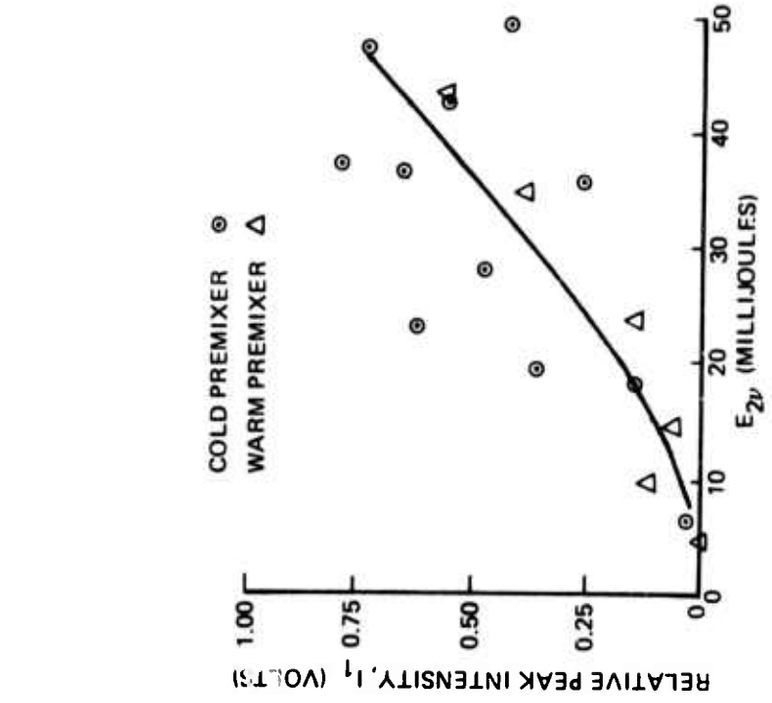

FIGURE 37. 2P(3) PEAK INTENSITY, $F_2 : H_2 : N_2 = 4 : 4 : 40$ TORR

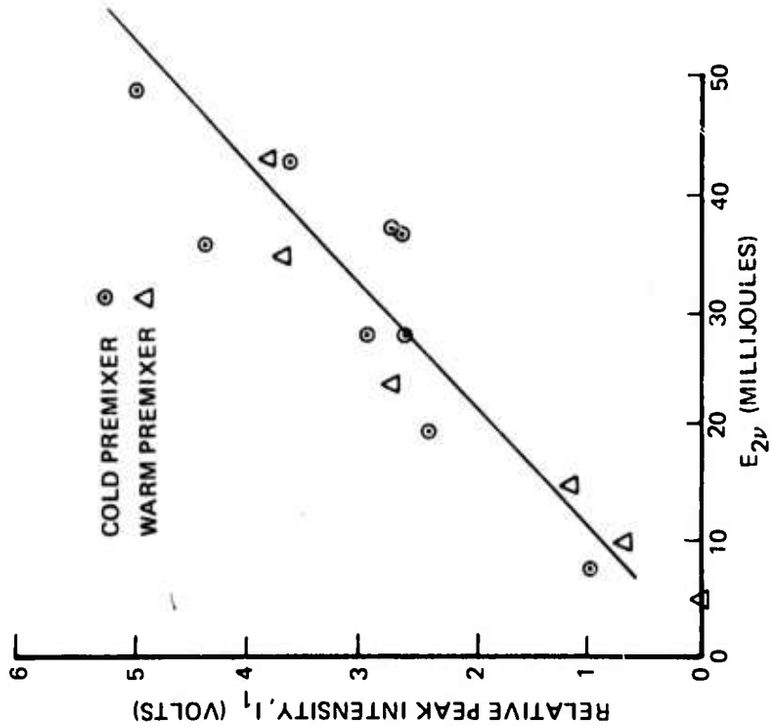

FIGURE 36. TOTAL–POWER PEAK INTENSITY, $F_2 : H_2 : N_2 = 4 : 4 : 40$ TORR

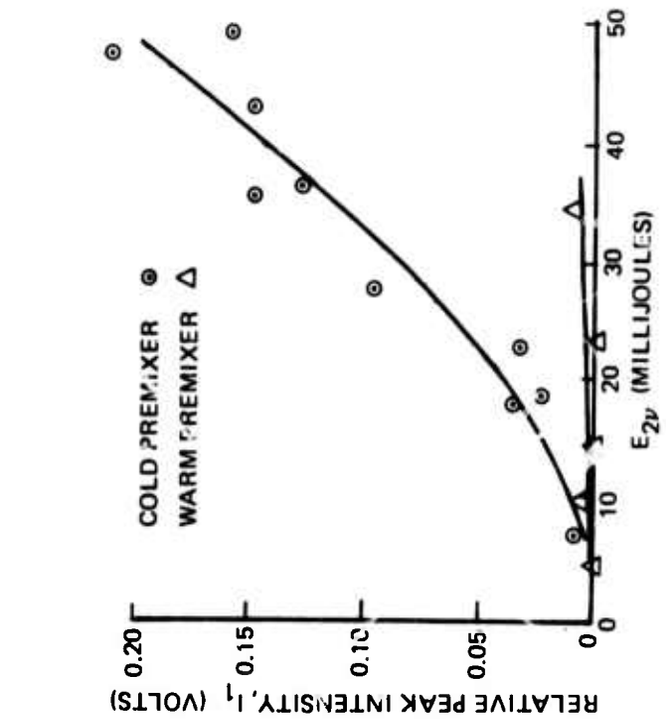

FIGURE 39. 2P(5) PEAK INTENSITY, $F_2 : H_2 : N_2 = 4 : 4 : 40$ TORR

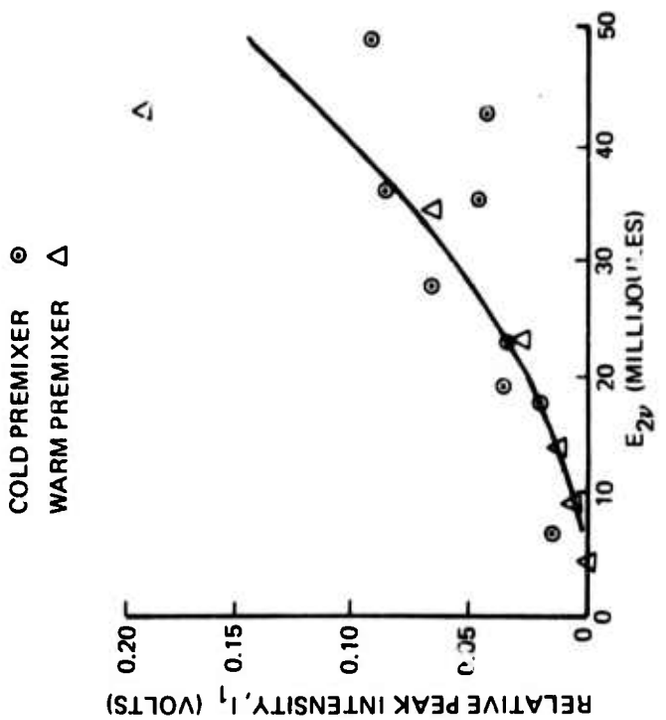

FIGURE 38. 2P(4) PEAK INTENSITY, $F_2 : H_2 : N_2 = 4 : 4 : 40$ TORR

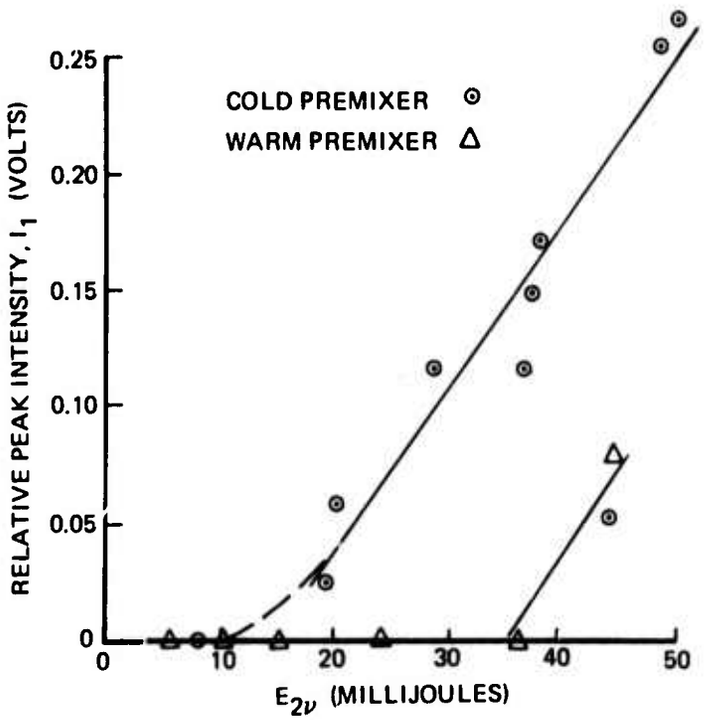

FIGURE 40. 1P(4) PEAK INTENSITY, $F_2 : H_2 : N_2 = 4 : 4 : 40$ TORR

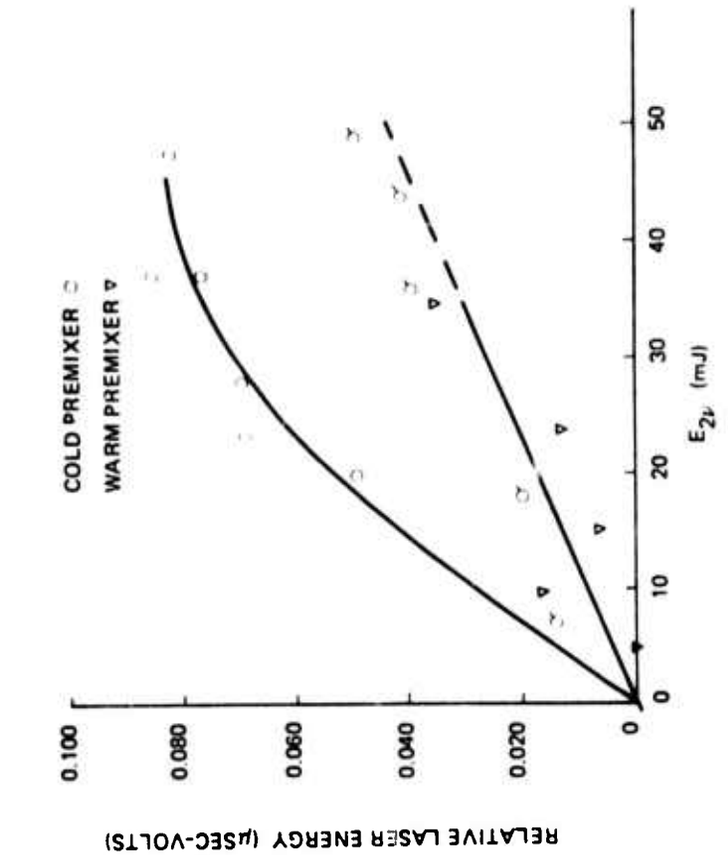

FIGURE 42. 2P(3) RELATIVE ENERGY, $F_2 : H_2 : N_2 = 4 : 4 : 40$ TORR

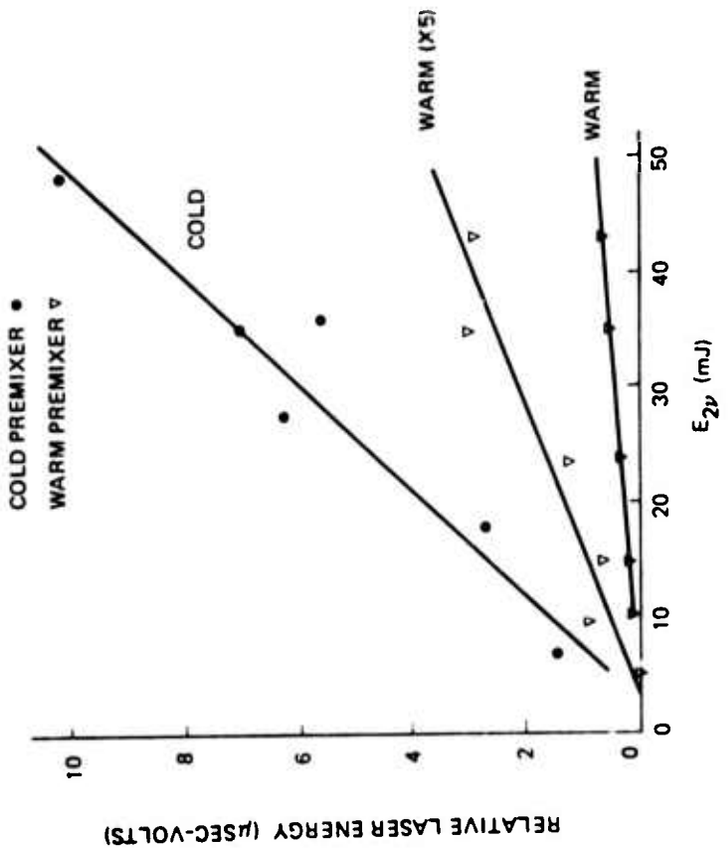

FIGURE 41. TOTAL RELATIVE ENERGY, $F_2 : H_2 : N_2 = 4 : 4 : 40$ TORR

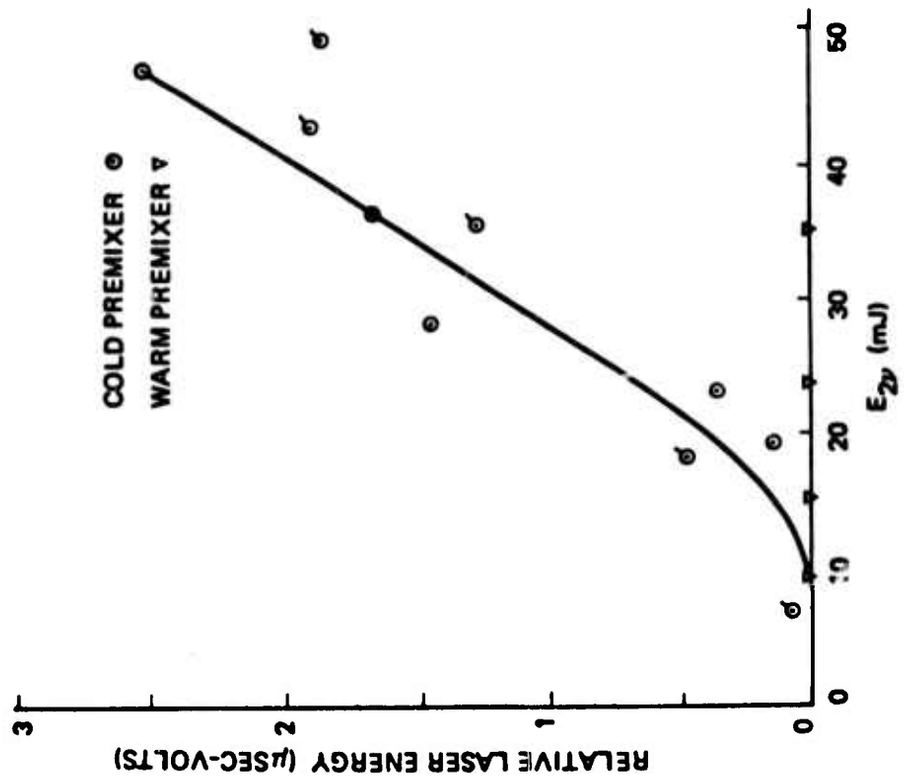

FIGURE 44. 2P(5) RELATIVE ENERGY, $F_2 : H_2 : N_2 = 4 : 4 : 40$ TORR

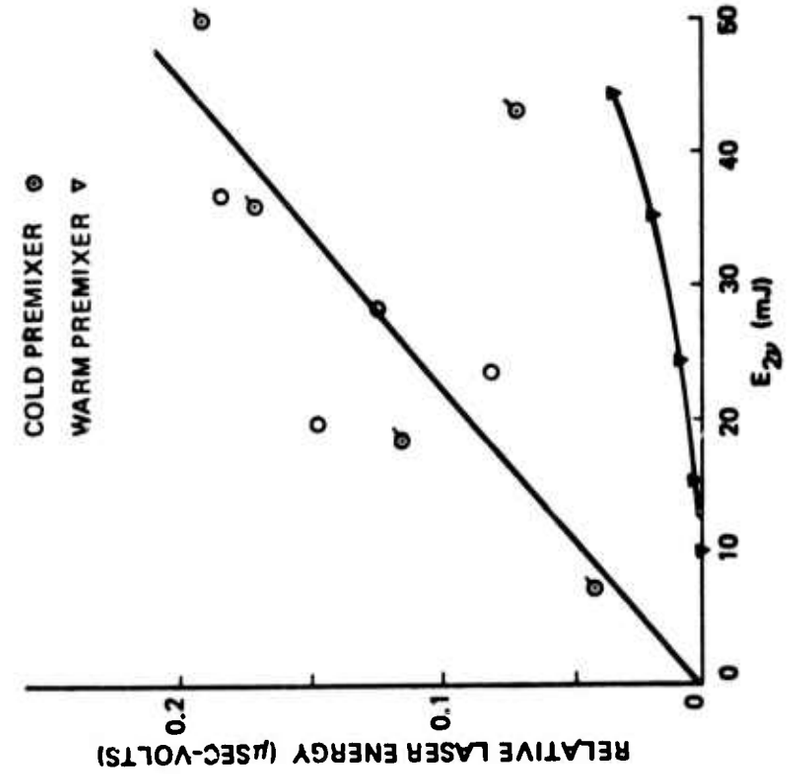

FIGURE 43. 2P(4) RELATIVE ENERGY, $F_2 : H_2 : N_2 = 4 : 4 : 40$ TORR

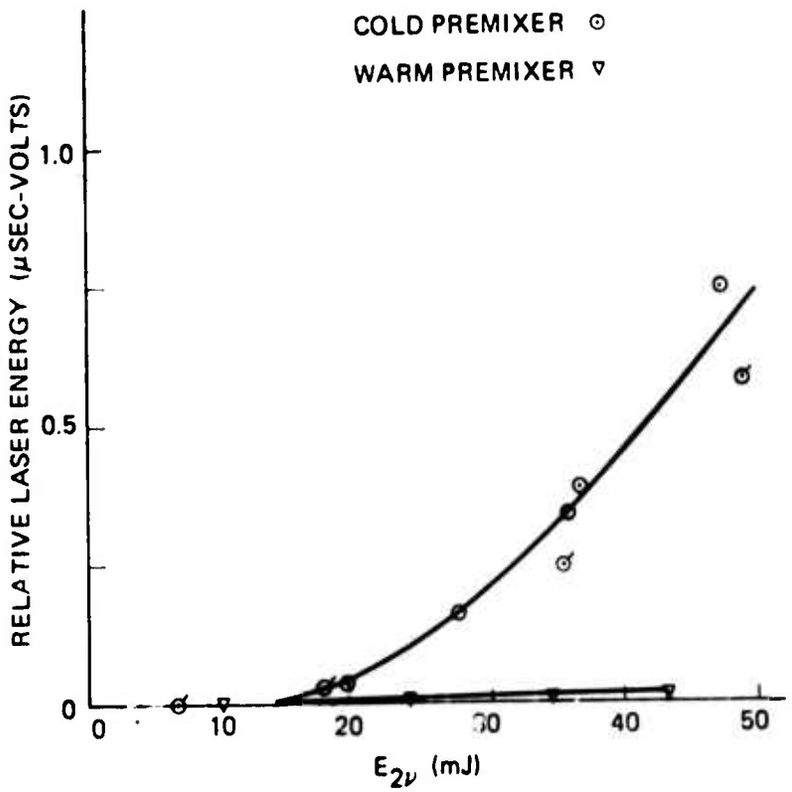

FIGURE 45. 1P(4) RELATIVE ENERGY, $F_2 : H_2 : N_2 = 4 : 4 : 40$ TORR

APPENDIX II

VARIATION OF PROPERTIES OF [HF] LASER EMISSION SPECTRA WITH INITIATING LIGHT $F_2:H_2:N_2$ = 8:8:80 TORR

Figs. 46-65 to follow exhibit detailed properties of total power and single line HF laser emission transients discussed in section V for the initial state $F_2:H_2:N_2$ = 8:8:80 torr. In each case the property is plotted against $E_{2\nu}$, and the figures are grouped to show a specific property in the order: total intensity/1P(5)/1P(6)/2P(3)/2P(4)/2P(5)/2P(6)/3P(2)/3P(5). Figs. 46-50 display initiation time relative to peak 2ν intensity (small negative values occurring in some cases may well be real, although accuracy of oscilloscope time base is not adequate to be definite on this point), Figs. 51-55 observable pulse duration, Figs. 56-60 peak emission intensity, and Figs. 61-65 relative/energy pulse. Principal characteristics of these transient properties are summarized by Fig. 20.

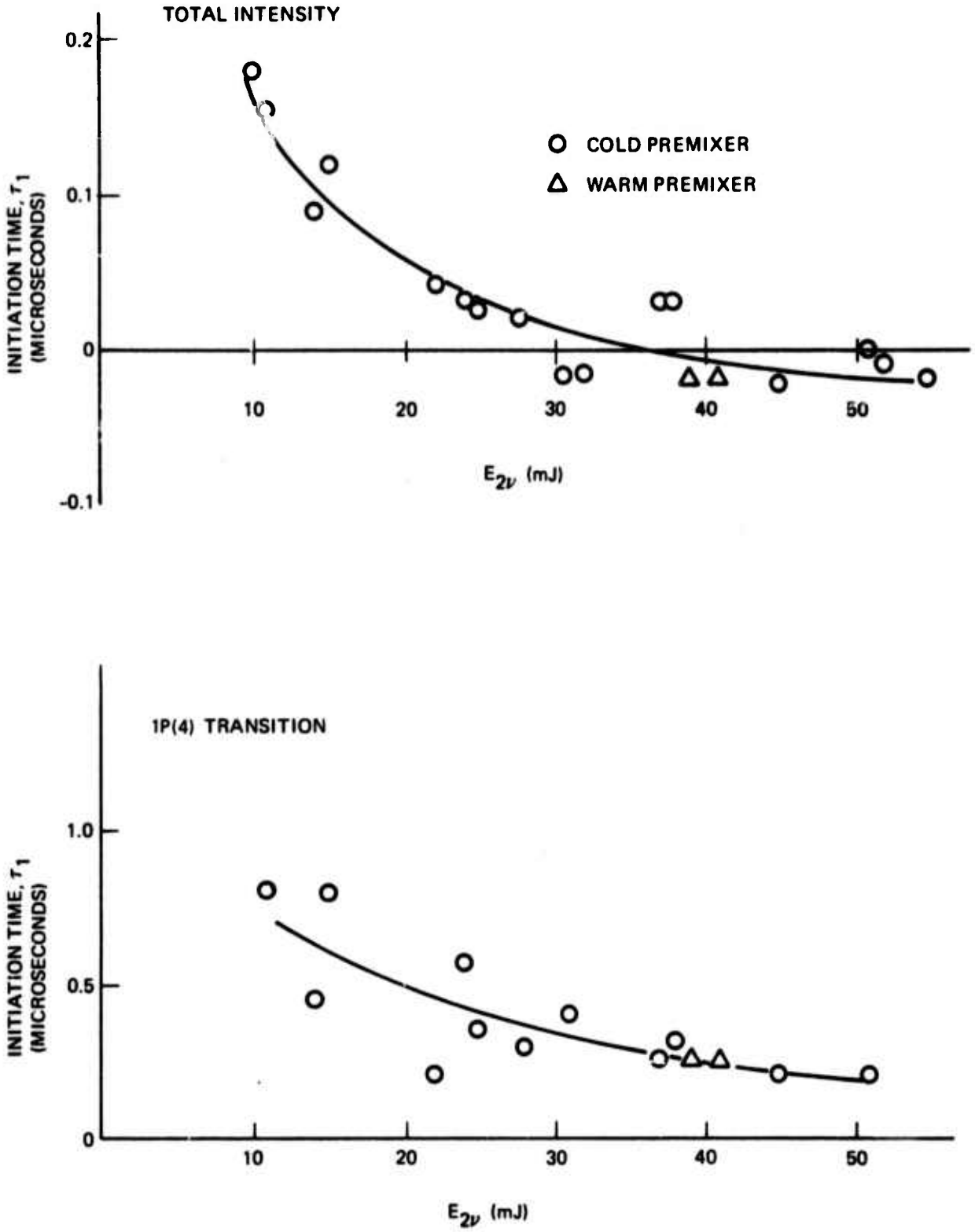

FIGURE 46. TOTAL--POWER AND 1P(4) INITIATION TIME, $F_2 : H_2 : N_2 = 8 : 8 : 80$ TORR

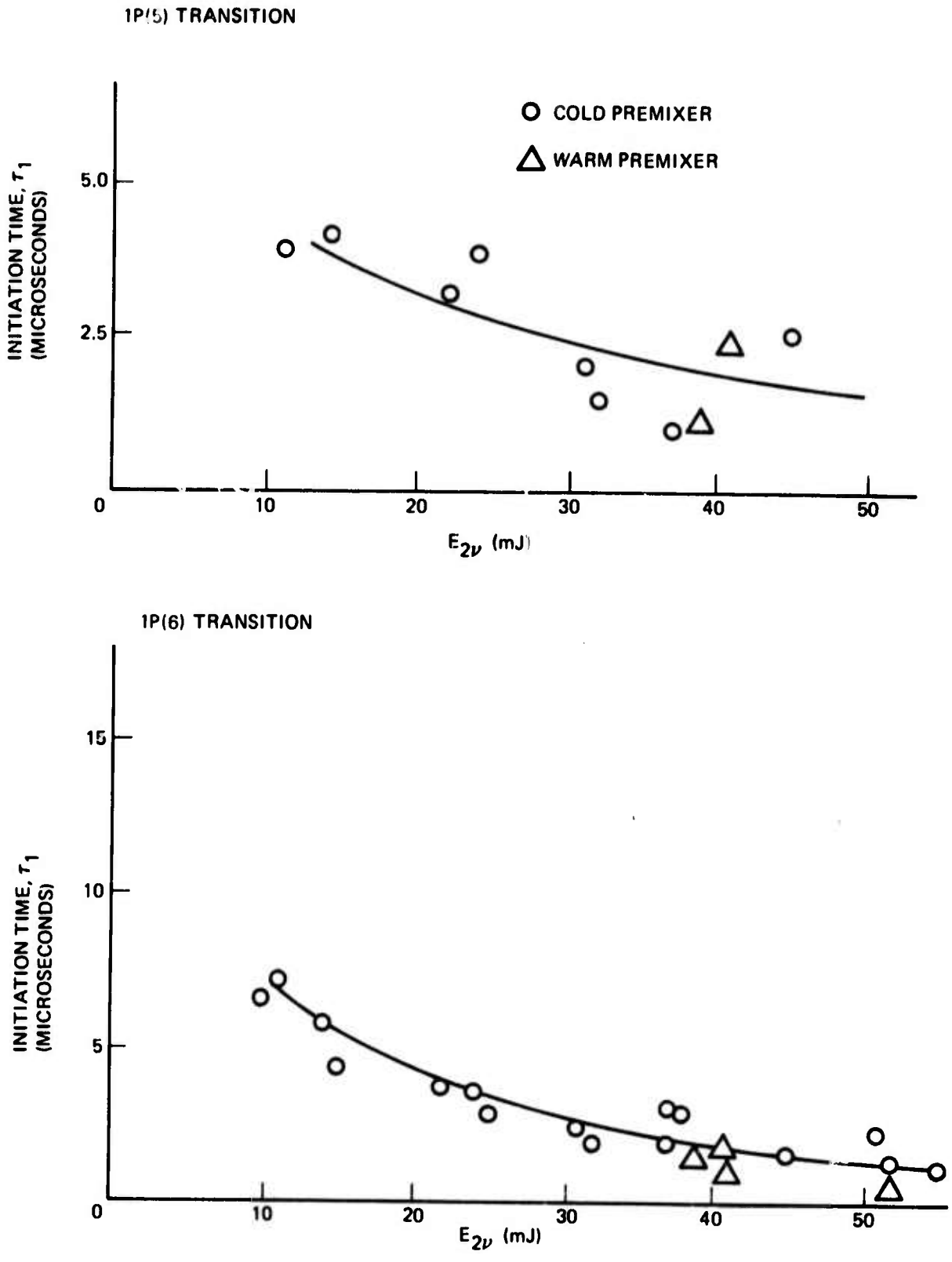

FIGURE 47. 1P(5) AND 1P(6) INITIATION TIME, $F_2 : H_2 : N_2 = 8 : 8 : 80$ TORR

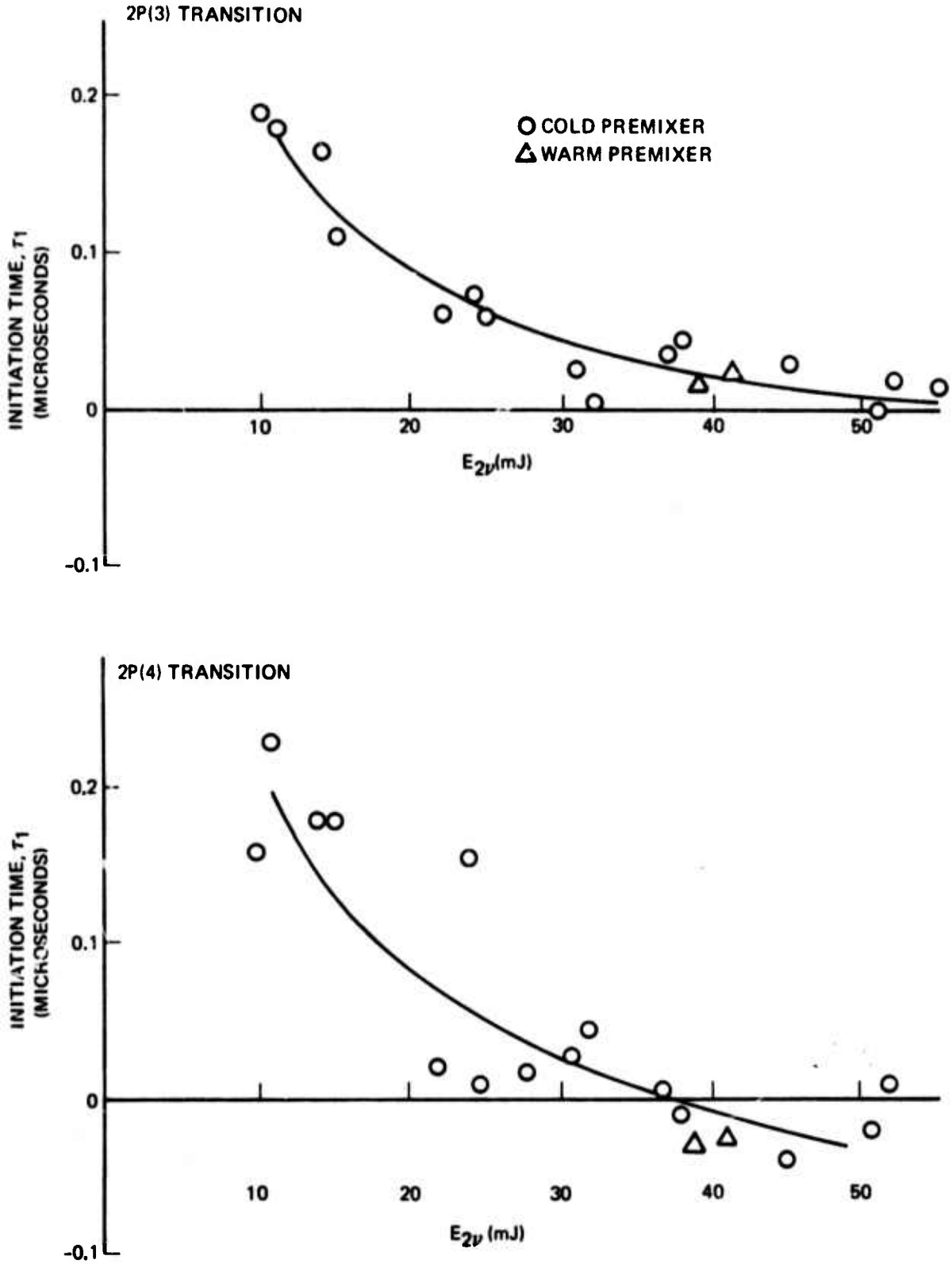

FIGURE 48. 2P(3) AND 2P(4) INITIATION TIME, $F_2 : H_2 : N_2 = 8 : 8 : 80$ TORR

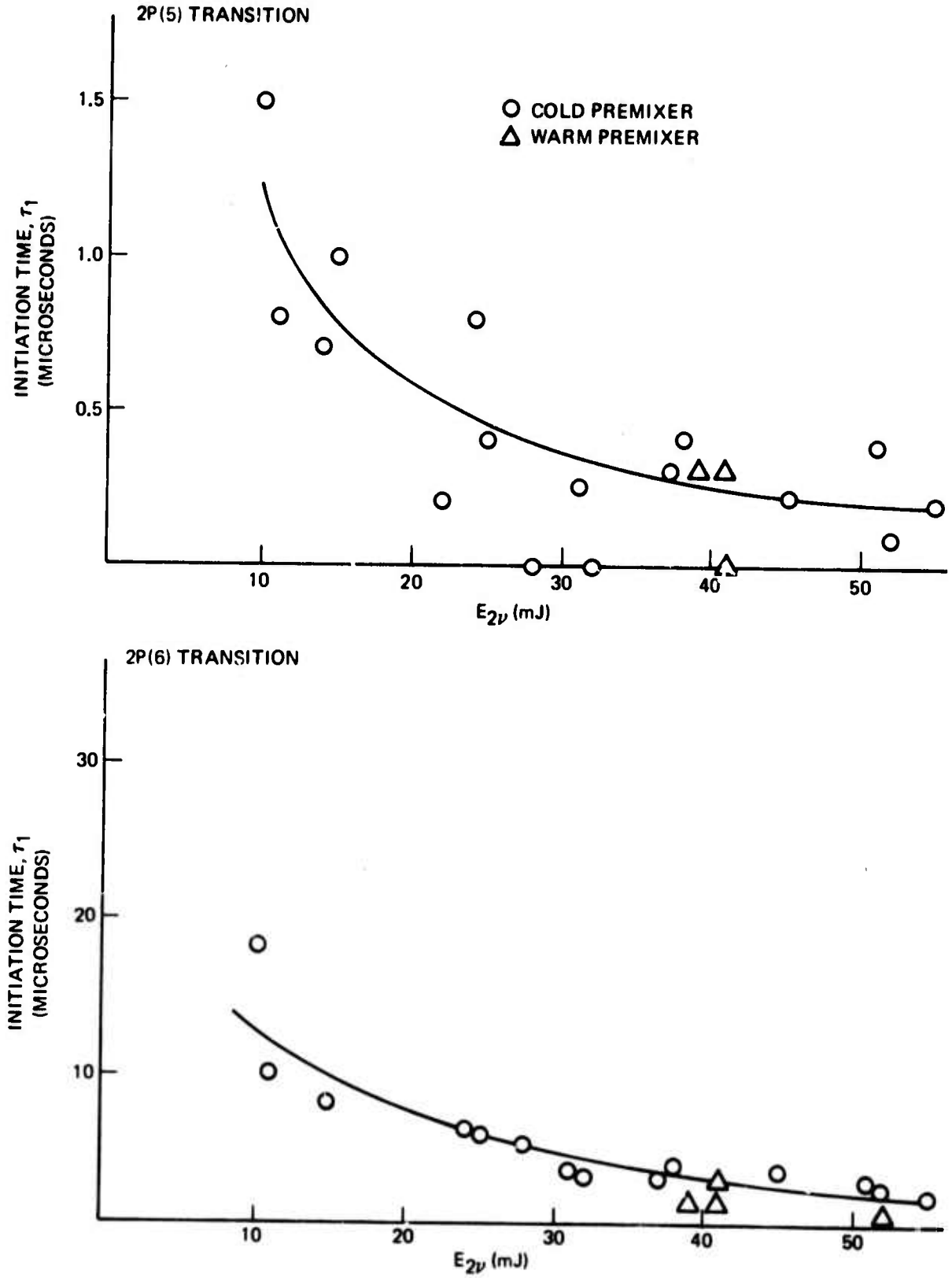

FIGURE 49. 2P(5) AND 2P(6) INITIATION TIME, $F_2 : H_2 : N_2 = 8 : 8 : 80$ TORR

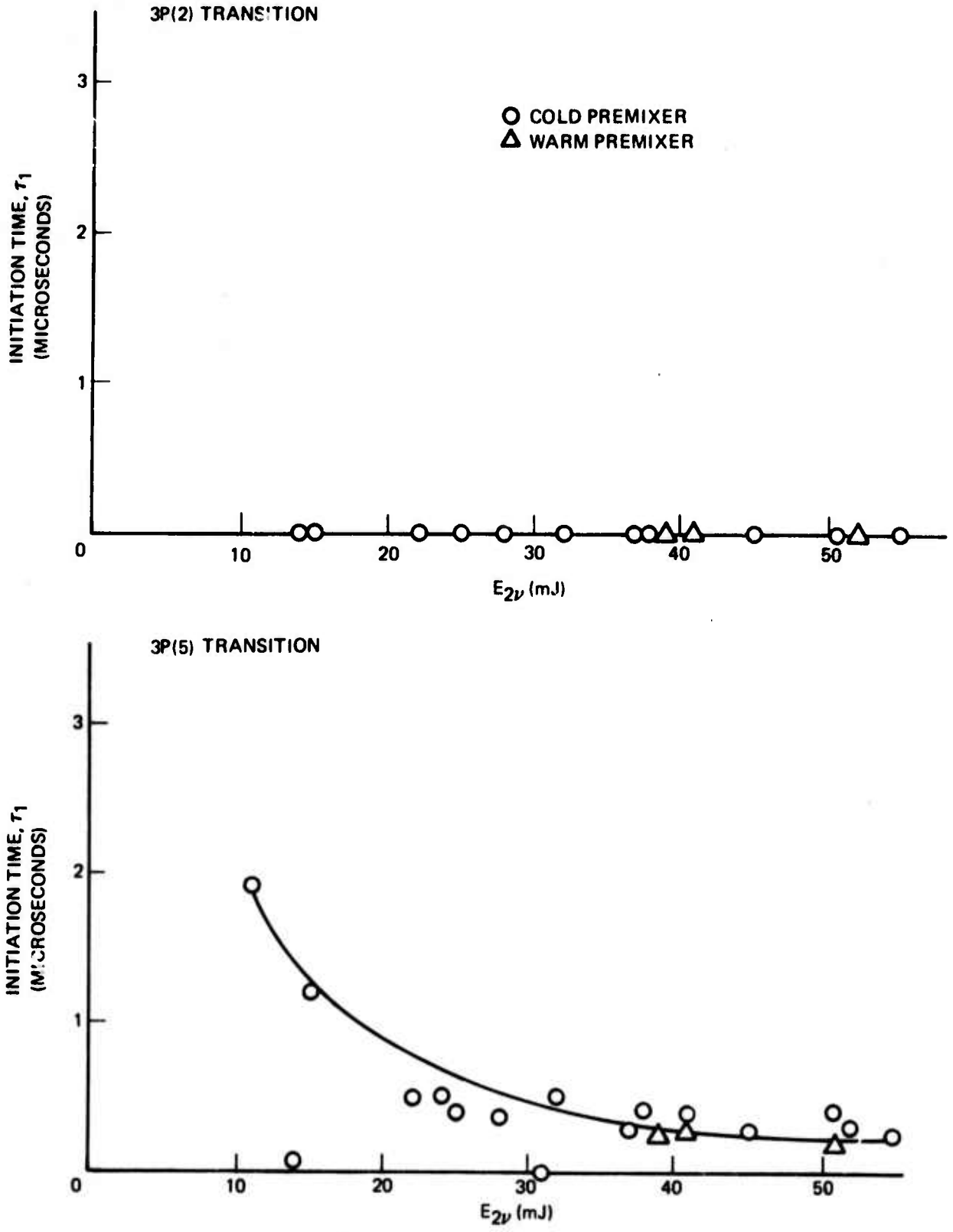

FIGURE 50. 3P(2) AND 3P(5) INITIATION TIME, $F_2 : H_2 : N_2 = 8 : 8 : 80$ TORR

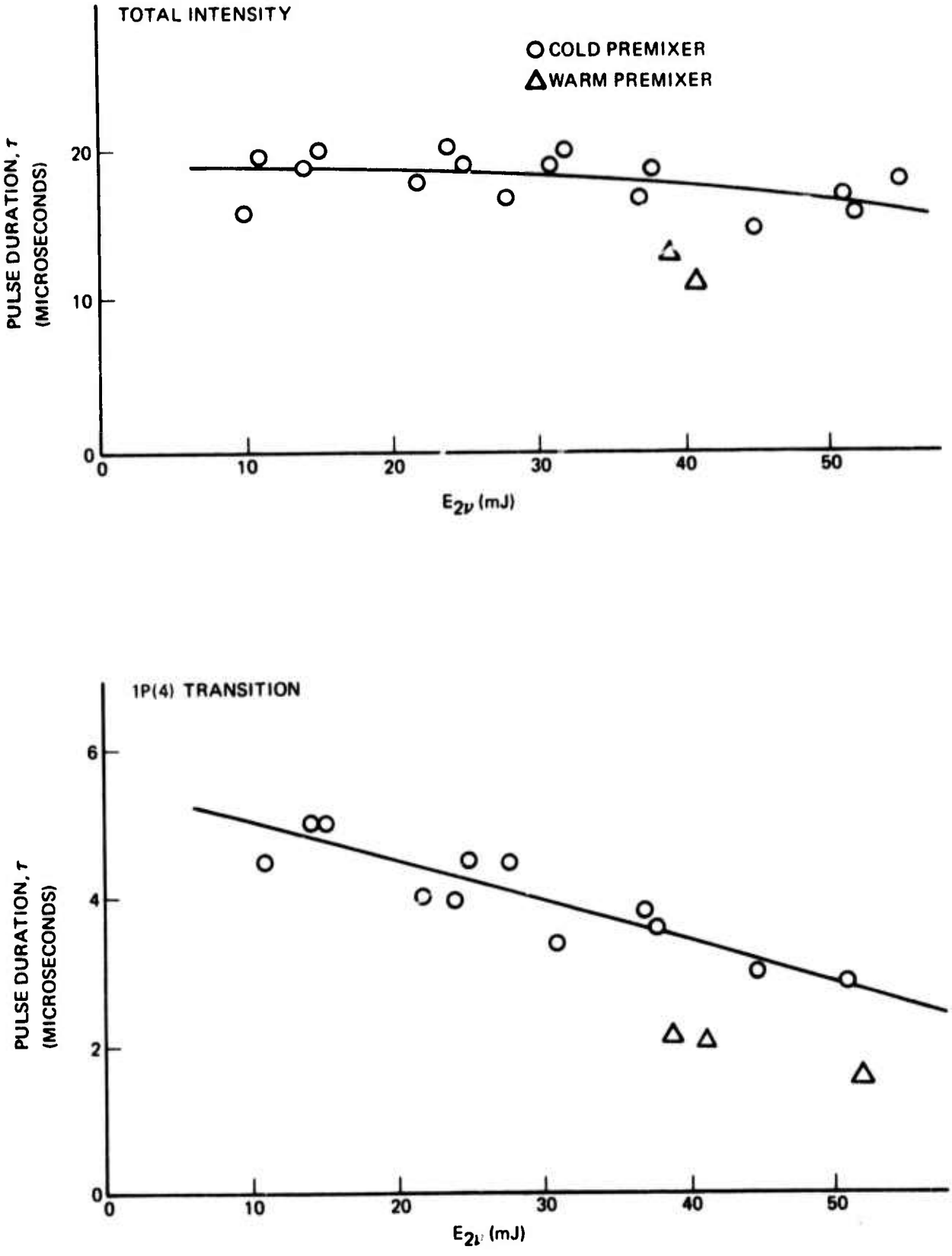

FIGURE 51. TOTAL AND 1P(4) PULSE DURATION, $F_2 : H_2 : N_2 = 8 : 8 : 80$ TORR

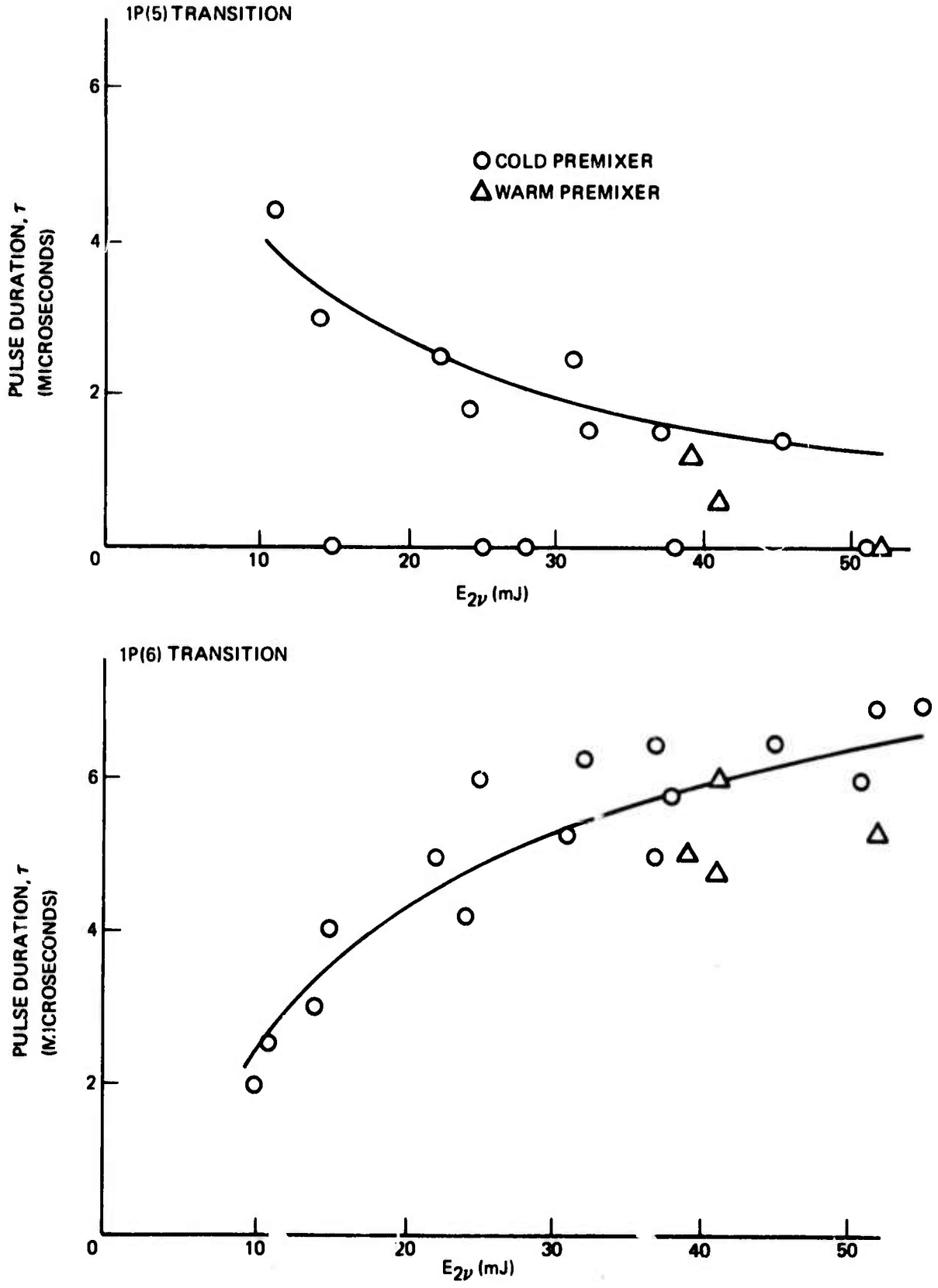

FIGURE 52. 1P(5) AND 1P(6) PULSE DURATION, $F_2 : H_2 : N_2 = 8 : 8 : 80$ TORR

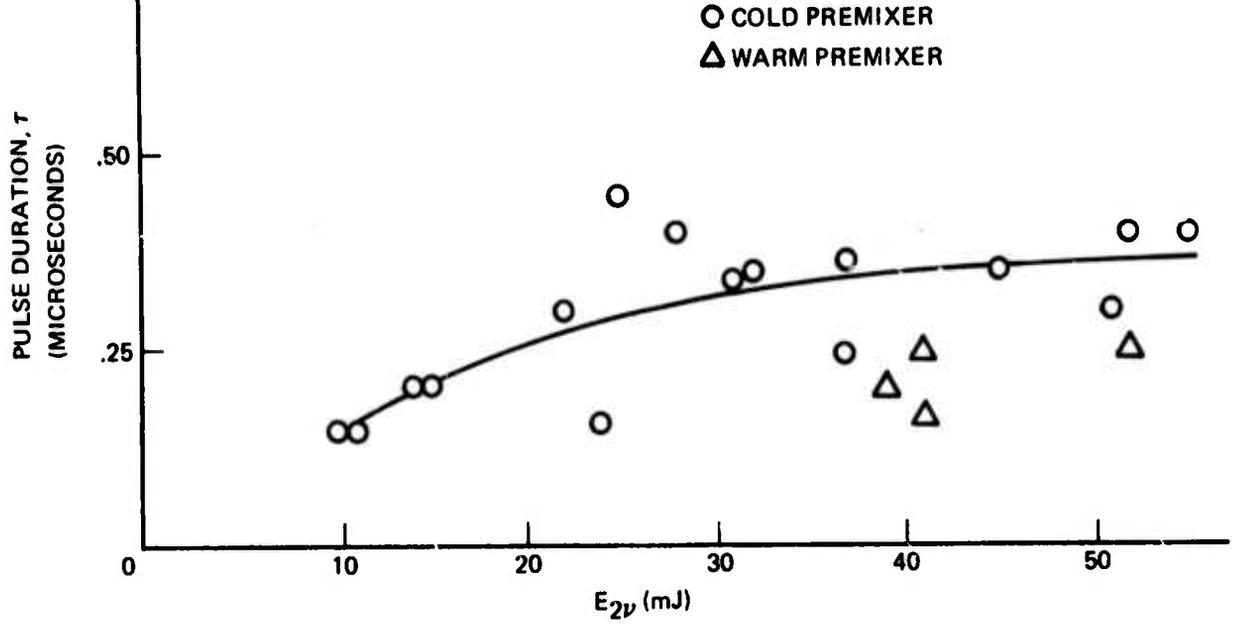

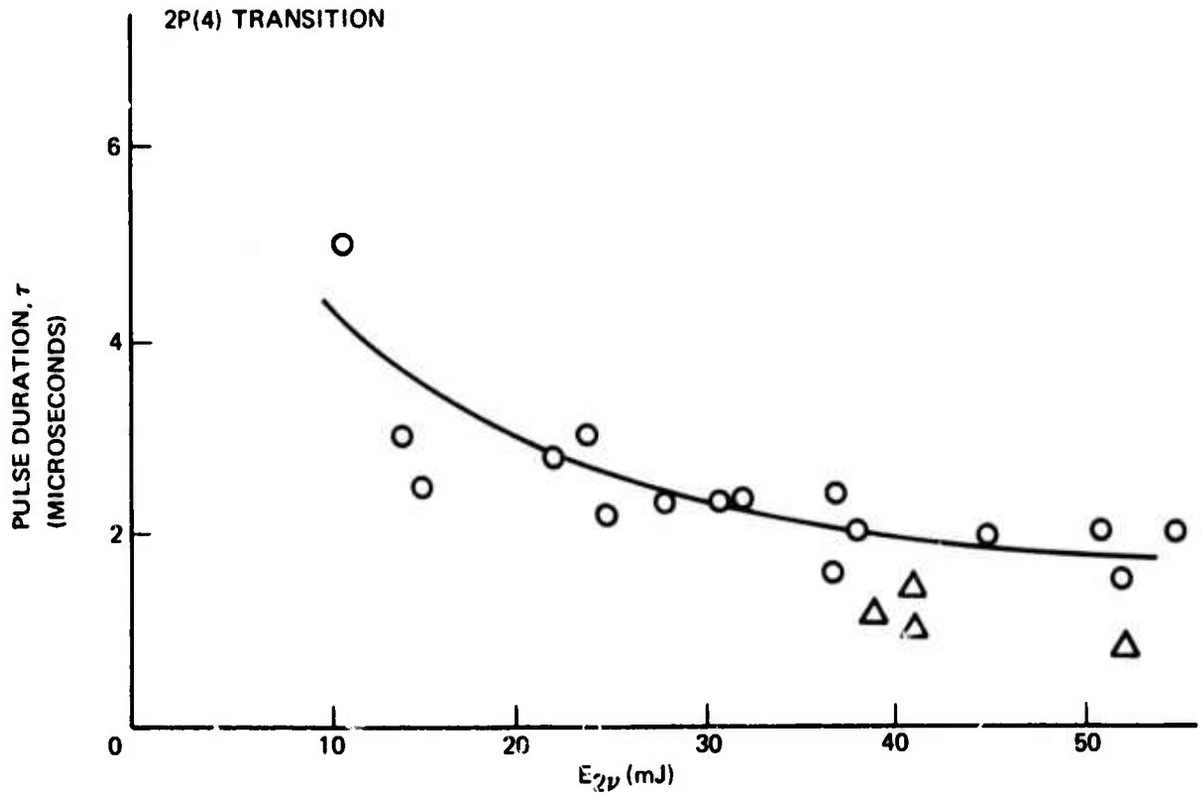

FIGURE 53. 2P(3) AND 2P(4) PULSE DURATION, $F_2 : H_2 : N_2 = 8 : 8 : 80$ TORR

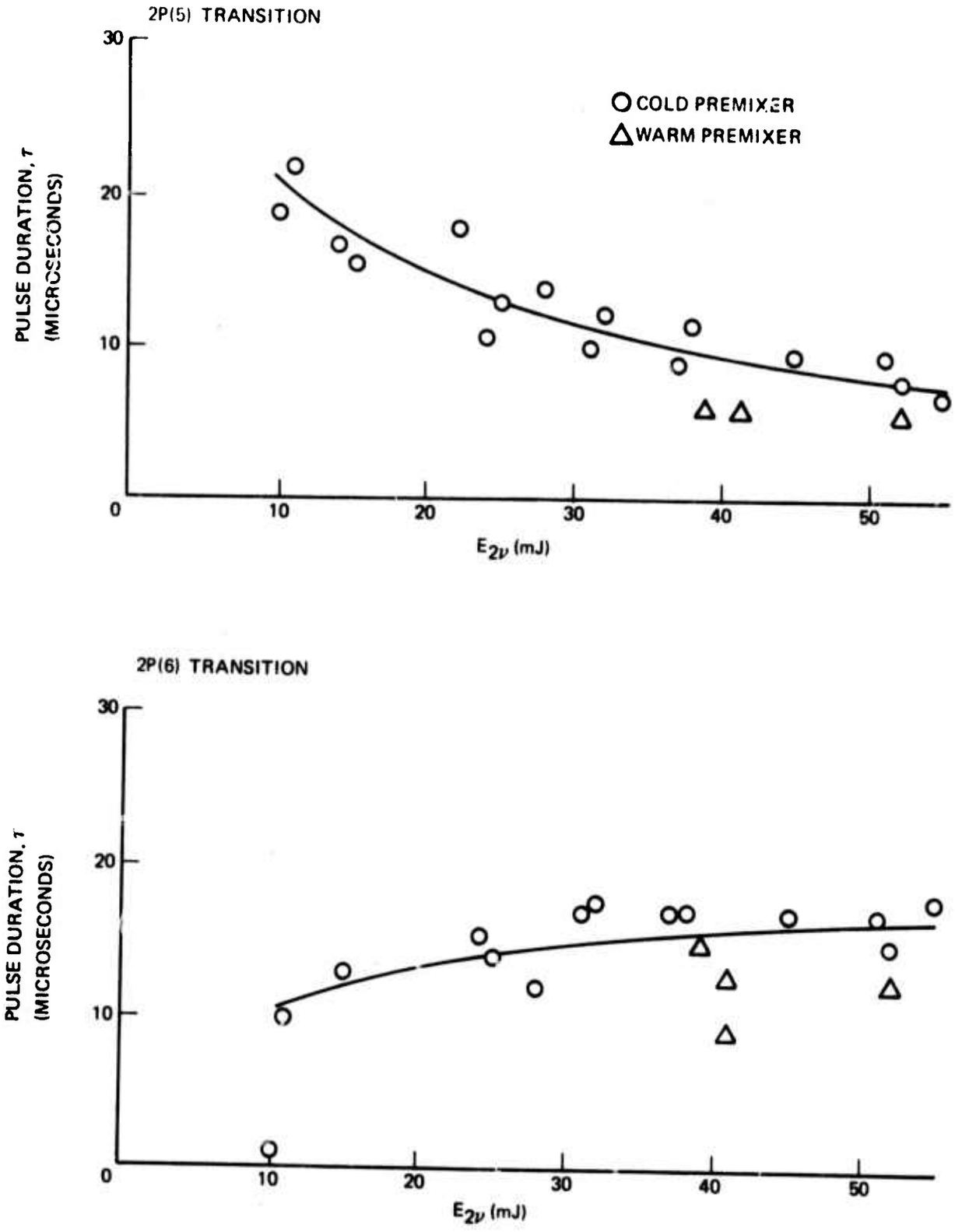

FIGURE 54. 2P(5) AND 2P(6) PULSE DURATION, $F_2 : H_2 : N_2 = 8 : 8 : 80$ TORR

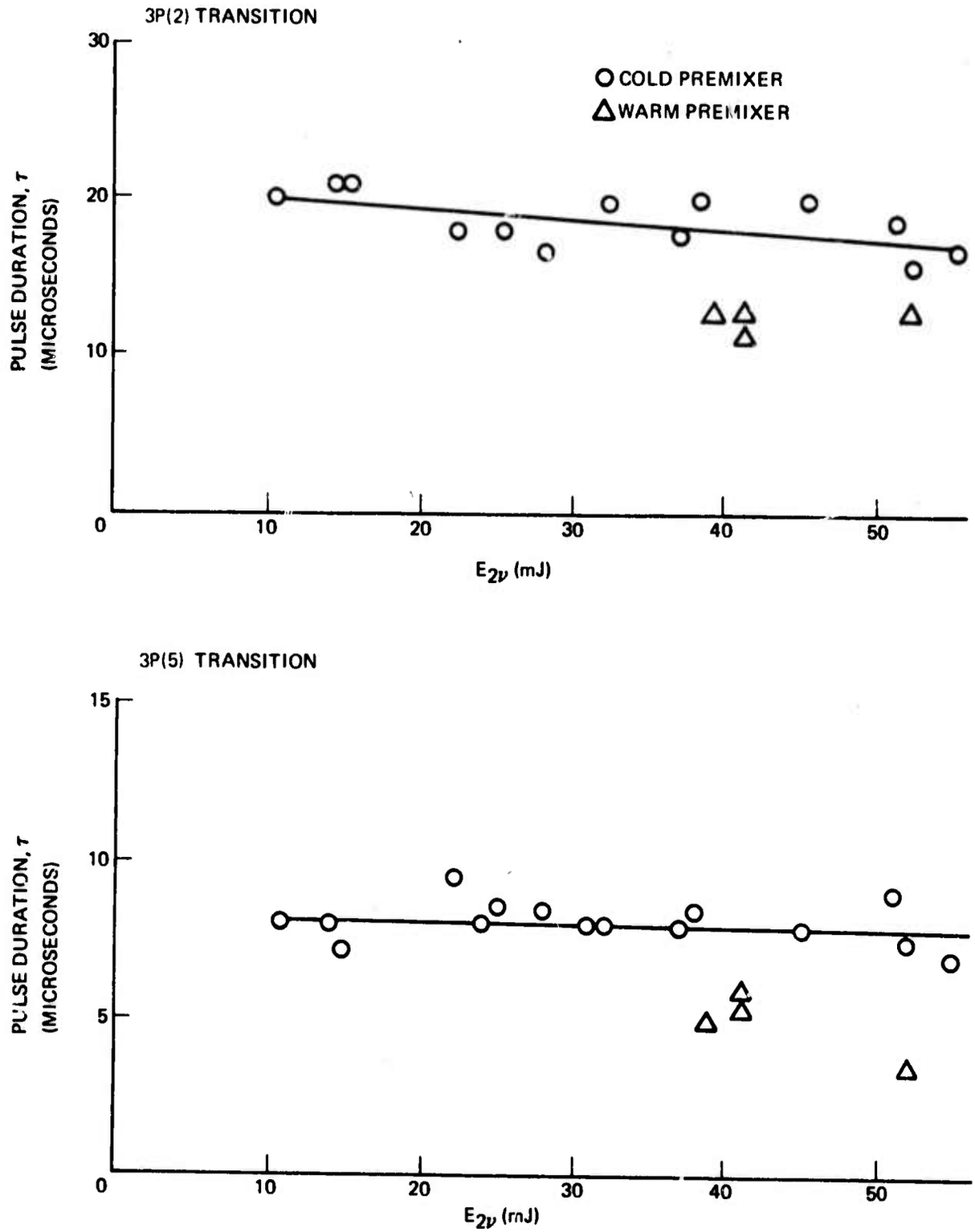

FIGURE 55. 3P(2) AND 3P(5) PULSE DURATION, $F_2 : H_2 : N_2 = 8 : 8 : 80$ TORR

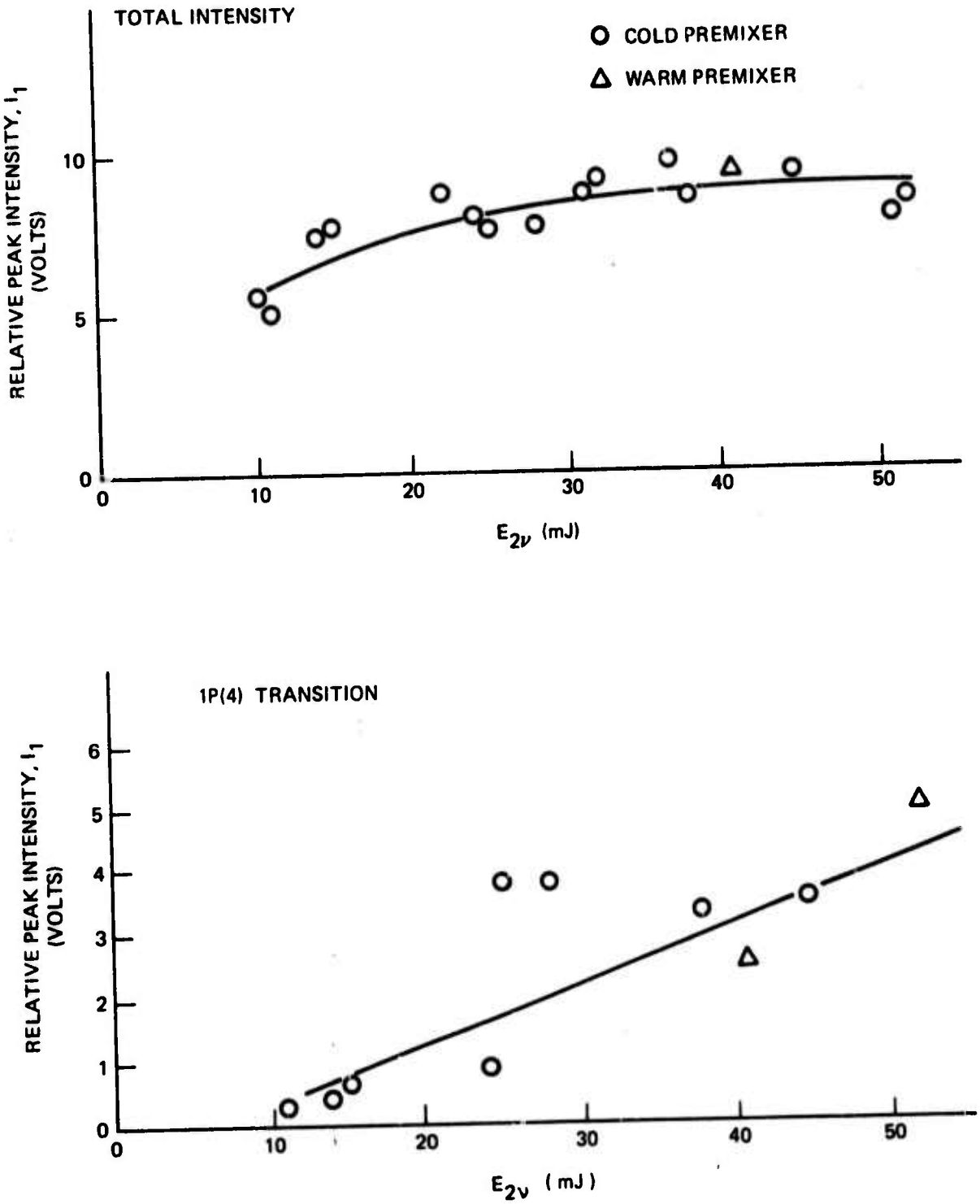

FIGURE 56. TOTAL AND 1P(4) PEAK INTENSITY, $F_2 : H_2 : N_2 = 8 : 8 : 80$ TORR

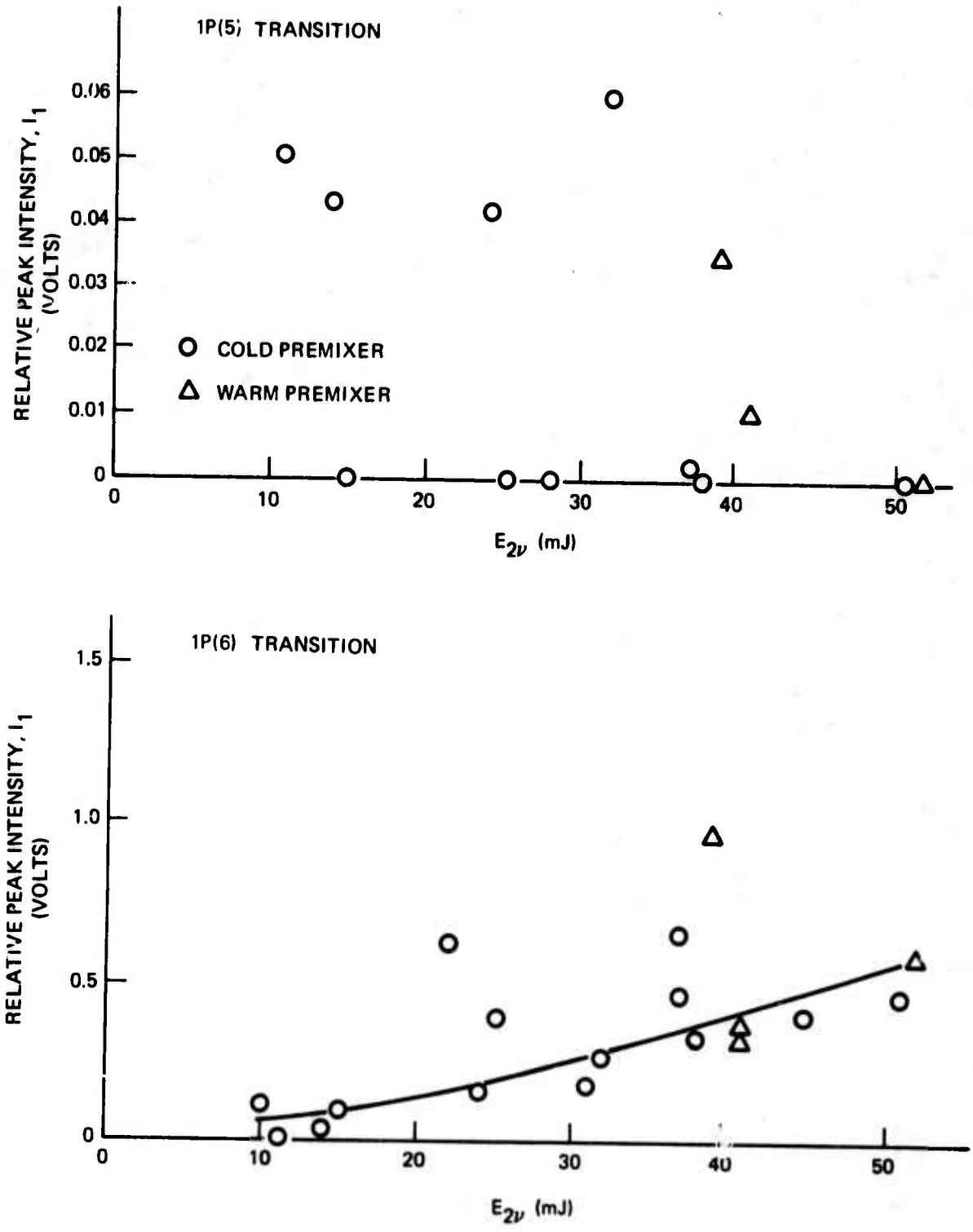

FIGURE 57. 1P(5) AND 1P(6) PEAK INTENSITY, $F_2 : H_2 : N_2 = 8 : 8 : 80$ TORR

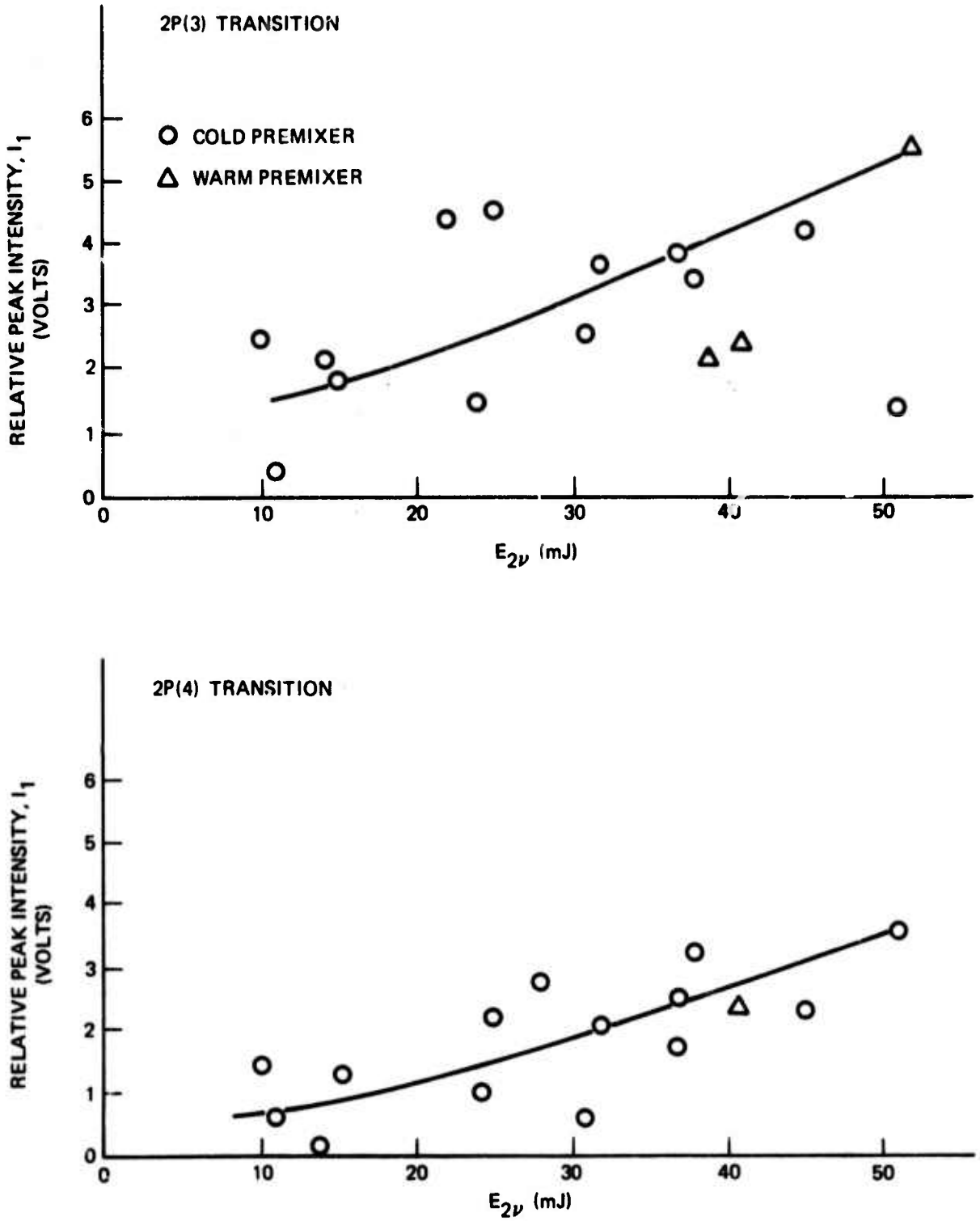

FIGURE 58. 2P(3) AND 2P(4) PEAK INTENSITY, $F_2 : H_2 : N_2 = 8 : 8 : 80$ TORR

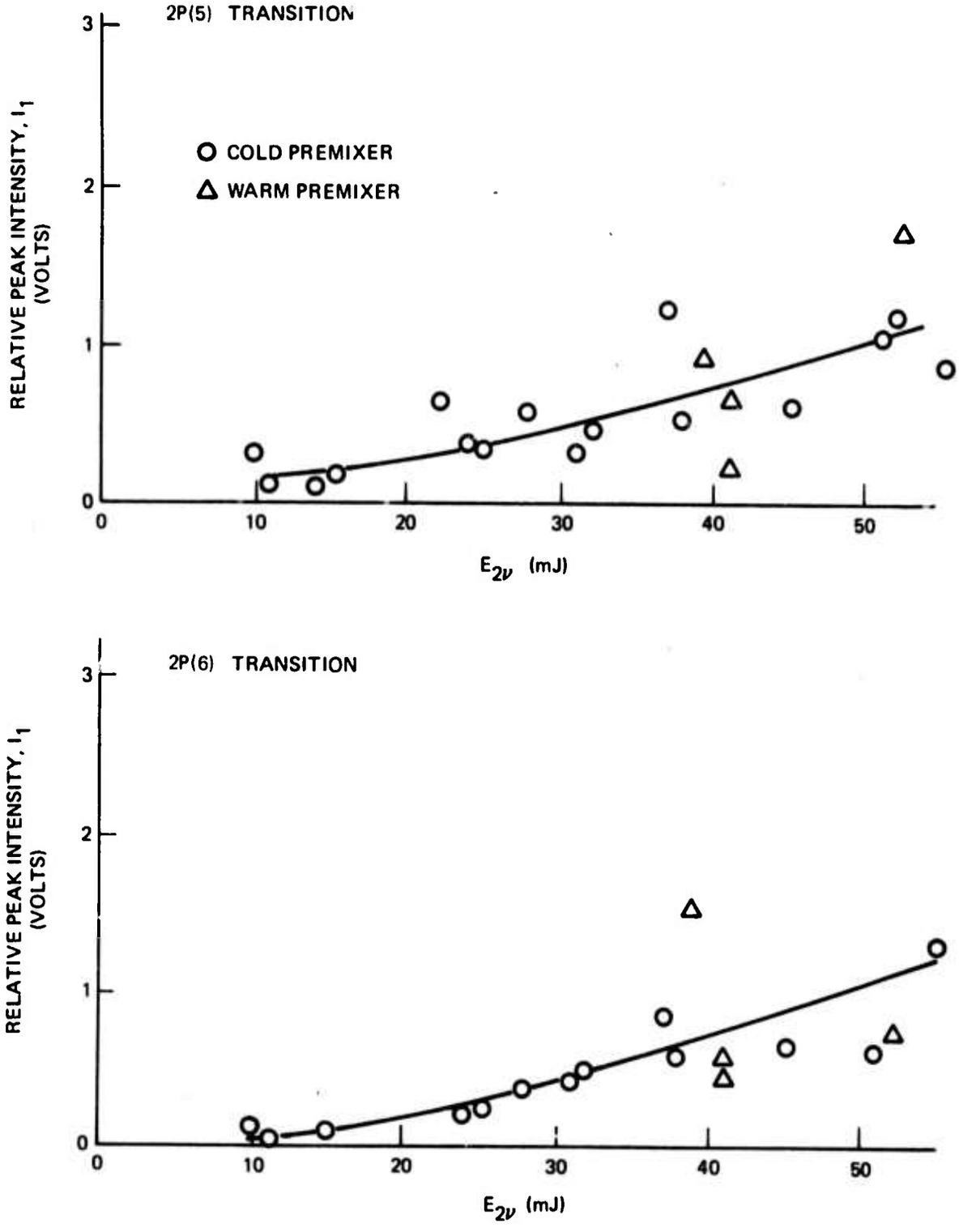

FIGURE 59. 2P(5) AND 2P(6) PEAK INTENSITY, $F_2 : H_2 : N_2 = 8 : 8 : 80$ TORR

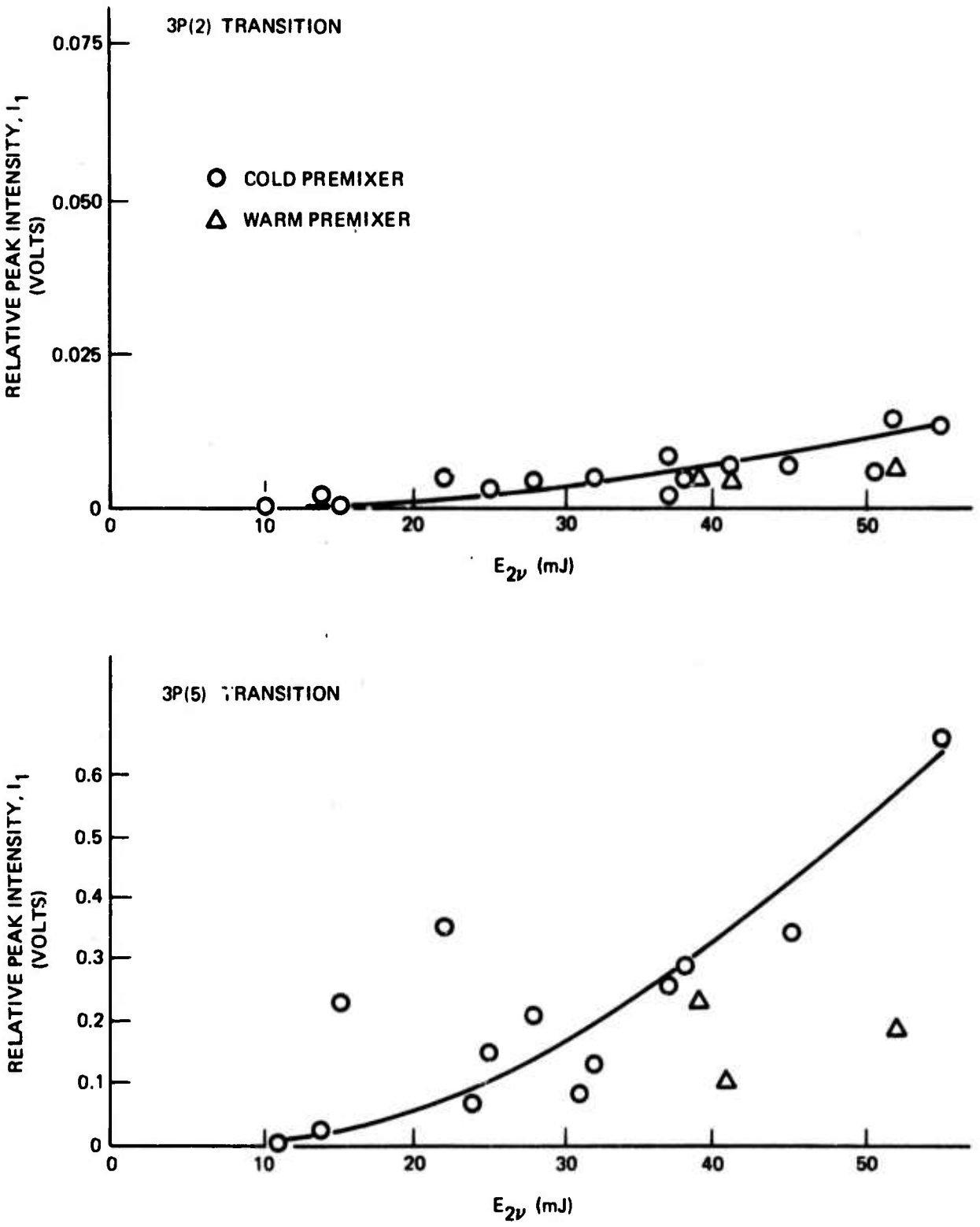

FIGURE 60. 3P(2) AND 3P(5) PEAK INTENSITY, $F_2 : H_2 : N_2 = 8 : 8 : 80$ TORR

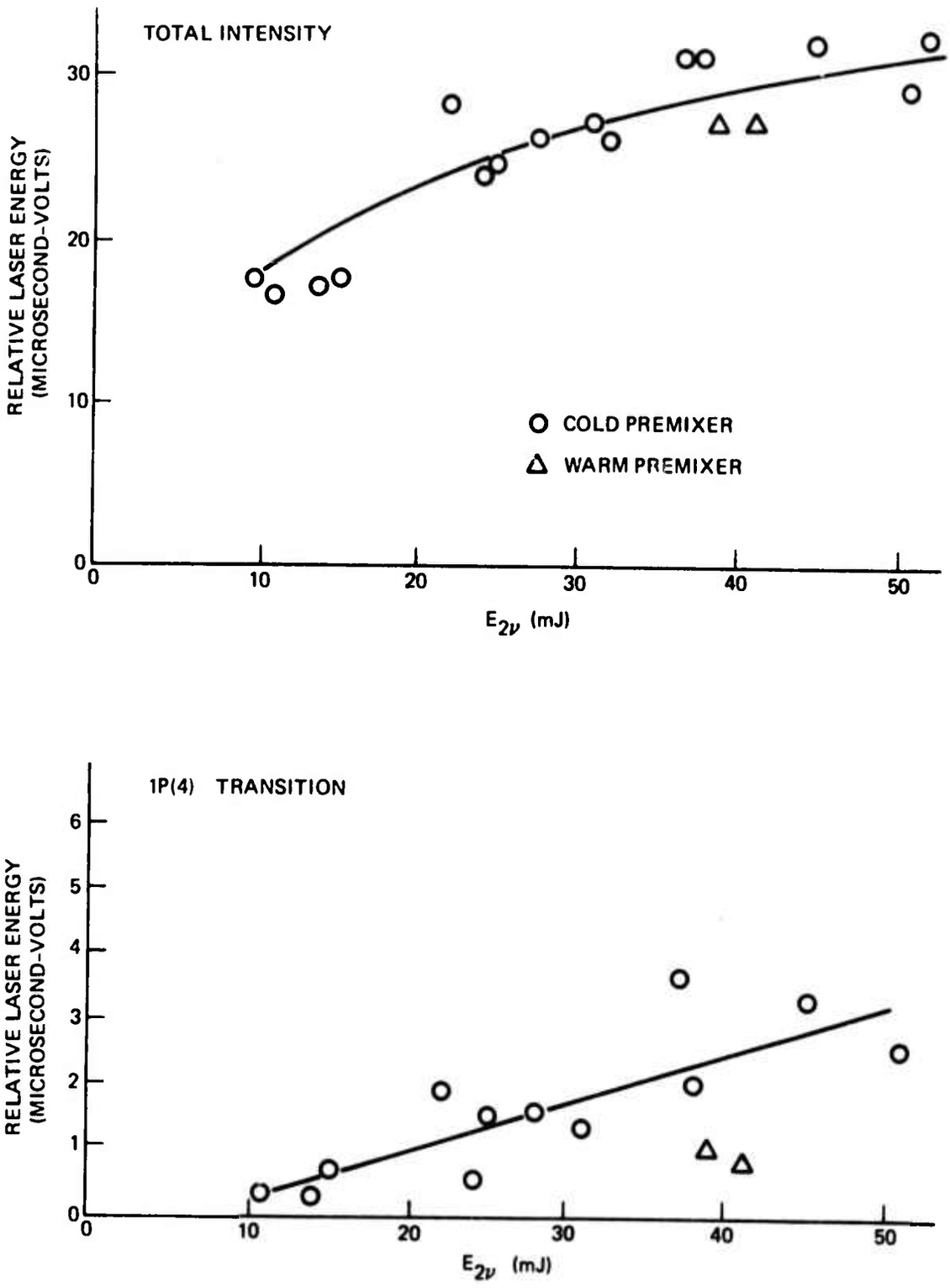

FIGURE 61. TOTAL AND 1P(4) RELATIVE ENERGY, $F_2 : H_2 : N_2 = 8 : 8 : 80$ TORR

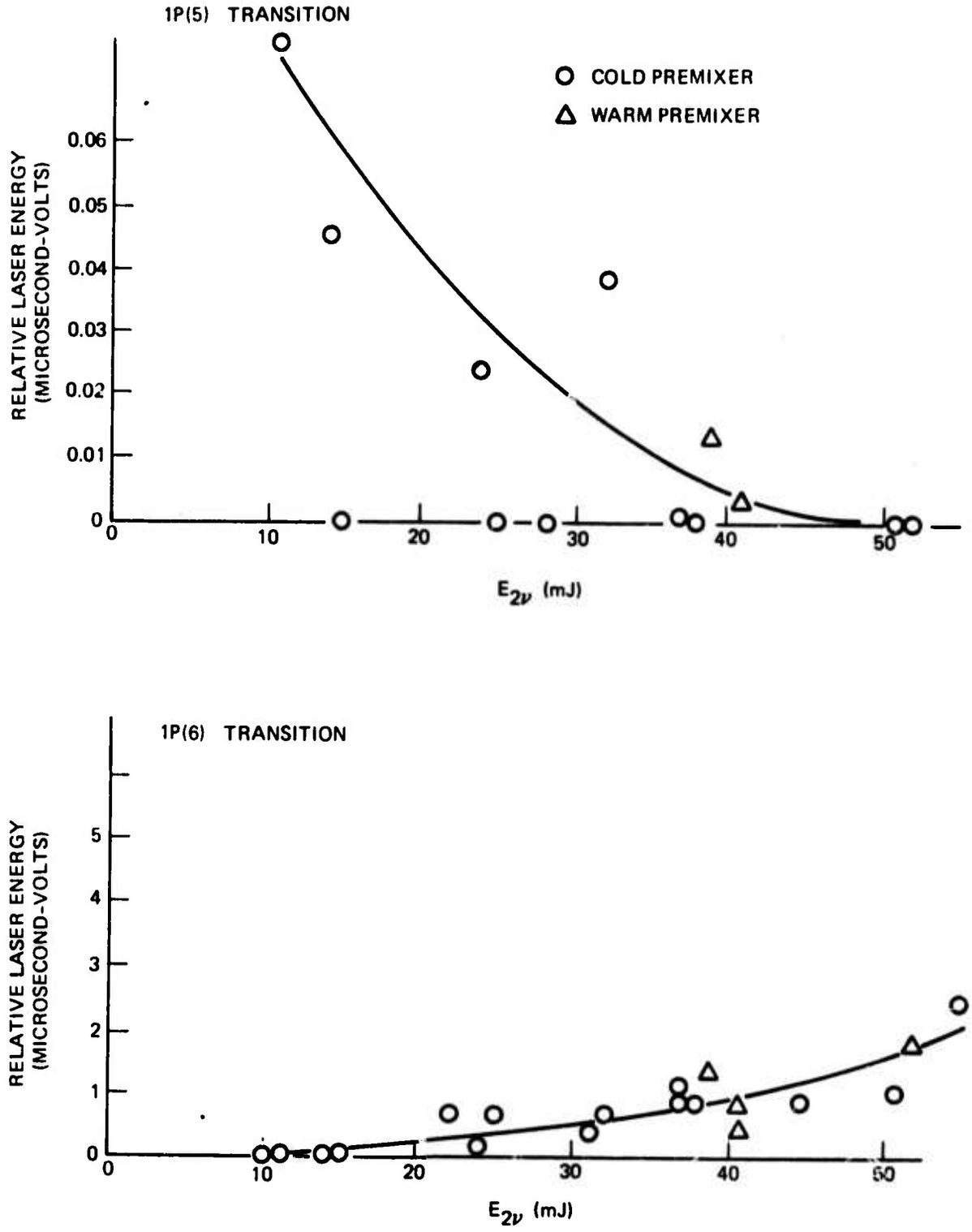

FIGURE 62. 1P(5) AND 1P(6) RELATIVE ENERGY, $F_2 : H_2 : N_2 = 8 : 8 : 80$ TORR

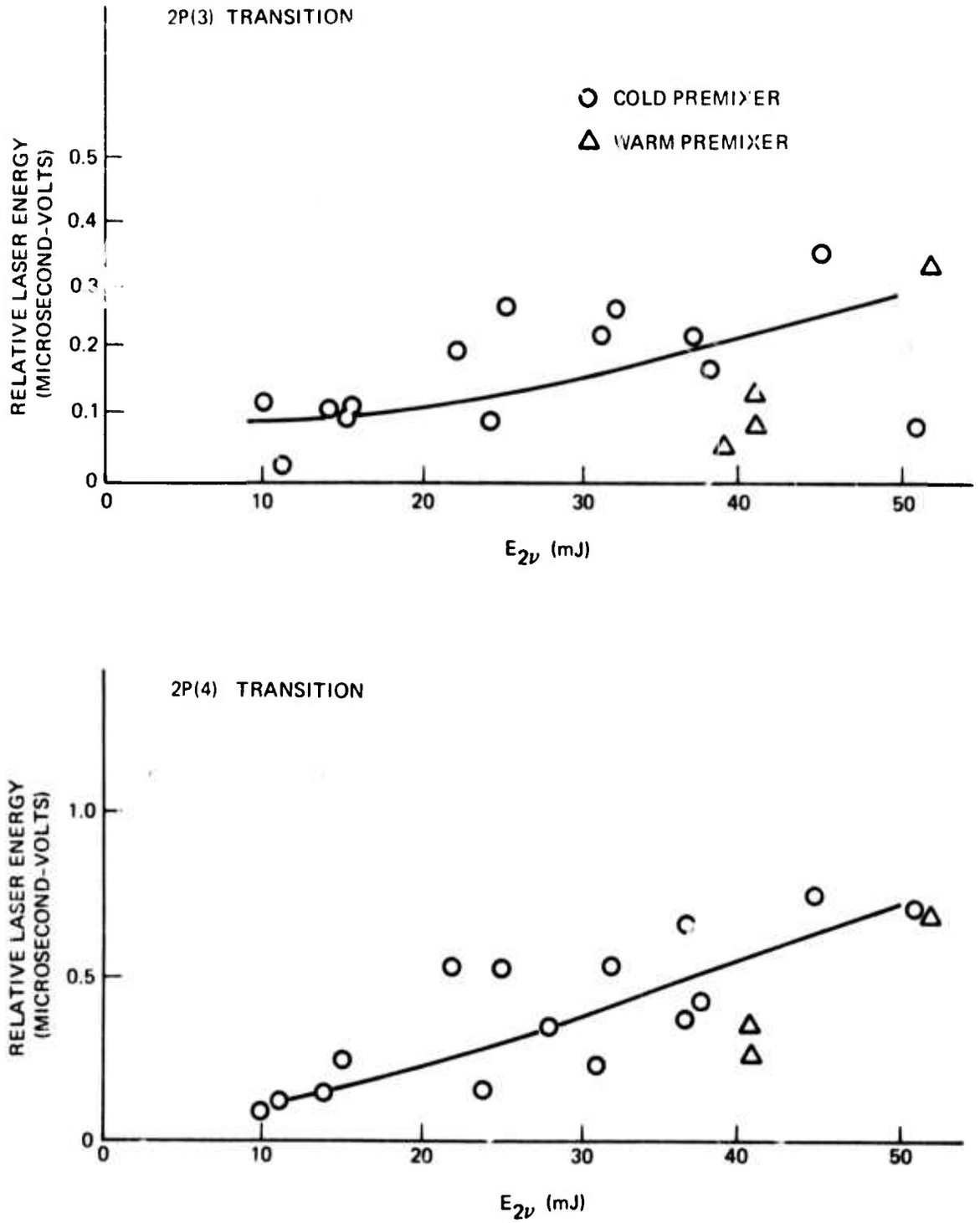

FIGURE 63. 2P(3) AND 2P(4) RELATIVE ENERGY, $F_2 : H_2 : N_2 = 8 : 8 : 80$ TORR

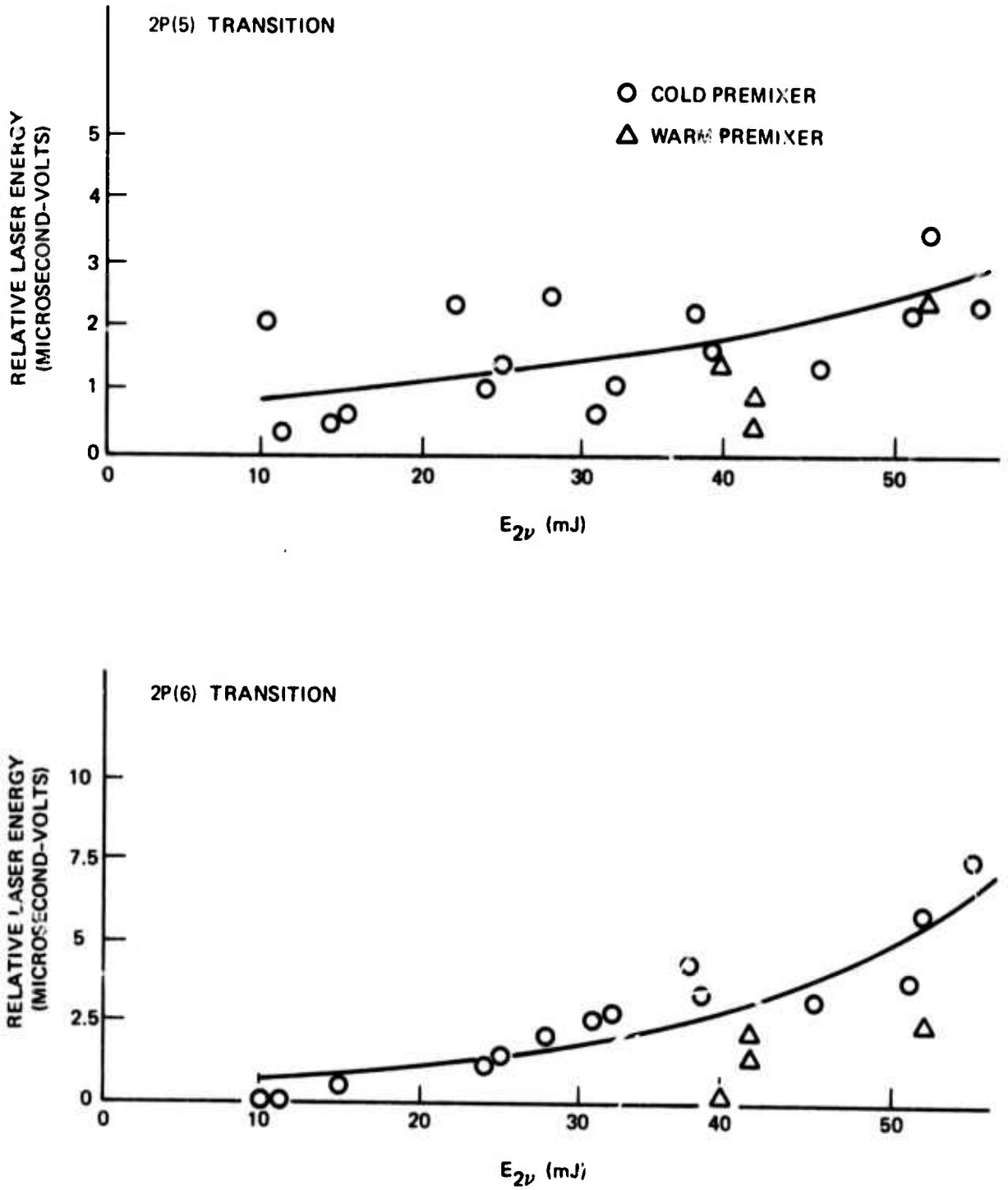

FIGURE 64. 2P(5) AND 2P(6) RELATIVE ENERGY, $F_2 : H_2 : N_2 = 8 : 8 : 80$ TORR

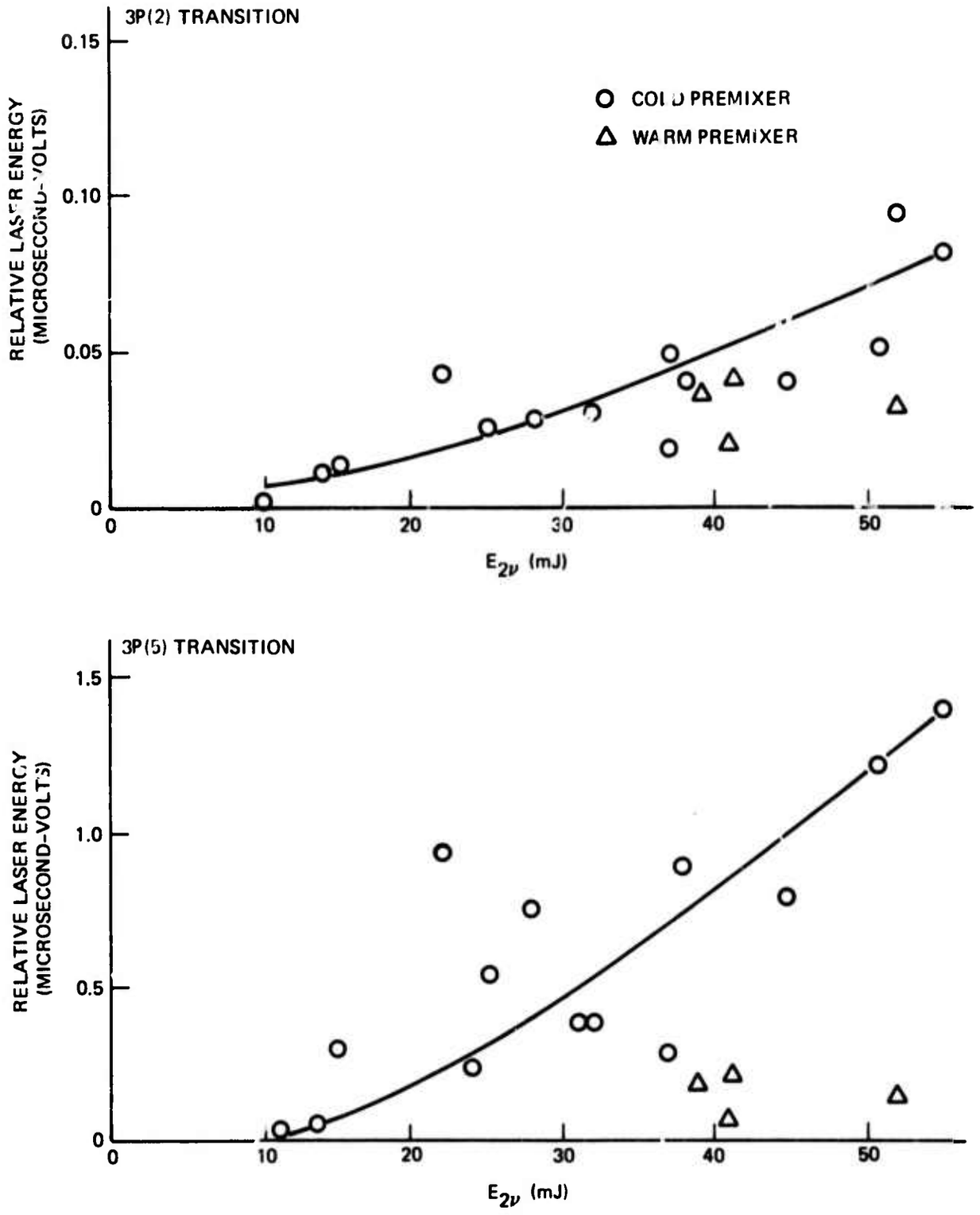

FIGURE 65. 3P(2) AND 3P(5) RELATIVE ENERGY, $F_2 : H_2 : N_2 = 8 : 8 : 80$ TORR

REFERENCES

1. Kasper, J.V.V. ,and Pimentel, G.C., 'HCl Chemical Laser,' Phys. Rev. Letters 14, 352 (1965).

2. Airey, J.R., 'Cl + HBr Pulsed Chemical Laser: A Theoretical and and Experimental Study,' J. Chem. Phys. 52, 156 (1970).

3. Corneil, P.H. ,and Pimentel, G.C., 'Hydrogen-Chlorine Explosion Laser.II. DCl,' J. Chem. Phys. 49, 1379 (1968).

4. Kompa, K.L., Parker, J.H., Pimentel, G.C., 'UF_6-H_2 Hydrogen Fluoride Chemical Laser: Operation and Chemistry,' J. Chem. Phys. 49, 4257 (1968).

5. Parker, J.H. ,and Pimentel, G.C., 'Vibrational Energy Distribution Through Chemical Laser Studies.I. Fluorine Atoms Plus Hydrogen or Methane,' J. Chem. Phys. 51, 91 (1969).

6. Basov, N.G., et al., 'Emission Spectrum of a Chemical Laser Using an H_2 + F_2 Mixture,' ZhETF Pis. Red. 9, 613 (1969).

7. Batovskii, O.M., et al., 'Chemical Laser Operating on Branched Chain Reaction of Fluorine with Hydrogen,' ZhETF Pis. Red. 9, 341 (1968).

8. [redacted]

9. Chester, A.N. ,and Hess, L.D., 'Study of the HF Chemical Laser by Pulse-Delay Measurements,' IEEE J. Quant. Electr. QE-8, 1 (1972).

10. Kerber, R. L., Emanuel, G., and Whittier, J.S., 'Computer Modeling and Parametric Study for a Pulsed H_2 + F_2 Laser,' J. Appl. Opt. 11, 1112 (1972).

11. Airey, J.R. ,and Smith, I.W.M., 'Quenching of Infrared Chemiluminescence: Rates of Energy Transfer from HF ($V \leq 5$) to CO_2 and HF, and from DF ($V \leq 3$) to CO_2 and HF,' J. Chem. Phys. 57, 1669 (1972).

12. Steunenberg, R. K. ,and Vogel, R.C., 'The Absorption Spectrum of Fluorine,' J. Am. Chem. Soc. 89, 901 (1956).

13. Levy, J.B. ,and Copeland, B.K.W., 'The Kinetics of the Hydrogen-Fluorine Reaction.III.The Photochemical Reaction,' J. Phys. Chem. 72, 3168 (1968).

REFERENCES (Continued)

14. Levy, J.B., and Copeland, B.K.W., 'The Kinetics of the Hydrogen-Fluorine Reaction. II. The Oxygen-Inhibited Reaction,' J. Phys. Chem. 69, 408 (1965).

15. Levy, J.B., and Copeland, B.K.W., 'The Kinetics of the Thermal Hydrogen-Fluorine Reaction. I. Magnesium Reactor,' J. Phys. Chem. 67, 2156 (1963).

16. Kapralova, G.A., Trofimova, E.M., and Shilov, A.E., 'The Upper Ignition Limit in the Reaction of Fluorine with Hydrogen,' Kinetika i Kataliz 6, 977 (1965).

17. Ultee, C.J., 'Compact Pulsed HF Lasers,' Rev. Sci. Instr. 42, 1174 (1971).

18. Shaw, B.M., and Lovell, R.J., 'Foreign-Gas Broadening of HF by CO_2,' J. Opt. Soc. Am. 59, 1598 (1969).

19. Emanuel, G., Adams, W.D., and Turner, E.B., 'RESALE-1: A Chemical Laser Computer Program,' Aerospace Corporation Report TR-0172-(2776)-1/Air Force Report SAMSO-TR-72-39, Unclassified (1972).

20. Meredith, R.E., and Kent, M.F., 'Line Strength Calculations for the 0-1, 0-2, 0-3, and 1-2 Vibration-Rotation Bands of HF,' Report of BAMIRAC 4613-125-T, Willow Run Laboratories, Univ. of Michigan (1966).

21. Mann, D.B., Thrush, B.A., Lide, D.R., Ball, J.J., and Acquista, N., 'Spectroscopy of Fluorine Flames. I. HF Flame and the Vibration-Rotation Emission Spectrum of HF,' J. Chem. Phys. 34, 420 (1961).

22. Benedict, W.S., Bullock, B.W., Silverman, S., and Grosse, A.V., 'Infrared Emission of the Hydrogen Fluoride (H_2 - F_2) Flame,' J. Opt. Soc. Am. 43, 1106 (1958).

23. Cool, T.A., Shirley, J.A., and Stephens, R.R., 'Operating Characteristics of a Transverse-Flow DF-CO_2 Purely Chemical Laser,' Appl. Phys. Letters 17, 278 (1970).

24. Kim, P., MacLean, D.I., and Valance, W.G., 'Reaction Kinetics of NO With F and With F_2 by ESR Spectroscopy,' Boston College Document Number FRK-122, Prepared for Contract N00014-69-A-0453, ONR, Unclassified (1972).

25. Cohen, N., 'A Review of Rate Coefficients for Reactions in the H_2 - F_2 Laser System,' Aerospace Corporation Rep. TR-0172(2779)-2/Air Force Report SAMSO TR-72-23, Unclassified (1971).

REFERENCES (Continued)

26. Jacobson, T.V., and Kimball, G.H., 'Transversely Pulse-Initiated Chemical Lasers: Atmospheric Pressure Operation of an HF Laser,' J. Appl. Phys. 42, 3402 (1971).

27. Molina, M.J., and Pimentel, G.C., 'Chemical Laser Studies of Vibrational Energy Distributions: The Equal-Gain and Zero-Gain Temperature Techniques,' IEEE J. Quant. Electr. QE-9, 64 (1973).

28. Polanyi, J.C., and Tardy, D.C., 'Energy Distribution in the Exothermic Reaction F + H_2 and the Endothermic Reaction HF + H,' J. Chem. Phys. 51, 5717 (1969).